DOE/MC/29222 --5219
(DE96004494)
Distribution Category UC-103

Experimental and Theoretical Investigation on the Mechanism of Transient Bubble Images in Fluidized-Bed Combustors
Systematic Interpretation and Analysis

Final Report
July 1992- July 1995

Work Performed Under Contract No.: DE-AC21 -92MC29222

For
U.S. Department of Energy
Office of Fossil Energy
Morgantown Energy Technology Center
P.O. Box 880
Morgantown, West Virginia 26507-0880

By
West Virginia University Research Corporation
Department of Civil Engineering
Morgantown, West Virginia 26505-6102

August 1995

Disclaimer

This report was prepared as an account of work sponsored by an agency of the United States Government. Neither the United States Government nor any agency thereof, nor any of their employees, makes any warranty, express or implied, or assumes any legal liability or responsibility for the accuracy, completeness, or usefulness of any information, apparatus, product, or process disclosed, or represents that its use would not infringe privately owned rights. Reference herein to any specific commercial product, process, or service by trade name, trademark, manufacturer, or otherwise does not necessarily constitute or imply its endorsement, recommendation, or favoring by the United States Government or any agency thereof. The views and opinions of authors expressed herein do not necessarily state or reflect those of the United States Government or any agency thereof.

ABSTRACT

The transient bubble behavior was experimentally investigated to fundamentally understand the transient motion of gas bubbles in freely bubbling fluidized beds, simulating the FBC systems. Due to the oversimplified traditional two phase flow model concepts developed and most of the related numerous experimental works from 1960s to 1980s, the transient bubble behaviors could not have received due attention, resulting in some fundamental misconception of the bubbling phenomena particularly in coarse fluidized beds.

For the improvement of the design and operation of the FBC systems, the insight into the intrinsic transient bubbling phenomena in freely bubbling fluidized beds is of vital importance. We have found several basic new bubbling mechanisms in this work experimentally, and some of them have not, to our best knowledge, been published in past literature. Using the two dimensional fluidized bed, the images of transient bubbling behavior were recorded by videos, and processed and analyzed by computers.

As the results of experiments, the following new experimental facts were found:

(1) Transient bubbles change and fluctuate their size and shape over very short time intervals (on the order of 30 milliseconds) .

(2) Bubble disappearance and reappearance occurred in the emulsion phase in addition to the known phenomena of coalescence and splitting. The bubble interaction occurred between the bubbles and adjacent emulsion phase and also among the transient bubbles.

(3) Bubblers velocity fluctuated significantly, e.g., 0.6 to 3.0 m/s.

(4) Under one single specific fluidization condition, two different fluidization patterns appeared to occur randomly shifting from one pattern to the other or vice verse.

(5) The erosion rates of in-bed tubes at ambient and elevated temperature could be predicted using material property data and transient behavior of bubbles.

By introducing a new quantitative criterion which we call a gas stress index in the emulsion phase, the comparison of the fluidization quality between two and three dimensional fluidized beds was accomplished. We found reasonable correspondence between the two beds, and concluded that the new findings of transient bubble behavior should hold true for both types of fluidized beds.

The conclusions of this work are in good agreement with the conclusion of the pioneering work of DOE/METC on the transient bubbling behavior in three dimensional coarse fluidized beds using the capacitance measurement method.

TABLE OF CONTENTS

0. EXECUTIVE SUMMARY

1. TECHNICAL BACKGROUND

2. EXPERIMENTAL METHODOLOGY

2.1 Key Point of General Strategy for Achieving Experiments

2.2 Experimental Apparatus and Others

3. RESULTS AND DISCUSSIONS

3.A. Behavior of Transient Bubbles in Two Dimensional Fluidized Beds

3.B. Two Dimensional Circulating Fluidized Bed

3.C. Fluidization Pressure Effect on the Transient Behaviors

3.D. Comparison of Two and Three Dimensional Fluidized Beds

4. EROSION: AN INDEX TO THE TRANSIENT MOTION OF SOLID IN FLUIDIZED BEDS

4.1. Introduction

4.2. Literature Review

4.3. Experimental

4.4. Experimental Results and Discussions

5. CONCLUSIONS

6. NOMENCLATURE

7. BIBLIOGRAPHY

LIST OF FIGURES

Figure 2.2.1 Experimental set up for coarse particle fluidization 17

Figure 2.3.2 Locations of pressure taps for pressure fluctuation measurement 19

Figure 3-AI1-1 Gas phase pressure fluctuation vs time at the points of P, to P_5 located horizontally in freely bubbling fluidized bed (t=0 to 5 see) . . 27

Figure 3-AI1-2 Gas phase pressure fluctuation vs time at the points of P, to P_5 located horizontally in freely bubbling fluidized bed (t=5 to 10 see) . 27

Figure 3-AI1-3 Gas phase pressure fluctuation vs time at the points of P_1 to P_5 located horizontally in freely bubbling fluidized bed (t=10 to 15 see) . 28

Figure 3-AI1-4 Gas phase pressure fluctuation vs time at the points of P, to P_5 located horizontally in freely bubbling fluidized bed (t=15 to 20 see) . 28

Figure 3-AI1-5 Pressure difference between P_4 and P_1 vs time 29

Figure 3-AI1-6 Pressure difference between P_4 and P_5 vs time 29

Picture 3-AI-N1 Transient bubble images under the experimental condition. 30

Picture 3-AI-N2 Transient bubble images under the experimental condition 31

Picture 3-AI-N3 Transient bubble images under the experimental condition. 32

Picture 3-AI-N4 Transient bubble images under the experimental condition. 33

Figure 3-AI2-N1 cross sectional area of transient bubbles vs time under experimental condition I (normal period) 36

Figure 3-AI2-N2 cross sectional area of transient bubbles vs time under experimental condition I (normal period) 37

Figure 3-AI3-N1 Roundness of transient bubbles vs time under experimental condition I (normal period) . . 38

Figure 3-AI3-N2 Roundness of transient bubbles vs time under experimental condition I (normal period) . . 39

Figure 3-AI4-N1 Vertical distance of transient bubbles vs time under experimental condition I (Normal period) 40

Figure 3-AI4-N2 Vertical distance of transient bubbles vs time under experimental condition I (Normal period) . . . . .0.. . . . ..*.* .000 .o 41

Figure 3-AI5-N1 Velocity of transient bubbles vs time under experimental condition I (normal period) 42

Figure 3-AI5-N2 Velocity of transient bubbles vs time under experimental condition I (normal period) 43

Figure 3-AI6-N1 Horizontal velocity of transient bubbles vs time under experimental condition I (normal period) 44

Figure 3-AI6-N2 Horizontal velocity of transient bubbles vs time under experimental condition I (normal period) 45

Figure 3-AI7-N1 Cross sectional area of transient bubbles vs vertical distance under experimental condition I (normal period) 46

Figure 3-AI7-N2 Cross sectional area of transient bubbles vs vertical distance under experimental condition I (normal period) 47

Picture 3.AI-An-1 Transient bubble images under the experimental condition I (abnormal period) 48

Picture 3.AI-An-2 Transient bubble images under the experimental condition I (abnormal period) 49

Picture 3.AI-An-3 Transient bubble images under the experimental condition I (abnormal period) 50

Picture 3.AI-An-4 Transient bubble images under the experimental condition I (abnormal period) 51

Figure 3-AI2-AN-1 Cross sectional area of transient bubbles vs time under experimental condition I (abnormal period) 54

Figure 3-AI3-AN-1 Roundness of transient bubbles vs time under experimental condition I (abnormal period) . 55

Figure 3-AI4-AN-1 Vertical distance of transient bubbles vs time under experimental condition I (abnormal period) 56

Figure 3-AI5-AN-1 Velocity of transient bubbles vs time under experimental condition I (abnormal period) 57

Figure 3-AI6-AN-1 Horizontal velocity of interacting bubbles under experimental condition I (abnormal period) 58

Figure 3-AI7-AN-1 Cross sectional area of transient Bubbles Vs vertical distance under experiment condition I (abnormal period) 59

Figure 3-A8-N1 Cross sectional area of transient bubbles Vs vertical location (t=0 to 1.96 seconds) 60

Figure 3-A8-AN Cross sectional area of transient bubbles Vs vertical location (t=13.89 to 14.92 seconds) . . . 60

Figure 3-AI9-N&AN Disappearance along vertical distance at U_0/U_{mf}=2.0 61

Figure 3-AI10-N&AN Two kinds of disappearance at U_0/U_{mf}=2.0 . 62

Figure 3-AI11-N&AN Splitting along vertical distance at U_0/U_{mf}=2.0 63

Picture 3-AII-1 Transient bubble images under the experimental condition II 65

Figure 3-AII2-N1 Cross sectional area of transient bubbles vs time under experimental condition II 67

Figure 3-AII3-N1 Roundness of transient bubbles vs time under experimental condition II 67

Figure 3-AII4-N1 Vertical distance of transient bubbles under experimental condition II 68

Figure 3-AII5-N1 Velocity of transient bubbles vs time under experimental condition II 68

Figure 3-AII6 Horizontal velocity of transient bubbles vs time under experimental condition II 69

Figure 3-AII7-N&AN Coalescence along vertical distance at U_0/U_{mf}=2.3 70

Picture 3-AIII-1 Transient bubble images under the experimental condition III . . . . . , ... 71

Figure 3-AIII2-N1 Cross sectional area of transient bubbles vs time under experimental condition III . 73

Figure 3-AIII3-N1 Roundness of transient bubbles vs time under experimental condition III 73

Figure 3-AIII4-N1 Vertical distance of transient bubbles under experimental condition III 74

Figure 3-AIII5-N1 Velocity of transient bubbles vs time under experimental condition III 74

Figure 3-AIII6-N1 Horizontal velocity of transient bubbles vs time under experimental condition III 75

Figure 3-AIII7-N&AN Coalescence along vertical distance at U_0/U_{mf}=2.3 76

Picture 3.B.1 Images of circulating fluidized bed at different U_0/U_{mf} 77

Picture 3.B.2 Images of circulating fluidized bed by time sequence at U_0/U_{mf}=20.5 77

Figure 3.B.1 Pressure fluctuation at UO=5.29 m/s 79

Figure 3.B.2 Pressure fluctuation at UO=4.51 m/s 80

Figure 3.B.3 Pressure fluctuation at UO=3.73 m/s 81

Figure 3.B.4 Power spectrum of frequency at UO=5.29 m/s , . 83

Figure 3.B.5 Power spectrum of frequency at U_0=4.51 m/s . . 83

Figure 3.B.6 Power spectrum of frequency at UO=3.73 m/s . . 84

Figure 3.C.1 Pressure fluctuation at different operating pressure 87

Figure 3.D.1 Pressure difference between two horizontal points 88

Figure 3.D.2 Pressure difference between P_4 and P_1 vs time . 89

Figure 3.D.3 Pressure difference between P_4 and P_5 vs time . 89

Figure 3.D.4 Pressure fluctuation for three dimensional bed 92

Figure 3.D.5 $\Delta\Delta P^{\#}$ vs gas velocity for two horizontal points (Z/H=0.5) 93

Figure 3.D.6 $\Delta\Delta P^{\#}$ vs gas velocity for single point (Z/H=0.5) 93

Figure 3.D.7 $\Delta\Delta P^{\#}$ vs bed height for two horizontal points (Z/H= 0.5) 94

Figure 3.D.8 $\Delta\Delta P^{\#}$ vs bed height for single point (Z/H= 0.5) 94

Figure 3.D.9 Comparison of single point $\Delta\Delta P_{max}$ vs two $\Delta\Delta P^{\#}_{max}$ 95

Figure 4.3.1 Correlation between the maximum pressure fluctuations and the maximum force (Kono et al., 1987) 101

Figure 4.3.2 Experimental set-up for erosion tests 105

Figure 4.3.3 Schematic diagram of the experimental setting . 106

Figure 4.3.4 Relation between the maximum pressure fluctuations and the dimensionless gas velocity 107

Figure 4.3.5 Erosion index versus maximum pressure fluctuations for the in-bed tubes 110

Figure 4.3.6 Correlation between the erosion index and $\Delta\Delta P_{max}$ 111

Figure 4.3.7 Correlation between the erosion index and the dimensionless characteristic erosion number 112

Figure 4.3.8 Effect of fluidized particles on the erosion index. 114

Figure 4.3.9 Peripheral measurement points on the in-bed tube 115

Figure 4.3.10 Distribution of maximum pressure fluctuation along the peripheral direction of the tube 116

Figure 4.3.11 Tube rings for the measurement of erosion rates in longitudinal direction 117

Figure 4.3.12 Erosion index in the longitudinal direction ofthein-bedtube 118

Figure 4.3.13 The effect of temperature on $\Delta\Delta P_{max}$.....119
Figure 4.3.14 Erosion vs $\Delta\Delta P$ and properties of material . . 120

LIST OF TABLES

Table 2.2.1 The measured data and their physical meanings . 21

Table 2.2.2 Experiment data derived from the images of transient bubbles and other transient phenomena . . 21

Table 3-AI-1 Analysis results of bubbles of normal period (t=l.46 to 1.96 seconds) 34

Table 3-AI-2 Analysis results of bubbles of abnormal period (t=1.99 to 2.49 seconds) 52

Table 3-AII Analysis results of bubbles of under experimental condition II (t=O.49 to 0.59 second) 66

Table 3-AIII Analysis results of bubbles of under experimental condition III (t=0.49 to 0.59 second) 72

Table 4.3.Oa Tensile strength and Young's modulus for aluminum alloy 6061-T6 at different temperature 102

Table 4.3.0b Tensile strength and Young's modulus for copper 122 at different temperature 103

Table 4.3.0b Tensile strength and YoungFs modulus for 304 stainless steel at different temperature 103

Table 4.3.1 Erosion index data (aluminum alloy) 108

Table 4.3.2 Erosion index data (copper) 108

Table 4.3.3 Erosion index data (stainless steel) 109

Table 4.3.4 Mechanical properties of test tubes . , ... 109

EXECUTIVE SUMMARY

The overall objective of this work was to fundamentally understand the transient motion of bubbles in freely bubbling fluidized beds. More specifically, the objective of this work is to systematically help interpret the transient bubble images seen by capacitance imaging method developed at DOE/METC in three dimensional fluidized beds. To accomplish this, experimental and theoretical studies of the behavior of transient bubbles in two dimensional fluidized bed were carried out to elucidate the intrinsic bubble behavior and the mechanism of transient bubble motion. Although bubbling phenomena has been heavily investigated in the classical fluidization papers from 1960s to 1980s, very little of the work deals with the transient bubble behavior. Most of past research for bubbling have been under very limited conditions where the bubbling gas was injected into an incipiently fluidized bed.

In the classical two phase flow model for fluidization, bubble behavior in a freely bubbling fluidized bed was assumed to be the same as an injected bubble into an incipient fluidized bed (Davidson, 1963). This was obviously oversimplified and misleading in view of actual bubbling phenomena. Unfortunately, this oversimplified two phase flow model was widely accepted to the gas-solid fluidized bed systems, leading to a series of critical practical problems particularly for fluidized bed combustion (FBC) systems. One of the purpose of this work was to correct the traditional misconcept by providing new experimental evidence.

Various types of the fluidized bed combustion system have been or are being developed. Examples of these systems include atmospheric bubbling, circulating, and pressurized fluidized bed combustors. Although many investigations were performed and published, the transient motion of bubbles in fluidized beds has not really yet been well understood, which sometimes made the design and operation of fluidized beds difficult.

The phenomena of transient motion of bubbles have also been one of the most fundamental key problem of fluidization science, which have not really been elucidated. Recently the images of transient motion of bubbles have been obtained by the capacitance methods in three dimensional fluidized bed at METC, e.g., Halow et al (1992) which can potentially provide a very deep insight into this fundamental problem of fluidization.

Accordingly, the overall objectives of this research were to provide the basic and systematic interpretation of the above transient bubble images through the experimental and theoretical studies and to fundamentally elucidate the mechanism of the transient motion of bubbles in various types of fluidization experimentally and theoretically.

Through our experimental research works, we have developed several new findings.

a) There was a considerable similarity between the transient bubble' motion in three and two dimensional fluidized beds by comparing the transient motion of bubbles; many observations from the three dimensional fluidized beds (capacitance image) and two dimensional fluidized beds (actual video image) are in good agreement. The advantage of two dimensional fluidized beds was that the direct visual observation could easily be carried out. Therefore, we could get a clear experimental evidence of the basic mechanism of transient bubble phenomena. On the other hand, we should not forget the limitation of two dimensional fluidized beds due to the wall effect. However it was experimentally verified that there is no substantial difference between two and three dimensional fluidized beds in terms of bubbling mechanism.

b) In contrary to the classical two phase flow theory, the bubble size and velocity in actual fluidized beds were not at all constant in fluidized beds. Gas bubbles could disappear into the adjacent emulsion phase or be generated from the adjacent emulsion phase, which was never reported in the past published gas-solid fluidization papers but was actually and experimentally observed both in three dimensional fluidized beds by capacitance imaging (Halow, 1991) and in two dimensional fluidized bed by video pictures in this work.

c) The properties of both bubbles and emulsion phases could generate fluctuations of voidage when the bubbles were passing through the bed. Especially, the various levels of voidage caused by turbulence in the emulsion phase could effect the transient forces of solid particles in fluidized beds.

Therefore, the interpretation of capacitance images of transient bubble motion had been accomplished in the following points:

- Elucidation on the mechanism of transient bubble motion in two and three dimensional fluidized beds
- Elucidation on the role of transient behavior of emulsion phase in fluidized beds
- Analysis of digitized video image of transient bubble motion together with the transient force signal
- Elucidation of transient bubble motion
- Application of basic understanding on the transient motion of bubble to the design and operation of fluidized bed combustors

The overall goal of the work was successfully accomplished

through the procedures described above, and the outline can be shown as follows.

Measurement of Transient Bubble Motion and Behavior in Two Dimensional Fluidized Beds and Its Comparison with the Capacitance Image in Three Dimensional Fluidized Beds

In case of two dimensional fluidized beds, transient bubble motion could easily and reproducibly be measured by using video technique, although the fluidization became slightly different due to the wall effect from the three dimensional bubble motion developed at METC. Through the newly developed experimental technique of measuring the fluctuation of gas phase stress forces in horizontal direction in the emulsion phase, the difference of two and three dimensional fluidized bed's behavior was found to be , quantitatively pretty close to each other, which has not, to our best knowledge, been known in past literature. The experimental results showed that many common characteristics could be observed both by capacitance method in three dimensional fluidized beds and by synchronized video technique in two dimensional fluidized beds. A database was built to store bubble parameters and related information. The data base was based on our data collections (tapes, photos, etc.). Some characteristic factors were considered, and analysis was made to determine the key factors and to find the relationship between these factors and bubble images. The transient behavior of bubble size, bubble shape, bubble motion, bubble coalescence/splitting were measured, analyzed, and compared with transient bubble motion images generated by two dimensional fluidized bed and compared with the capacitance method in three dimensional fluidized beds.

Conversion of Video Bubble Images into Computer Data for Numerical Analysis

It was found that the transient video bubble images could provide insight into the transient bubble motion, video bubble image signals obtained in two dimensional freely bubbling fluidized beds could be further digitized and analyzed by computer. This technique was developed in our lab to build a bubble image collection system. The computerized bubble image collection signals were used for classification and further analysis of the data. To be more specific, the systematic simultaneous data takings were carried out, including bubble size, bubble location, bubble shape, bubble velocity, local stress force's fluctuation in emulsion phase, maximum solid force, etc., all of which behave very transiently. Further all these transient data were analyzed and shown as function of time, the time interval being 0.033 sec. The accumulation of the precisely analyzed above data could build most reliable argument on experimental facts, which should be one of the most comprehensive experimental data collection describing the

properties of transient bubbles in freely bubbling fluidized beds.

Analysis of transient behavior of bubble motion in freely bubbling fluidized beds.

Using the database constructed, statistical analysis was carried out and a stochastic model was developed. Unlike most computer models in the literature, this model could provide very interesting, important conclusion for a freely bubbling fluidized bed under the standard fluidization condition. (U_0/U_{mf}=1.8 to 2.3, H/Dt=1, fluidized particles of 1 mm spherical glass beads).

- Bubble sizes were changing transiently sometimes very quickly, sometimes less quickly through coalescence and/or splitting with adjacent bubbles or by the other ways of the interaction between the bubbles and the emulsion phases. The above bubbling mechanism verified through experiments was significantly different from classical two phase flow of Davidson. Note that Davidson's model only hold true for the bubbles injected into incipient fluidized beds, in which the bubble size remained constant and has constant rising velocity.
- Bubble shape were changing very rapidly by the same mechanism explained for bubble size changes. Among the adjacent bubbles and the emulsion phase there occurred the intensive gas flow interaction, inducing the bubble shape change ϕ_c (Carman's shape factor) in the range of 0.8 to 0.1 in 0.067 sec. The classical assumption of bubble cap shape could only hold true for the limited case of the injected bubble into the incipient fluidized bed.
- Bubbling rising velocity could change, e.g., from -0.4 m/s to +2.0 m/s in 0.067 sec.
- The gas phase stress in the same vertical level at half the bed height could change, e.g., 0.7 to 1.0 kPa in 0.03 second and this stress value changed very transiently.
- All these transient changes could occur due to the transient flow exchanges of gas flow among adjacent bubbles and/or of gas flow from bubbles to the emulsion phase or vice versa. Sometimes, a bubble could disappear into the emulsion phase and a bubble could reappear from the emulsion phase.
- The effect of these transient behaviors of bubble on the erosion rate of in-bed tubes in fluidized bed was confirmed experimentally.

The Study on Intrinsic Mechanism of Transient Motion of Bubbles and Transient Behavior of the Emulsion Phase

The disappearance of bubbles into the adjacent emulsion phase was experimentally verified by photographs and the sudden generation of bubble from the emulsion phase could actually be confirmed, which could not be explained by the classical two phase flow model. The elucidation of this mechanism will experimentally and theoretically be investigated by using an emulsion structure

model. The structure of the emulsion phase could change transiently, causing the transient motion of bubbles. The transient structural change "of emulsion phase was experimentally measured.

Interpretation of the Capacitance Image of Transient Bubble Motion in Three Dimensional Fluidized Beds

Through the accomplishments of 1 through 4, we could have a deep insight to the transient bubble motion. Then, the interpretation of the capacitance image of transient bubble was improved. Particularly we used these transient bubble data for the better design and operation of fluidized combustion system.

Transient Bubble Motion in Circulating Fluidized Beds

Based upon the accumulated understanding on the transient bubble motion described in 1 through 4, the transient bubble motion of circulating fluidized bed was investigated experimentally and theoretically. As experiment pieces of equipment, two dimensional circulating cold fluidized beds was installed (10cm(width) X 100cm (height) X lcm (thickness)) together with a cyclone and a return cycle system. Because the fluidization conditions (flow pattern) can be vitally important for the basic design of circulating fluidized beds, which has been missing in the past research. We found the importance of transient behavior in time averaged particle density profile mostly reported in CFB. The wave-like motion of particle on the inside wall of vessels seem to play a key role.

Transient Bubble Motion in Pressurized Fluidized Beds

The transient motion of bubble will experimentally be measured in a two dimensional pressurized fluidized bed (cold model, pressure: 5-10 atmospheres, size: 10cm (width) X 100cm (height) X 1cm (thickness)).

The approach and analysis of experiments will be in the same way as described in 1 through 4. The transient bubble motion was predicted form the gas phase tensor fluctuation.

An understanding of the transient behavior of the emulsion phase was developed to assess the erosion rate of several materials at ambient and elevated temperature and develop a predictive model for erosion and compare to the measured erosion rates.

The transient motion and behavior of the emulsion phase in a fluidized bed were measured and characterized in a fluidized bed at ambient and elevated temperature.

The erosion rates of several specific materials with known mechanical properties were measured at ambient and elevated

temperatures in a fluidized bed at several fluidization conditions.

Using the measured erosion rate, the measurement and understanding of the emulsion phase behavior, and the results of the transition bubble and emulsion phase behavior (contract original statement of work) a predictive model for erosion rates were developed and compared to the measured rates. The model incorporated the physical and mechanical properties of the materials and the effect of temperature of the erosion rate.

1. TECHNICAL BACKGROUND

The overall objective of this work was to fundamentally understand the transient motion of bubbles in freely bubbling fluidized beds. More specifically, our objective is to systematically help interpreting the transient bubble images by capacitance method developed at DOE/METC in three dimensional fluidized beds by accomplishing additional experimental and theoretical studies and to elucidate the transient bubble images and their motion mechanism. Although the bubbling phenomena were much investigated in the classical fluidization papers, the most of transient bubble behavior has still not been well understood. As the most of past research for bubbling have been accomplished under the very limited condition where the bubbling gas was injected into an incipient fluidization.

In the classical two phase flow model for fluidization, the bubble behavior in a freely bubbling fluidization bed was assumed the same as the injected bubble behavior in an incipient fluidization (Davidson, 1963), which was obviously oversimplified and misleading in view of actual bubbling phenomena. Unfortunately, this oversimplified two phase flow model was widely applied to the gas-solid fluidized bed systems, generating a series of problems particularly for fluidized bed combustion (FBC) systems. One of the purpose of this work was to correct the traditional misconcept experimentally.

The various types of the fluidized bed combustion system have been or are being developed. Examples of these systems include atmospheric bubbling, circulating, and pressurized fluidized bed combustors. Although many investigations were accomplished and published, still the transient motion of bubbles in fluidized beds has not really yet been well understood, which sometimes made the design and operation of fluidized beds difficult.

The phenomena of transient motion of bubbles have also been one of the most fundamental key problem of fluidization science, which have not really been elucidated. Recently the images of transient motion of bubbles have been obtained by the capacitance methods in three dimensional fluidized bed at METC, which can potentially provide a very deep insight into this fundamental problem of fluidization.

Accordingly, the overall objectives of this research were to provide the basic and systematic interpretation of the . above transient bubble image through the additional experimental and theoretical studies and to fundamentally elucidate the mechanism of the transient motion of bubbles in various types of fluidization experimentally and theoretically.

Through our experimental research works, we could have found several new findings.

a) There was a considerable similarity between the transient bubble motion in three and two dimensional fluidized beds by comparing the transient motion of bubbles; many observations from the three dimensional fluidized beds (capacitance image) and two dimensional fluidized beds (actual video image) are in good agreement. The advantage of two dimensional fluidized beds was that the direct visual observation could easily be carried out. Therefore, we could get a clear experimental evidence of the basic mechanism of transient bubble phenomena. On the other hand, we should not forget the limitation of two dimensional fluidized beds due to the wall effect. However, it was experimentally verified that there was no substantially difference of fluidization quality between two and three dimensional fluidized beds.

b) In contrary to the classical two phase flow theory, the bubble size and velocity in actual fluidized beds were not at all constant in fluidized beds. Gas bubbles could disappear into the adjacent emulsion phase or be generated from the adjacent emulsion phase, which was never reported in the past published gas-solid fluidization papers but was actually and experimentally observed both in three dimensional fluidized beds by capacitance imaging (Halow, 1991) and in two dimensional fluidized bed by video pictures in this work.

c) The properties of both bubbles and emulsion phases could generate fluctuations of voidage peaks when the bubbles were passing through the bed. Especially, the various levels of voidage caused by turbulence in the emulsion phase could effect the transient forces of solid particles in fluidized beds.

Therefore, the interpretation of capacitance images of transient bubble motion had been accomplished in the following view points:

- Elucidation on the mechanism of transient bubble motion in two and three dimensional fluidized beds
- Elucidation on the role of transient behavior of emulsion phase in fluidized beds
- Analysis of digitized video image of transient bubble motion together with the transient force signal
- Elucidation of transient bubble motion
- Application of basic understanding on the transient motion of bubble to the design and operation of fluidized bed combustors

Historically the bubble motion and its properties (size, shape, cloud, wake, etc.) in fluidized beds had been investigated very intensively by many researchers including famous classical works by Davidson et al (1963) and by Rowe et al (1962).

However, past researchers investigated mostly the behavior of the bubble in incipient fluidized beds. Therefore, their results should not directly be applicable to the transient behavior of bubbles in freely bubbling fluidized beds. The transient behavior of bubbles in fluidized beds could not have been predicted by the past open literature. Ironically, the transient motion of bubbles became very significant in fluidized beds (fluidized bed combustion systems or gasifiers) using coarse particles (>0.5 mm), in which fluidization was generally not homogeneous and large bubbles were formed. Qualitatively, the size and shape of bubbles were partially investigated but actually the transient bubble behaviors in fluidized beds had not been clarified (Rowe 1968).

Some attempts were made to determine the bubble parameters. Viswanathan and Rao (1984) used a simple method to estimate average bubble size at various height in fluidized beds. Clough and Weimer (1985) developed avoid propagation equation to describe a bubbling fluidized bed, and predicted the dynamic response to step changes in inlet gas flow of bubble volume fraction at any axial position. Gyure and Clough (1987) estimated the bubble frequency and bubble velocity in a fluidized bed from the cross-correlation function of pressure measurements during dynamic changes in fluidizing conditions. However, strangely all these estimates were still based on the classical two phase flow theory. The bubble volume or size obtained were the average, and could not reflect the transient bubble behavior in fluidized beds. A laser-based technique were developed by Sung and Burgess (1987) for the measurement of bubble velocities and sizes in a two dimensional fluidized bed. Lim, Agarwal and O'neill (1990) used image analysis to measure bubble parameters in a two dimensional fluidized bed. Their technique greatly improved the accuracy of bubble parameter measurement. However, the transient motion of bubbles (slugs) has still not been well clarified, especially when coalescence and splitting take place.

Recently, Halow et al (1989, 1990, 1991) made a clear break-through to measure the transient motion of bubbles in fluidized beds by using a capacitance method. On the other side, Kono et al (1988, 1990) also developed three methods to measure and characterize the transient forces of solid particles in fluidized beds, which can be used to interpret the transient motion of the bubbles (slugs). Furthermore a very interesting observation was obtained by Kono et al (1991) in a two dimensional fluidized bed: bubble size and velocity can drastically be changed in its transient motion. This observation was in good agreement with the findings of Halow's group in three dimensional fluidized beds. We also found that the emulsion phase voidage fluctuate transiently within the remarkable range in continuously bubbling fluidized beds. Our experimental approach was to recognize the transient motion of bubbles by measuring and characterizing transient forces of solid particles, and to support the interpretation of the capacitance images of transient bubble motion in three dimensional

fluidized bed. For that purpose, a video image technique in two dimensional fluidized beds was used.

Even though many computational techniques were known (Sinclair and Jackson, 1989; Ding and Gidaspow, 1990), some of their assumptions were still not convincing. They could have shown a kind of bubble images, using various adjusting parameters. However, they found the difficulty of finding and explaining the development of bulk density fluctuation in the emulsion phase of fluidized beds. We developed a two dimensional hydrodynamic two phase flow model describing the transient bubbling behavior with additional supplementary equations (equation of continuity, gas and solid momentum balance equation, relevant drag coefficient equation and the emulsion deformation equation). In stead of using the very artificial intensity function of particle temperature (T) proposed by R. Jackson (1989), we introduced the emulsion phase's packing structure randomness model. According to the preliminary work, we could generate the simulated computer image of transient bubble motion which seems to be supporting our two dimensional experiment results.

Based upon the consideration discussed so far, we planned to attain an understanding of the fundamentals of transient bubble motion in operating bubbling, circulating, and pressurized fluidized bed combustors (FBC) and develop a working model that can predict this phenomena. The working model was based on experimental results (not theoretical) and reflected the actual bubbling phenomena. One interesting example of mispresentation of computer simulation results were demonstrated for the case of circulating fluidized beds at Fluidization Conference VIII, Tours, France (1995) by Knowlton, Geldart and Matson. The time average computation results indicated no physical meaning at all, when it is compared with the corresponding experimental data (images) shown in this work.

We have been successfully obtaining the transient behavior of bubbles and found that the irregular activated transient bubble motion could occur time to time very suddenly (approximately 20% - 30% of the total observation period in our experiment) under a specific' fluidization condition. Traditionally, most of the common sense of hydrodynamics, showed that the flow characteristics should be determined by a specific given flow condition. On the contrary, we found a very interesting stochastic behavior of fluidization characteristics in coarse particle fluidized beds. Under the same given fluidized bed condition, in terms of equipments and flow condition, obviously more than two significantly different fluidization behaviors could stochastically coexist, which were defined in this work as "normal" and "abnormal" fluidization. This peculiar characteristics has at least to our knowledge not reported nor known. This could be a significant impact to understand the erosion problem, which is so important in terms of application. Therefore, the understanding of the transient behavior of the

emulsion phase (solid particles) caused by the above transient motion of bubble became very important. This additional approach was useful to achieve this project more precisely and also to attain the practical application (the prediction of the erosion rate) .

As an index of the transient behavior of the emulsion phase, various physical parameters were considered. The erosion rate of in-bed tubes can be a good index representing the transient behavior of the emulsion phase particles, because the erosion rate was only sensitive to the transient maximum motion but not much to the average motion of the solid particles. Furthermore, this index had a very important generous application significance for the science of fluidization.

This work was carried out to understand and predict the transient behavior of the emulsion phase (solid particles) at the ambient and elevated temperatures, using" the erosion rate data obtained under the ambient condition, together with a novel characterization method of the mechanical properties of the materials of construction concerned.

According to the basic fracture theory of solid, the erosion of in-bed tubes and other bed components should logically be caused by the following factors: the properties of materials concerned (tube/components and particles) , and the transient maximum particle forces and its frequency. When the maximum transient motion of solid particles is specified, the properties of concerned materials (such as tensile strength and Young's modulus) should play the decisive roles to determine the erosion rates.

The maximum transient forces of solid particles were measured under various fluidization conditions and in various size of fluidized beds with three different measurement methods. The maximum transient force of solid particles was found to be the determining major factor which controls the erosion rates of in-bed components (in-bed tubes, vessel walls etc.) in fluidized beds.

Furthermore, we could obtain an interesting experimental observation in a two dimensional fluidized bed: i.e., bubble size and velocity could drastically be changed in its transient motion. This observation was in good agreement with the findings of Halow's group in three dimensional fluidized beds. We found that the emulsion phase voidage fluctuated transiently within the remarkable range in continuously bubbling fluidized beds. Especially, the various levels of voidage caused by turbulence in the emulsion phase could effect the transient forces of solid particles in fluidized beds. All these phenomena were caused by the interaction between bubbles or between bubbles and emulsion phases.

In another recent research, we measured erosion rates for various materials with different mechanical properties under

specific fluidization conditions and at ambient and elevated temperature. The effect of the characteristic mechanical property of the materials concerned on the erosion rates was investigated by changing the testing materials with different mechanical strength and elastic modulus.

We found that the erosion rates could be well predicted using material characteristic properties (tensile strength and Youngts modulus) and the maximum particle forces, regardless of the various materials used, the scale and type of fluidized beds, and the operating conditions. The erosion rate index is well correlated with a characteristic function consisting of maximum particle forces, and material characteristic properties (tensile strength and Young's modulus). The term $\Delta\Delta P_{max}$, the maximum gas pressure fluctuation, corresponds the maximum particle forces, since reliable correlation between $\Delta\Delta P_{max}$ and maximum particle forces exists (Kono 1990) . Furthermore, a new interpretation of gas phase pressure fluctuation in the horizontal direction was developed and defined as the stress force fluctuation $(\Delta\Delta P)_{\#}$ in fluidized beds.

It was our intent to determine the transient motion of bubbles by measuring and characterizing transient forces of solid particles at both ambient and high temperatures. The proposed research will apply the conclusion of the understanding of the transient motion and behavior of bubbles and emulsion phase to the erosion assessment of fluidized bed combustion systems.

An empirical predictive erosion characteristic equation, expressed by the maximum force of solid particles in the beds and the properties of the bed components, was obtained. This approach was generalized to predict the erosion rates at elevated temperature. This erosion data were also found to be useful to characterize the transient property of fluidization. In this work, we developed the predictive method to assess the effect of property change of material caused by temperature on the erosion rate. The characteristic mechanical properties of the materials, and their changes at elevated temperature, were collected from the literature. The erosion rates of various materials at elevated temperature were experimentally measured. Furthermore, the erosion process, which consists of the fracture of solid particles, would comprehensively be expressed and interpreted by introducing erosion characteristic function ϕ, and $\phi = f\ (F_{max}, \sigma_t, Y)$.

The overall goal of the proposed work was thus successfully accomplished through the procedures described above, and the outline was shown as follows.

1. Measurement of Transient Bubble Motion and Behavior in Two Dimensional Fluidized Beds and Its Comparison with the Capacitance Image in Three Dimensional Fluidized Beds

In case of two dimensional fluidized beds, transient bubble motion could easily and reproducibly be measured by using video technique, although the fluidization became slightly different due to the wall effect from the three dimensional bubble motion developed at METC. The experimental results showed that many common characteristics could be observed both by capacitance method in three dimensional fluidized beds and by synchronized video technique in two dimensional fluidized beds. A database was built to store bubble parameters and related information. The data base was based on our data collections (tapes, photos etc.). Some characteristic factors were considered, and analysis was made to determine the key factors and to find the relationship between these factors and bubble images. The transient behavior of bubble size, bubble shape, bubble motion, bubble coalescence/splitting were measured, analyzed, and compared with transient bubble motion images generated by-two dimensional fluidized bed and compared with the capacitance method in three dimensional fluidized beds.

2. Conversion of Video Bubble Images into Computer Data for Numerical Analysis,

It was found that the transient video bubble images could provide insight into the transient bubble motion, video bubble image signal obtained in two dimensional freely bubbling fluidized beds could be further digitized and analyzed by the computer. This technique were developed in our lab to build a bubble image collection system. The computerized bubble image collection were used for classification and further analysis. To be more specific, the systematic simultaneous data takings were carried out, including bubble size, bubble location, bubble shape, bubble velocity, local stress force's fluctuation in emulsion phase, maximum solid force, etc., all of which behave very transiently. Further all these transient data were analyzed and shown as function of time, the time interval being 0.033 sec. The accumulation of precisely analyzed above data could build most reliable argument on experimental facts, which should be one of the most comprehensive experimental data describing the property of transient bubble in freely bubbling fluidized beds.

3. Analysis of transient behavior of bubble motion in freely bubbling fluidized beds.

Using the database constructed, statistical analysis was carried out and a stochastic model was developed. Unlike most computer models in the literature, this model could provide very interesting, important conclusion for a freely bubbling fluidized bed under the standard fluidization condition. (U_0/U_{mf}=1.8 to 2.3, H/Dt=1, fluidized particles of 1 mm spherical glass beads).

- Bubble sizes were changing transiently sometimes very quickly, sometimes less quickly by the way of coalescence and/or splitting

of adjacent bubbles or by the other way of the interaction between the bubbles and the emulsion phases. The above bubbling mechanism verified through experiments is significantly different from classical two phase flow of Davidson. Note that Davidson's model only hold true for the bubbles injected into incipient fluidized beds, in which the bubble size remained constant with a constant rising velocity.

- Bubble shape were changing very rapidly by the same mechanism explained for bubble size changes. Among the adjacent bubbles and the emulsion phase there occur the intensive gas flow interaction, inducing the bubble shape change ϕ_c (Carman's shape factor) in the range of 0.8 to 0.1 in 0.067 sec. The classical assumption of bubble cap shape could only hold true for the injected bubble into the incipient fluidized bed.
- Bubbling rising velocity could change, e.g., from -0.4 m/s to +2.0 m/s in 0.067 sec.
- The gas phase stress in the same vertical level at the half of the bed height could change, e.g., 0.7 to 1.0 kPa in 0.3 second and this stress value changed very transiently.
- All these transient changes could occur due to the transient flow exchanges of gas flow among adjacent bubbles and/or of gas flow from bubbles to the emulsion phase or vice versa. Sometimes, a bubble could disappear into the emulsion phase and a bubble could reappear from the emulsion phase.
- The effect of these transient behaviors of bubble on the erosion rate of in bed tube in fluidized bed was confirmed experimentally.

4. The Study on Intrinsic Mechanism of Transient Motion of Bubbles and Transient Behavior of the Emulsion Phase

The disappearance of bubbles into the adjacent emulsion phase was experimentally verified by photographs and the sudden generation of bubble from the emulsion phase could actually be confirmed, which can not be explained by the classical two phase flow model. The elucidation of these mechanism will experimentally and theoretically be investigated by using an emulsion structure model. The structure of the emulsion phase could change transiently, causing the transient motion of bubbles. The transient structural change of emulsion phase was experimentally measured.

5. Interpretation of the Capacitance Image of Transient Bubble Motion in Three Dimensional Fluidized Beds

Through the accomplishments of 1 through 4, we could have a deep insight to the transient bubble motion. Then, the interpretation of the capacitance image of transient bubble was improved. Particularly we used these transient bubble data for the better design and operation of fluidized combustion system.

6. Transient Bubble Motion in Circulating Fluidized Beds

Based upon the accumulated understanding on the transient bubble motion described in 1 through 4, the transient bubble motion of circulating fluidized bed was investigated experimentally and theoretically. As experiment pieces of equipment, two dimensional circulating cold fluidized beds was installed (10cm(width) X 100cm (height) X 1cm (thickness)) together with a cyclone and a return cycle system. Because the fluidization conditions (flow pattern) can be vitally important for the basic design of circulating fluidized beds, which has been missing in the past research. We found the importance of transient behavior in time averaged particle density profile mostly reported in CFB. The wave like motion of particle on the inside was of vessels seem to play a key role.

7. Transient Bubble Motion in Pressurized Fluidized Beds

The transient motion of bubble will experimentally be measured . in a two dimensional pressurized fluidized bed (cold model, pressure: 5-10 atmospheres, size: 10cm (width) X 100cm (height) X 1cm (thickness)).

The approach and analysis of experiment will be in the same way as described in 1 through 4. The transient bubble motion was predicted from the gas phase tensor fluctuation.

8. Erosion Rate of In-Bed Tubes in Fluidized Bed at Ambient and Elevated Temperature

An understanding of the transient behavior of the emulsion phase was developed to assess the erosion rate of several materials at ambient and elevated temperature and develop a predictive model for erosion and compare to the measured erosion rates. T h e transient motion and behavior of the emulsion phase in a fluidized bed were measured and characterized in a fluidized bed at ambient and elevated temperature. The erosion rates of several specific materials with known mechanical properties were measured at ambient and elevated temperatures in a fluidized bed at several fluidization conditions.

Using the measured erosion rate, the measurement and understanding of the emulsion phase behavior, and the results of the transition bubble and emulsion phase behavior (contract original statement of work) a predictive model for erosion rates were developed and compared to the measured rates, showing good agreement.

2. EXPERIMENTAL METHODOLOGY

2.1 Key Points of General Strategy for Conducting Experiments

(a) Based upon the considerations discussed in the preceding section, we understand that the fundamental property difference of bubbles in freely bubbling fluidized beds and that in incipient fluidized beds is that the bubbles in the former case could vigorously interact with each other and also with the adjacent emulsion phase, while the bubble in latter case could not. Therefore, the experimental confirmation and verification of these facts is a significant goal.

(b) Now, to characterize the transient behaviors of bubbles, we had to measure and record the size, shape and volume of bubble, bubble velocity, the gas phase stress in the emulsion phase at specific locations, the erosion rate (corresponding to the maximum of solid particle's receiving stress) simultaneously, all of which are *very* transient and fluctuating. The time interval of data taking should be in the range of 30 to 100 milliseconds. The data acquisitions needs to be well synchronized.

(c) The interpretationof averaging the transient phenomenon's data must carefully be accomplished. For example, the bubble sizes and shapes changed on the order of 30 to 100 milliseconds and bubbles interacted very extensively with the adjacent emulsion phase. Thus, the gas diffusion model used in the classical two phase flow would not predict this behavior and be reformulated.

(d) The stochastic occurrences of some bubbling phenomena was also a critical point to be considered for fluidization phenomena using coarse particle, which can sometime take place in FBC. Under certain constant fluidization conditions, we found there could be stochasticaly two different types of fluidization, which was named the one as "normal" and the other as "abnormal" fluidization. This finding seems to be important because two different flow mechanism could shift from one to the another fluidization quite stochastically.

(e) The 'pro and con' of using two dimensional fluidized beds was investigated using a new fluidization quality index of $(\Delta\Delta P)'$, which will be explained in the following section.

2.2 Experimental Apparatus and Others

2.2.1 Fluidized bed systems

For a systematic study of transient characteristics in coarse particle fluidized bed systems, the experimental set-up as shown in Figure 2.2.1 was constructed. This set-up mainly consists of: (1) a two dimensional fluidized bed, (2) pressure sensors, (3) a timer, (4) a video camera, (5) anA/D converter, (6) a desk-top computer.

There is no page 17.

The configuration of the experimental apparatus was designed to study the transient behavior of gas and solid particles by utilizing: (1) transient pressure fluctuations, and (2) image analysis techniques all together in a synchronized fashion. A TTL signal box which sets the time was manufactured to achieve simultaneous video recording and data sampling. This device was connected to a timer to provide on-screen timing.

The two dimensional fluidized bed was made of transparent plexi-glass material with dimensions of 1.0 x 0.254 x 0.012 m. The dimensions of the three dimensional fluidized bed was 0.11 m I.D. X 1.50 m in height. The gas distributors are metal porous plates with an average pore size of 200 μm for both beds. The beds contain enough volumes under the distributor plates to provide uniform gas flux. An advantage of two dimensional beds was that it was very easy to observe and record both phases which in turn yields high quality images.

There have been many methods developed for the investigation of fluidization. Various methods such as differential pressure probes and light probes have the disadvantage of probe interference with the bubbles as they rose. On the other hand, the non-intrusive methods such as the X-ray method do not interfere with the flow inside the bed. However, they have the following disadvantages: (1) the picture is necessarily a silhouette and bubbles behind or partially behind another can not be distinguished clearly; (2) to penetrate to a bed of realistic thickness containing X-ray transparent material, quite high tube voltages are necessary; (3) since the fluidized bed is a dynamic system with particle and bubble velocities extremely high, a high X-ray flux density is necessary to obtain an adequate response. Consequently, the utilization of two dimensional beds among other methods practically becomes advantageous.

2.2.2 Pressure fluctuation measurements

Five equally spaced pressure taps were mounted horizontally onto the fluidized bed for pressure fluctuation measurements. The locations of these sampling points were schematically shown in Figure 14. The taps were connected to pressure sensors through flexible plastic tubing. Validyne (Model P305D) pressure transducers were used in the experiments. The DC output of these pressure transducers was fed to an A/D converter and then to a desk-top computer for data acquisition and storing.

2.2.3. Image capturing and analysis

The experiments were recorded by an RCA video camera. The recordings were then played on a TV set and the images were captured by using a Quick Capture frame grabber and a software package. The time interval between each image was as small as 0.033 seconds.

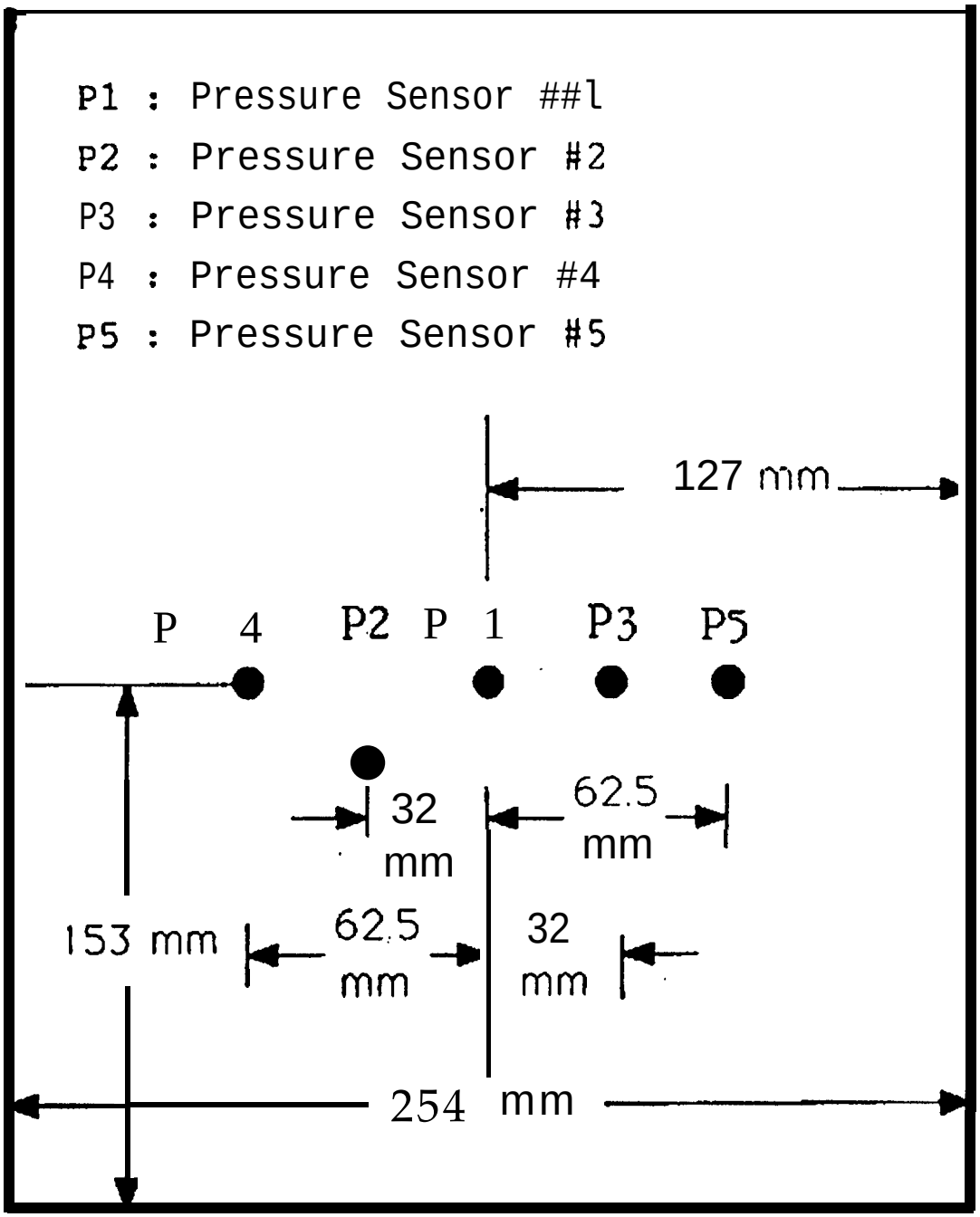

Figure 2. 3.2 Locations of pressure taps for pressure fluctuation measurements

After the completion of capturing, each image was processed and analyzed by using Global Lab Image software. In this way, a complete data bank composed of images and processed data was formed.

2.2.4 Materials and Experimental Conditions

In the experiments, 1 mm spherical glass beads (U_{mf}=0.46 m/s) were used as fluidized particles. Air supplied by a compressor via flowmeter was the fluidizing medium. Three different superficial gas velocities (U_0/U_{mf}=1.8, 2.0, and 2.3) were utilized. In all the experiments, the bed height was 0.25 m, i.e., the bed aspect ratio of H/D=1.0. The fluidization conditions used in the experiment were named as I, II and III in the following way:

Experimental condition I: U_0/U_{mf}=2.0
Experimental condition II: U_0/U_{mf}=2.3
Experimental condition III: U_0/U_{mf}=1.8

2.2.5 Simultaneous data taking system for transient behaviors of bubbles in freely bubbling fluidized beds

Combining 2.2.1 t02.2. 4, the transient bubble behavior, i.e., the size, shape and volume of bubbles, bubble velocity, bubble coalescence, disappearance, and/or reappearance phenomena could be measured simultaneously. All the data taking was accomplished by computers. Bubble images were analyzed by the system of 'Globe Lab Image' .

2.2.6 Data organization system

The comprehensive data taking systems are summarized in Table 2.2.1. All of the data are synchronizingly taken by using TTL signals at the measurement interval of 1/30 second for the periods of several seconds. Namely all the data could be obtained as the function of time.

Through the analysis and processing the originally obtained data, the following data were derived, as shown in Table 2.2.2

2.2.7 Circulating fluidized beds

The two dimensional transparent circulating fluidized bed (1000mm (height) X 92mm (width) X 10mm (thickness)) was installed, using spherical glass beads of 0.5 mm in diameter as the fluidized particles.

2.2.8 High pressure fluidized beds

The effect of elevated pressure on the behavior of transient bubbles was investigated using a two dimensional fluidized bed under high pressure (1 to 4 atm). Although the visual observation is not easy, the $\Delta\Delta P_{max}$ measurement is easy. As we have a plenty of data accumulation between the transient bubble image and $\Delta\Delta P_{max}$ in

Table 2.2.1 The measured data and their physical meanings

Measured data .	Physical meaning etc.
(1) transient bubble images in the 2-D fluidized bed as function of time	Overall view of transient bubble images are provided in the picture form
(2) bubble areas (volume) and perimeters as the function of time	Bubble size and volume can be calculated. Bubble coalescence and splitting can be observed. Bubble shape factor can be obtained.
(3) bubble centroids of X and Y (X: horizontal, Y: vertical) as the function of time	bubble positions in the bed can be provided, from which bubble velocity can be obtained too.
(4) gray average as the function of time	This value should be related to the density of the emulsion phase. But this was not used for this work due to the lack of reproducibility.
(5) gas pressure fluctuation at the half of the bed height as the function of time	Measuring the gas pressure at $Z=H_{mf}/2$ at five different points located horizontally. The gas pressure differences among these points show the gas phase stresses in the emulsion phase.

Table 2.2.2 Experimental data derived from the images of transient bubbles and other transient phenomena

a. Pressure fluctuation of gas phase at the five horizontally located positions, and transiently occurring gas phase stresses in the emulsion phase
b. Analyzed transient bubble's properties, e.g., cross sectional area (i.e., corresponding volume) , roundness (i.e., shape factor ϕ_c), bubble motion in horizontal and vertical direction.
c. Bubble size (cross sectional area) versus vertical distance from the gas distributor
d. Difference between normal and abnormal fluidization, which occurred quite stochastically from one type of fluidization to another or vice versa under the same certain given condition.

two dimensional fluidized bed, we decide to measure $\Delta\Delta P_{max}$ by using two dimensional fluidized bed under high pressure (1 to 4 atm). The behavior of transient bubble can be predicted through the gas phase pressure fluctuation.

2.2.9 Comparison of two and three dimensional fluidized beds

The comparison of two and three dimensional fluidized beds were accomplished. As the two dimensional fluidized bed, we used the same one shown in Figure 2.2.1. For the three dimensional fluidized beds, the 4" cylindrical fluidized bed were used. To make the quantitative comparison, the $(\Delta\Delta P)''$ (the transient gas stress gradient existing between two points located horizontally) was used.

3. EXPERIMENTAL RESULTS AND DISCUSSIONS

In this section, results were presented and discussed with respect to the following works:

(A) Behavior of transient bubbles in two dimensional fluidized beds.
(B) Behavior of transient bubbles in two dimensional circulating fluidized beds.
(C) Behavior of transient bubbles in two dimensional fluidized beds at elevated pressure (P=1 to 4 atm).
(D) Comparison of transient bubble-behavior in two and three dimensional fluidized beds.

3.A. Behavior of Transient Bubble in Two Dimensional Fluidized Beds

The detail experimental data of transient bubble behavior were obtained in two dimensional fluidized beds by changing gas velocity; i.e., under experiment condition I (U_0/U_{mf}=2.0), under experiment condition II (U_0/U_{mf}=2.3), and under experiment condition III (U_0/U_{mf}=1.8). Detail experimental conditions were described in Section 2.2. Furthermore, under the respective experimental conditions, we found two different fluidization modes, normal and abnormal fluidization, which could coexist stochastically in parallel.

Using the examples of experimental condition of I, a basic concept of normal and abnormal fluidization was discussed here. To evaluate the transient bubble performance, the gas phase pressure fluctuation was measured by using pressure taps P_1, P_2, P_3, P_4 and P_5, which located horizontally as shown in Figure 2.3.2. The gas phase pressure at P_1, P_2, P_3, P_4 and P_5 were fluctuating as shown in Figures 3-AI1-1 to 3-AI1-4.

From these figures, it is clear that the gas phase pressure fluctuation patterns seem to be not periodical but significantly stochastic. As already shown in Figure 2.3.2, the gas pressure measurement points were located at the same height horizontally. Therefore, if it were in acordance with the classical Davidson's prediction, the pressure differences such as P_4-P_1 would be zero in fluidized beds. However, as shown in Figures 3-AI1-5 and 3-AI1-6, the experimental results indicated that there were *very* significant gas pressure stress transiently existing between P_1 and P_4. These experimental facts indicated that there were a considerable interaction among the transient bubbles and also among the location of the emulsion phase.

By reviewing Figures 3-AI1-1 to 3-AI1-4, we found two different types of the gas phase pressure fluctuation patterns, i.e., within the time intervals of from t=2.0 seconds to t=3.0 seconds, of from t=12.7 seconds to t=14.7 seconds, and of from 17.7

seconds to t=18.2 seconds, the gas phase pressure fluctuation patterns were obviously different from the rest of time, which were named as "abnormal" periods. And the rest of the periods were called as normal periods. It is very important to recognize that there could be two different type of fluidization patterns coexisting under the same definite fluidization condition. The effect of the difference of "normal" and "abnormal" fluidization on the behavior of transient bubbles will be discussed later.

3.A.I Normal fluidization

3.A.I.1N Transient bubble images

The transient bubble images under the experimental condition I during the time interval of 1.46 seconds to 1.96 seconds (normal fluidization period) were shown in the pictures of from Pictures 3-AI-N1 to Pictures 3-AI-N4, where respective pictures were taken at the time interval of 1/30 second. There we could observe several new phenomena, which no classical fluidization theory could predict. Namely, the transient bubble behavior could be qualitatively summarized as follows:

(a) Bubble can change its size in a very short period of time (in 1/30 second), thus there is a plenty of evidence that the bubble can exchange gas with the adjacent emulsion phase.

(b) Beyond the known coalescence and splitting, the bubble disappearance into the emulsion phase and the bubble reappearance from the emulsion phase can take place stochastically under the certain fluidized bed condition.

(c) The shape of bubble can change also in a very short period of time in the order of 30 milliseconds.

(d) The motion of transient bubbles are transient and the bubble motion velocity is transient and stochastic.

All of the description on the transient bubbling phenomena indicated significant difference from the classical reported bubble characteristics in the past literature. The transient bubble properties were summarized in Table 3-AI-1 in terms of bubble size (cross sectional area), bubble positions in the beds, roundness, and perimeters. Although gray-average was obtained and can potentially be correlated to the density of the emulsion phase, the treatment was not included to avoid any oversimplification.

3.A.I.2N The bubble size (cross sectional area) versus time

The growth of bubbles in terms of the bubble's residence time (0 to 2 seconds) is shown in Figures 3-AI2-N1 and 3-AI2-N2. From these Figures, the bubble size growth was not at all straight forward nor constant in the freely bubbling fluidized beds.

Therefore, the well know Davidson's bubble rising speed equation (U_B=const X $(gD)^{0.5}$) can only be applicable to the bubbles injected into the incipient fluidized beds but not to the freely bubbling fluidized beds.

3.A.I.3N The bubble roundness versus time

The shape of bubbles was traditionally considered to be the so-called bubble-cap shape. The experimental results of roundness of bubbles of bubbling images described were analyzed and shown in Figure 3-AI3-N1 and 3-AI3-N2, indicating that the roundness of bubbles were fluctuating in the range of from 0.1 to 0.8 in terms of Carman's shape factors. These new experimental facts indicated potentially the intensive exchange of gas between bubble and emulsion phases, which would effect the mass transfer mechanism of bubbles in reactors.

3.A.I.4N Vertical distance of transient bubbles from the gas distributor versus time

The vertical distance of transient bubbles from the gas distributor is shown in Figures 3-AI4-N1 and 3-AI4-N2 as the function of time in the time range of 0 to 2 seconds. From these figures, the bubble splitting and coalescence schemes, and bubble disappearance and reappearance schemes could well be visualized. The bubble rising velocity's changes could also be obtained from the slope of bubble moving lines.

3.A.I.5N&6N Transient bubble's moving velocity

The effective velocities of transient bubbles in freely bubbling fluidized beds are shown in Figures 3-AI5-N1 and 3-AI5-N2 in the time range of 0 to 2 seconds. It is extremely interesting the bubble velocity reached sometimes as fast as 2.0 to 3.0 m/s before coalescence, while the mean velocity was approximately 0.4 to 0.5 m/s. The bubble velocity in horizontal direction is also shown in Figures 3-AI6-N1 and 3-AI6-N2 in the time range of 0 to 2.0 seconds. It is surprising that the horizontal velocity could reach as fast as 3.0 m/s, which was not known in the past literature.

3.A.I.7N Bubble size (cross sectional area) versus the vertical distance from the gas distributor

The data of bubble cross sectional area vs. vertical distance from the gas distributor are shown in Figures 3-AI7-N1 and 3-AI7-N2. The figures indicated that there were intensive bubble interaction in the lower half portion of fluidized beds. Only at the high portion of the fluidized beds, the bubble interaction becomes negligible in case of coarse particles's fluidization. Therefore, if the bubbling phenomena may be observed on the top of

fluidized beds, the understanding of bubbling phenomena will be very much misled, which happened frequently in the past classical research (Davidson, 1962) .

3.A.I Abnormal fluidization period

3.A.I.1.AN The images of transient bubble behavior

The transient bubble images under the experimental condition I during the abnormal fluidization period (t=1.99 to 2.5 seconds) were shown in Pictures 3-AI-AN1 to 3-AI-AN4. Using these original data, the analysis was carried out and the results were summarized in Table 3-AI-2. The basic data of transient bubble's in terms of bubble cross sectional area and perimeter, bubble position, roundness etc. were calculated by computer processing of transient bubble images.

3.A.I.2-7.AN Characteristic properties of transient bubbles

The cross sectional area of transient bubble at the time range of t=1.00 to 2.oO seconds are shown in Figures 3-AI2-AN1 and 3-AI2-AN2. The roundness (Carman's shape factor ϕ_c of transient bubbles is shown in Figure 3-AI3-AN1. The vertical distance of transient bubbles from th-e gas distributor was shown as the function of time in Figure 3-AI4-AN1. The effective velocity and horizontal velocity of transient bubbles are shown respectively in Figure 3-AI5-AN1 and 3-AI6-AN1. The bubble size (cross sectional area) versus vertical distance from the gas distributor is illustrated in Figure 3-AI7-AN1 .

3.A.I Comparison of "abnormal" and "normal" fluidization

To compare the "abnormal" and "normal" fluidization modes, the statistical analysis were made under the experimental condition of U_0/U_{mf}=2.0. With respect to the relation between the bubble size (the cross sectional area) and the vertical distance position from the gas distributor, the difference could be found as shown in Figure 3-AI8-N and Figure 3-AI8-AN. It indicated that the bubble interaction prevails generally more intensive at the bottom portion of fluidized bed during the normal fluidization period and the interaction prevails more widely all over the entire bed during the abnormal fluidization period. The figure's results show the same tendency as the figures of Halow et al.' (1992) for bubble rising velocity.

The disappearance of transient bubbles in the axial direction of the bed was more widely distributed in case of abnormal fluidization period than that of "normal" period as shown in. Figures 3-AI9-N&AN. The regular disappearance of transient bubbles was prevailing more in case of "abnormal" fluidization period as shown in Figures 3-AI10-N&AN. The splitting of transient bubbles

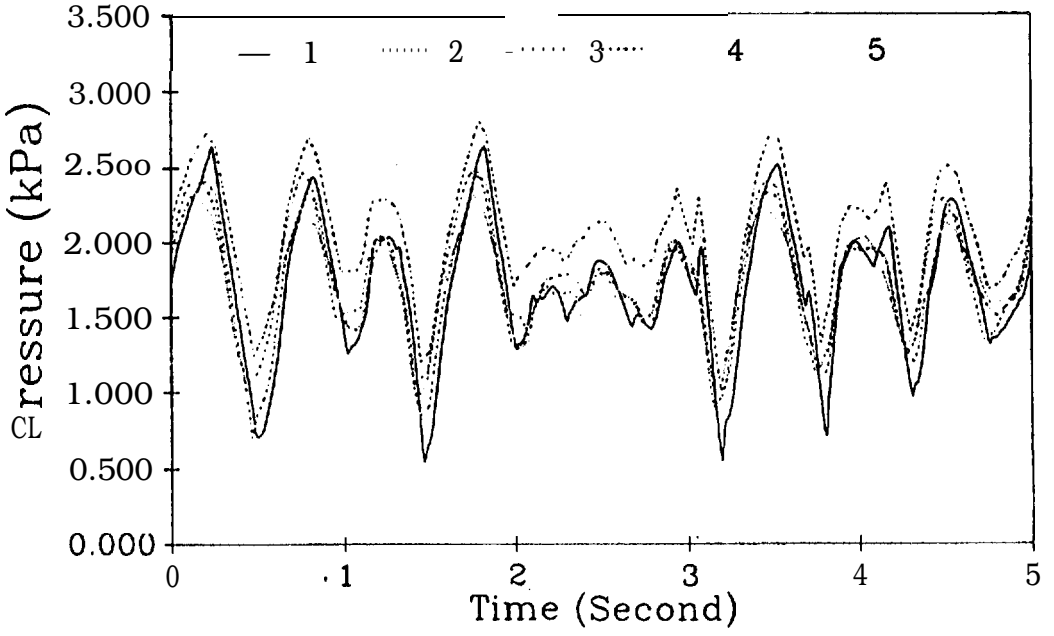

Figure 3-AI1-1 Gas phase pressure fluctuation vs time at the points of P_1 to P_5 located horizontally in freely bubbling **fluidized** bed

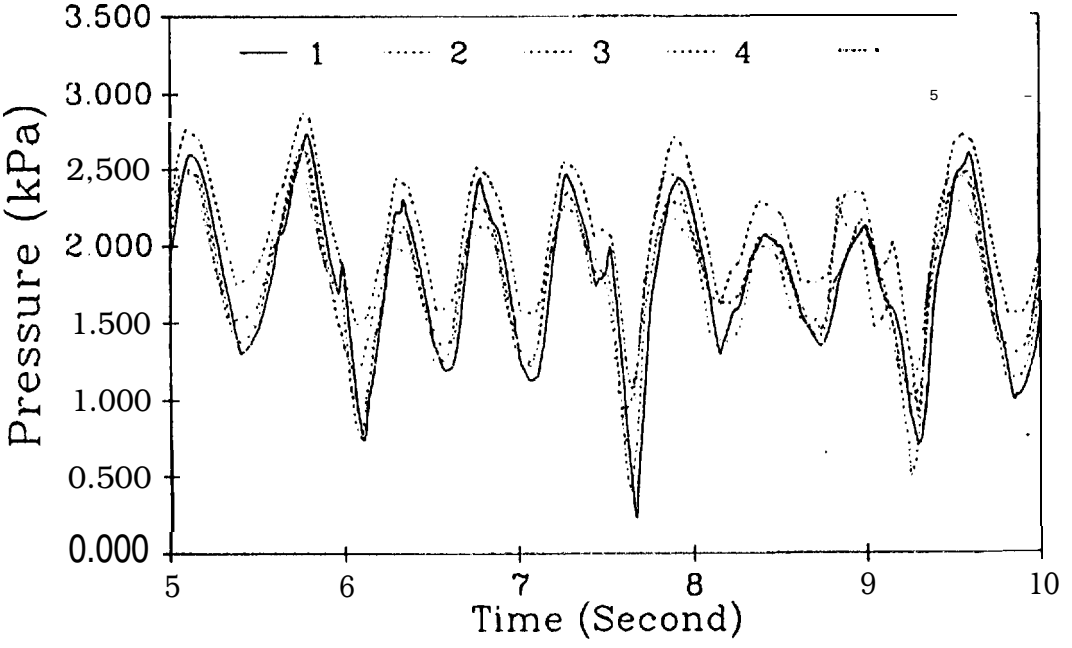

Figure 3-AI1-2 Gas phase pressure fluctuation vs time at the points of P_1 to P_5 located horizontally in freely bubbling **fluidized** bed

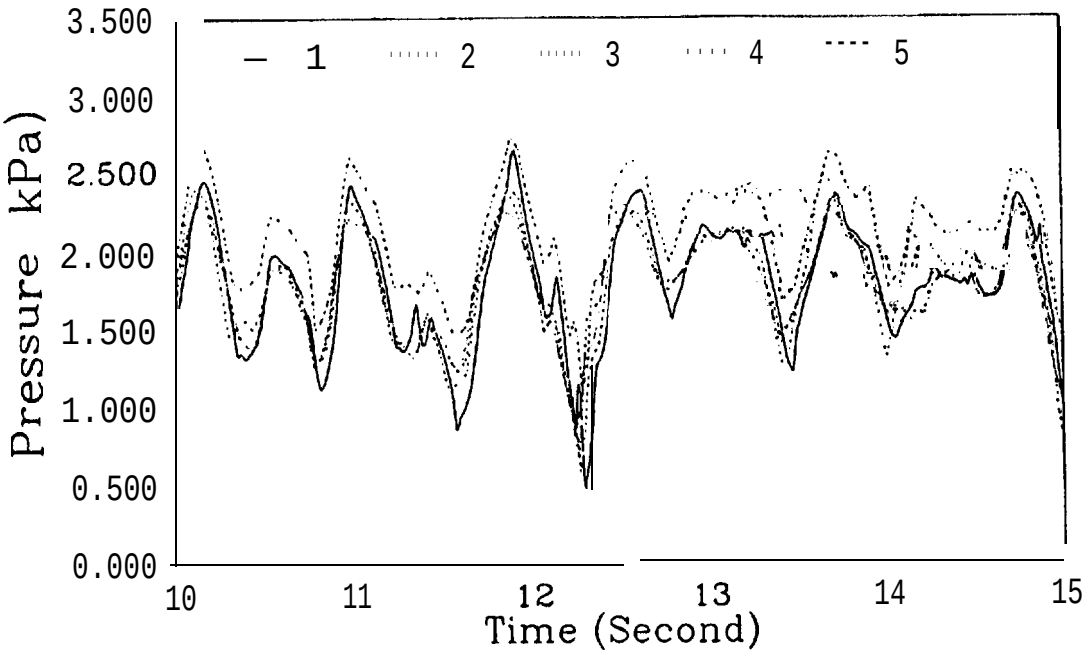

Figure 3-AI1-3 Gas phase pressure fluctuation vs time at the points of P_1 to P_5 located horizontally in freely bubbling fluidized bed

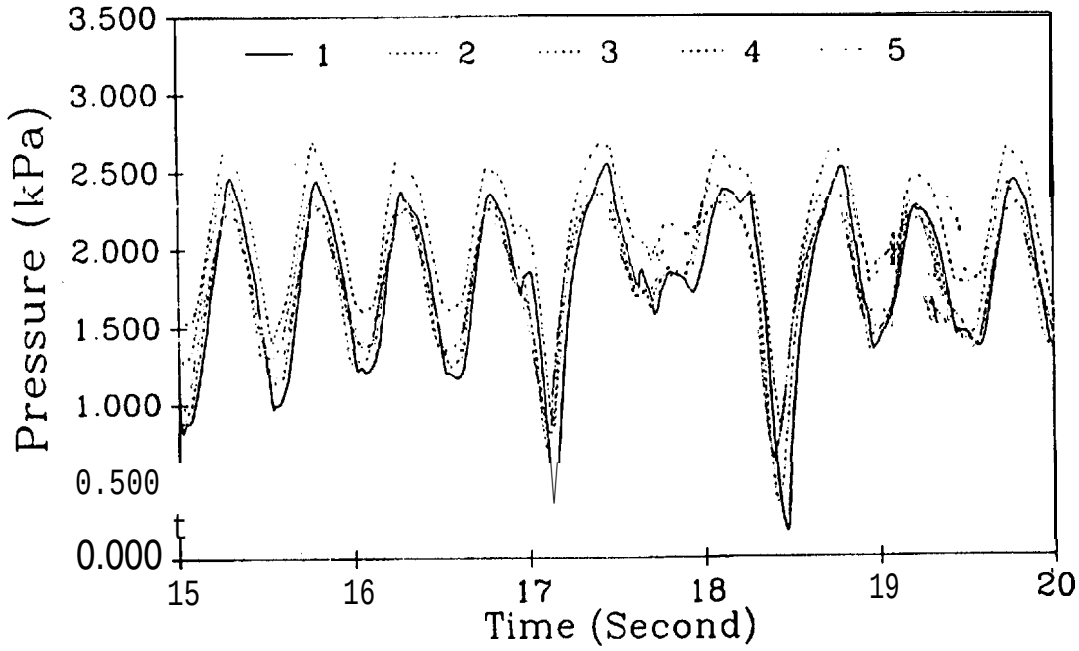

Figure 3-AI1-4 Gas phase pressure fluctuation vs time at the points of P_1 to P_5 located horizontally in freely bubbling fluidized bed

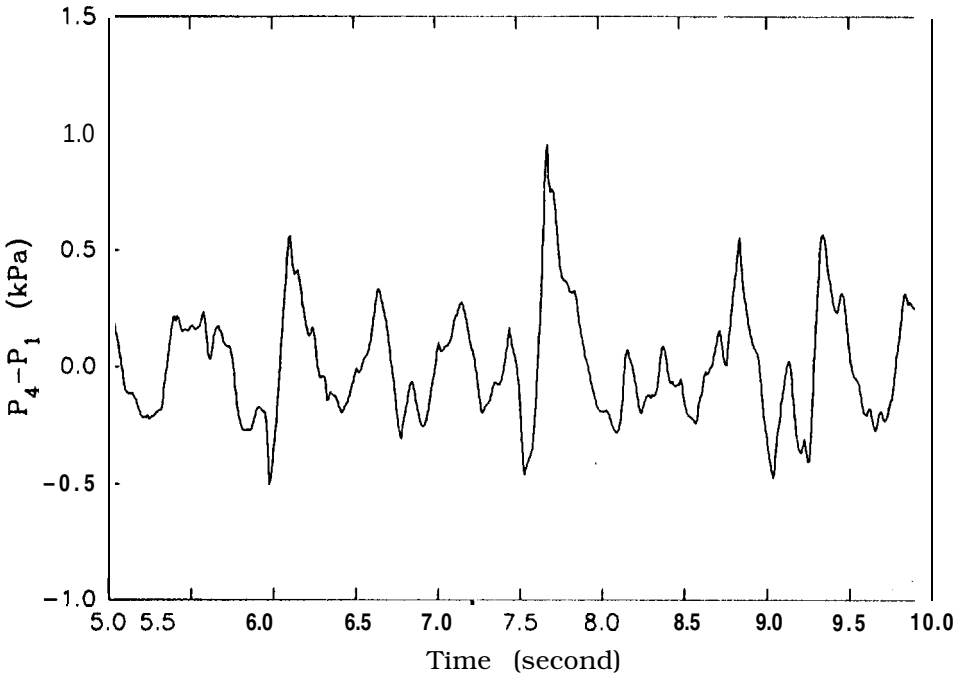

Figure 3-AI1-5 Pressure difference between P_4 and P_1 vs time

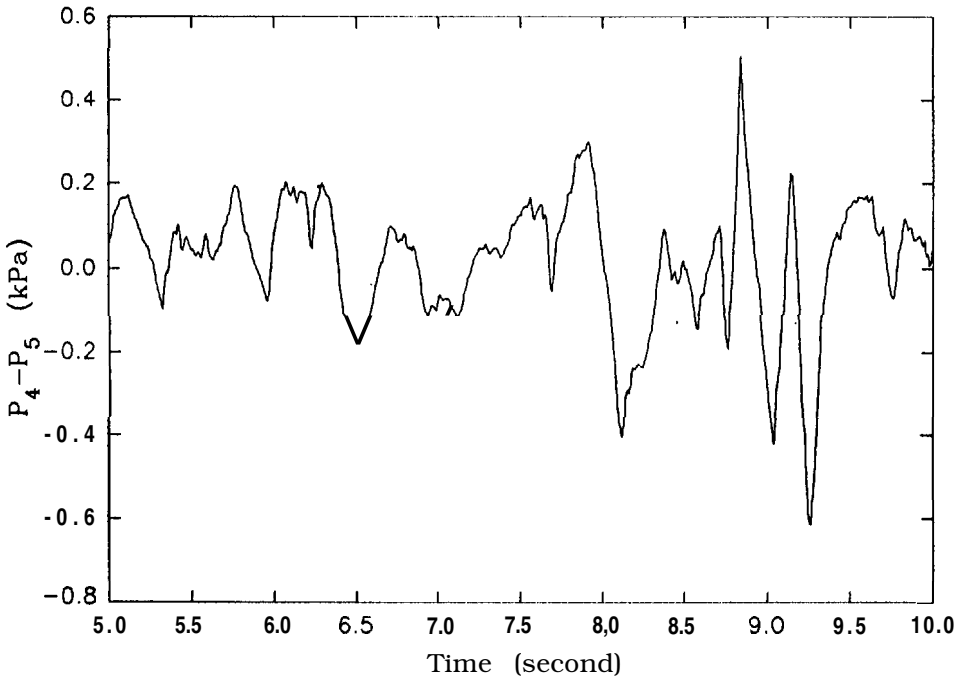

Figure 3-AI1-6 Pressure difference between P_4 and P_5 vs time

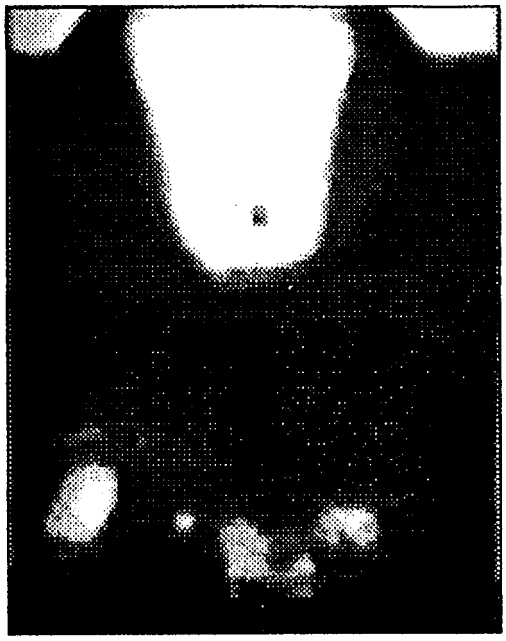

Time = 001.46

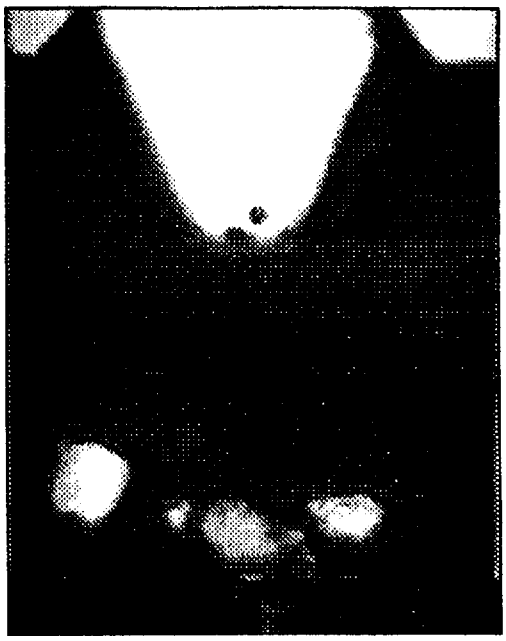

Time = 001.49

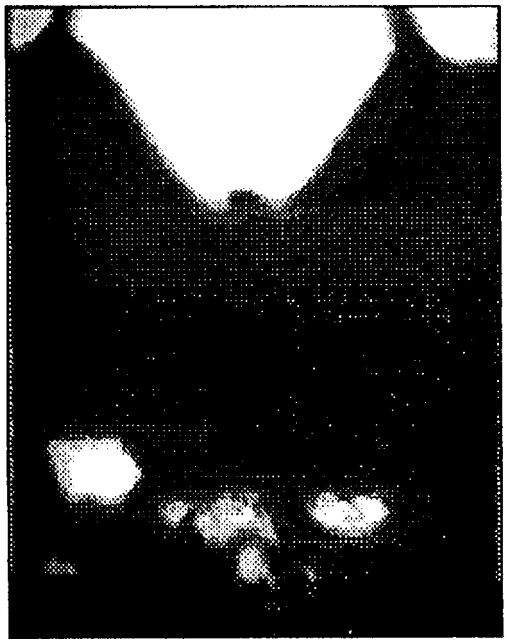

Time = 001.53

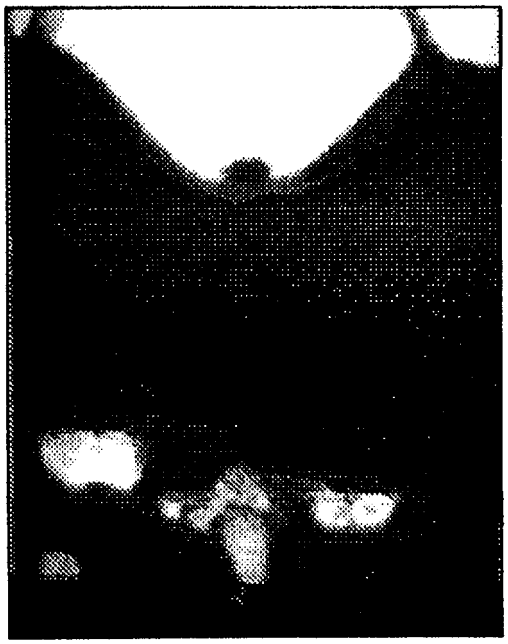

Time = 001.56

Picture 3-AI-N1 Transient bubble images under the experimental condition I (normal period)

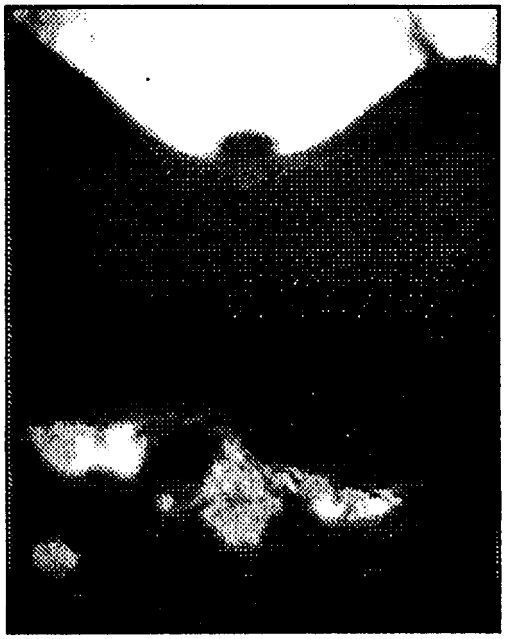

Time = 001.59

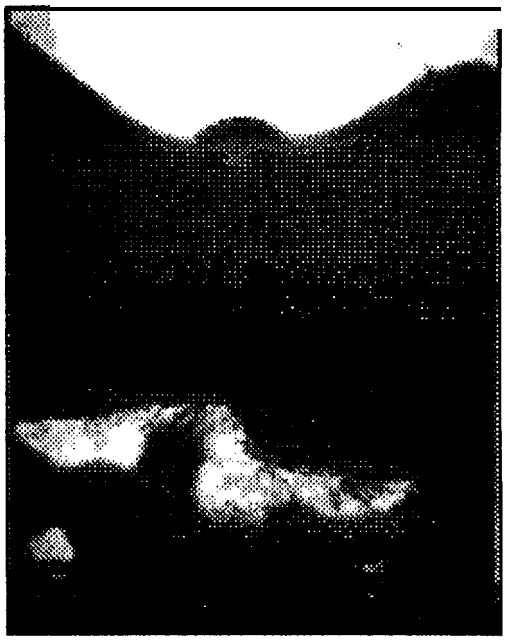

Time = 001.63

Time = 001.66

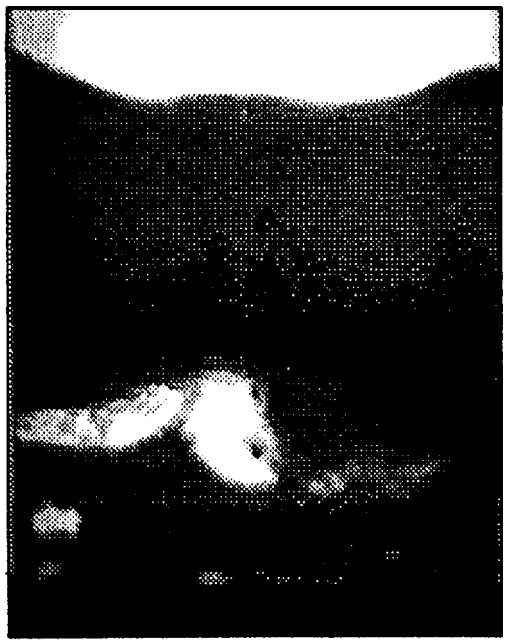

Time = 001.69

Picture 3-AI-N2 Transient bubble images under the experimental condition I (normal period)

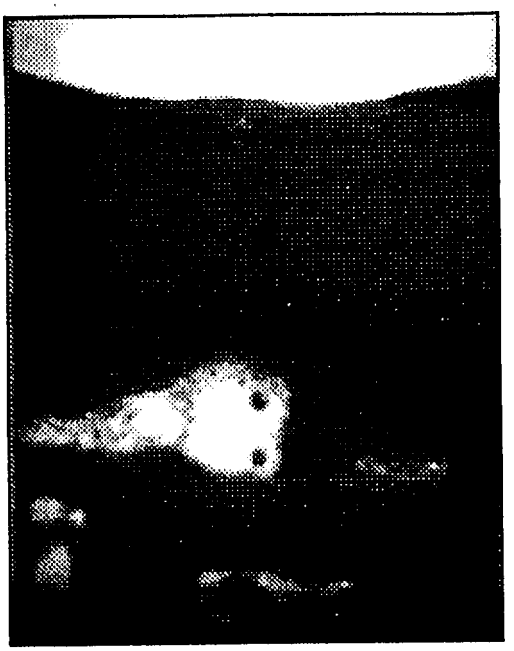

Time = 001.73

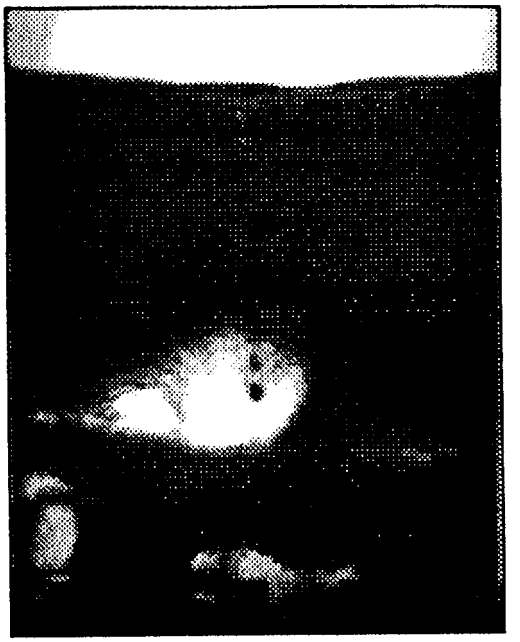

Time = 001.76

Time = 001.79

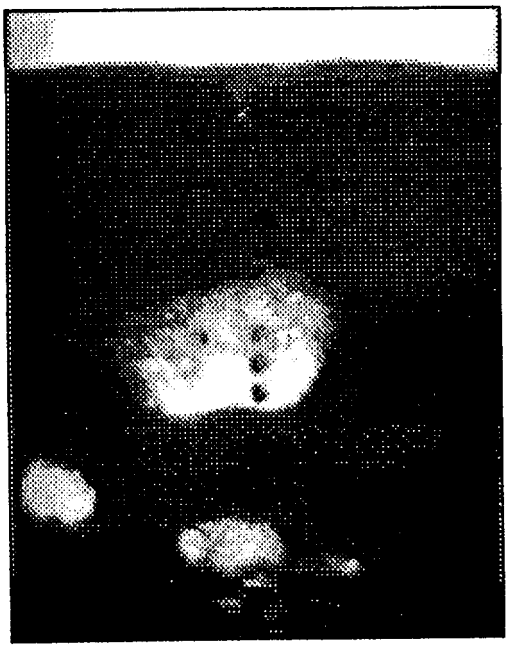

Time = 001.83

Picture 3-AI-N3 Transient bubble images under the experimental condition I (normal period)

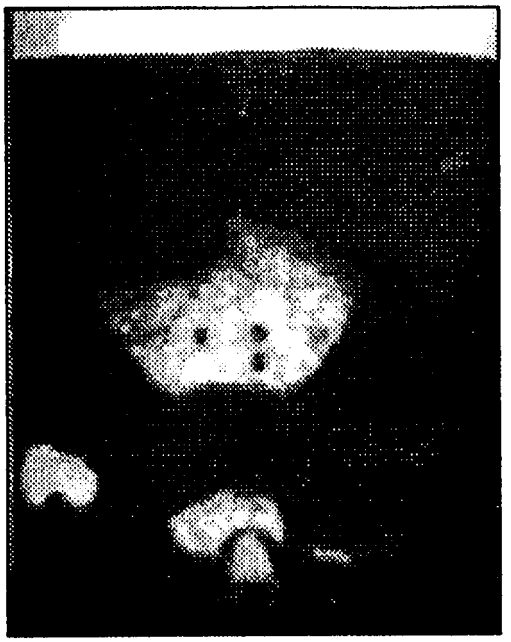

Time = 001.86

Time = 001.89

Time = 001,93

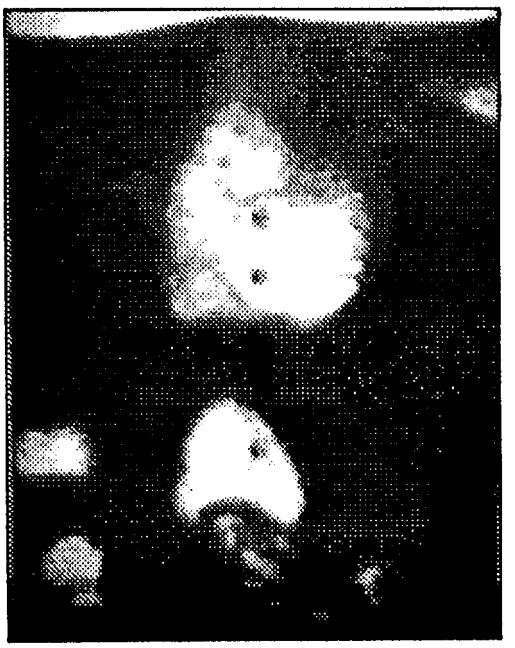

Time = 001.96

Picture 3-AI-N4 Transient bubble images under the experimental condition I (normal period)

Table 3-AI-1 Analysis results of bubbles of normal period (t=1.46 to 1.96 second)

Time (Sec.)	Bubble Num.	Area (sq.mm)	CentroidX (mm)	CentroidY (mm)	Perimeter (mm)	Roundness (o-1)	GrayAvg. {0-256)
1.46	0	75 7.%8480	128".19740	31.64916	262.08080	.13863	118.97480
1.46	1	73.54625	91.04838	48.58946	50.92088	.35650	142.31110
1.46	2	518.27660	176.76480	47.26087	180.04070	.20095	152.04650
1.46	3	1125.26900	38.53781	58.13962	280.46480	.17980	178.16510
1.49	0	904.89010	119.22270	45.70610	166.78980	.40883	136.98430
1.49	1	114.92020	85.77701	54.86755	47.28096	.64611	136.35070
1.49	2	703.07520	173.86590	54.88888	119.13360	.62260	175.73850
1.49	3	1303.16500	39.25438	72.51084	149.22260	.73556	195.03920
1.53	0	181.33250	123.52370	26.15600	86.94102	.30152	124.01810
1*53	1	766.42180	173.97210	54.48424	242.34200	.16402	178.24130
1.53	2	927.43370	108.89820	52.09116	294.44640	.13445	138.83130
1.53	3	1376.43800	41.06693	77.52248	295.70800	.19784	195.14270
1.56	0	151.61520	23.80035	27.87499	52.09882	.70207	83.73476
1 . 5 6	1	885.19480	175.13580	59.17074	151.97100	.48172	173.64520
1.56	2	1602.07400	113.90960	52.92244	277.36100	.26174	125.90190
1.56	3	1476.39500	41.25291	85.24398	183.25770	.55254	187.47790
1.59	0	256.98020	21.60868	31.10891	68.14832	.69548,	101.34040
1.59	1	62.05603	79.74240	61.16703	32.28639	.74822	101.08770
1.59	2	2843.75200	138.04220	64.74783	372.02440	.25824	143.01400
1*59	3	1568.85700	40.76988	90.82612	182.62340	.59123	182.68140
1.63	0	280.26340	20.33475	37.05495	76.49039	.60207	109.03880
1.63	1	2938.56500	133.49240	75.34269	395.25670	.23640	162.82590
1.63	2	1811.19200	42.37941	96.79077	234.10820	.41535	177.15940
1.66	0	286.73360	22.18057	44.31070	70.97865	.71534	119.20830
1.66	1	151.67500	200.50640	71.77863	61.29846	.50733	107.76900
1.66	2	4714.39300	91.94113	92.90891	515.77810	.22273	178.31300
1.69	0	272.53600	21.77635	51.66669	70.96844	.68012	129.05180
1.69	1	29.50302	157.79670	71.76381	20.88264	.85030	91.62963
1.69	2	67.77301	167.24600	74.99024	35.60286	.67199	90.74194
1.69	3	4485.62900	84.08313	103.32810	432.20680	.30180	189.43090
1.73	0	60.12606	133.23900	23.79485	40.82132	.45349	82.07273
1.73	1	49.65776	102.48140	25.78672	42.26184	.34944	84.85714
1.73	2	250.97540	20.09748	32.08859	70.74332	.63031	.98.08658
1.73	3	265.90290	20.20209	61.73237	83.24939	.48223	112.60410
1.73	4	4799.71200	90.80795	110.71260	408.66210	.36122	191.81240
1.76	0	35.05045	170.37860	23.33739	26.13294	.64505	84.25000
1.76	1	291.21020	126.81260	26.72952	89.21809	.45982	118.19510
1.76	2	67.63754	97.89463	30.66306	38.40845	.57626	102.90320
1.76	3	575.60150	20.31178	43.44190	107.66450	.62412	124.61320
1.76	4	156.71580	13.54564	72.04762	62.92591	.49744	117.89620
1.76	5	42.78714	15.51339	108.62050	31.19426	.55265	96.48101
1.76	6	4723.99900	100.16190	118.62030	381.09620	.41130	194.62960
1.79	0	63.52813	170.93860	24.49941	40.93369	.47652	89.27586
1*79	1	140.15100	96.95670	35.88733	51.21520	.67156	124.21010
1.79	2	639.55910	122.83050	30.93231	113.97240	.61882	138.00340
1.79	3	847.25400	21.69733	58.53999	118.90500	.75319	150.58680
1.79	4	5152.54700	107.79160	129.43140	369.63100	.47398	181.86700
1.83	0	51.48168	172.84950	29.29486	37.15190	.46878	88.17021
1.83	1	1115.48900	112.71680	40.36090	165.60960	.51118	155.43540
1.83	2	1004.35300	21.66484	67.77531	135.24980	.69009	162.62880
1.83	3	5543.64500	115.09100	143.34320	389.94790	.45820	178.32660
1.86	0	71.15919	164.73230	32.64220	50.51989	.35042	95.64616
1*86	1	1753.60500	112.23110	45.89026	250.88530	.35016	154.80940
1.86	2	1008.95600	20.96735	74.38495	145.31820	.60051	161.63010
1.86	3	6434.69800	118.43400	158.14840	428.61380	.44022	176.45500
1.89	0	2367.15200	112.62600	55.90033	225.65880	.58426	172.79030

1.89	1	958.84470	20.66063	79.84460	137.62990	.63623	164.78960
1.89	2	7384.70300	122.80910	175.05720	485.62110	.39356	179.30700
1.93	0	221.84490	31.81687	28.24748	59.23341	.79471	96.58823
1.93	1	939.82700	21.89052	84.54025	146.33640	.55161	165.68610
1.93	2	2768.46900	114.70040	68.46188	250.15980	.55601	196.22850
1.93	3	8321.97900	127.37390	192.59650	482.01440	.45017	185.61170
1.96	0	43.84472	184.95350	24.26450	29.61251	.62841	88.60000
1.96	1	79.75368	126.56750	31.57787	44.13750	.51454	95.31507
1.96	2	510.94710	31.44614	31.90674	94.60342	.71755	117.81910
1.96	3	28.91891	113.26940	43.85532	23.06903	.68298	91.92453
1.96	4	69.81280	111.32340	52.61825	37.49607	.62409	95.87500
1.96	5	882.60860	20.78197	88.93030	130.00720	.65633	166.47910
1.96	6	3152.10700	116.48540	82.56025	257.80930	.59605	209.48240
1.96	7	9302.66100	128.73590	212.02850	466.00020	.53840	197.28700

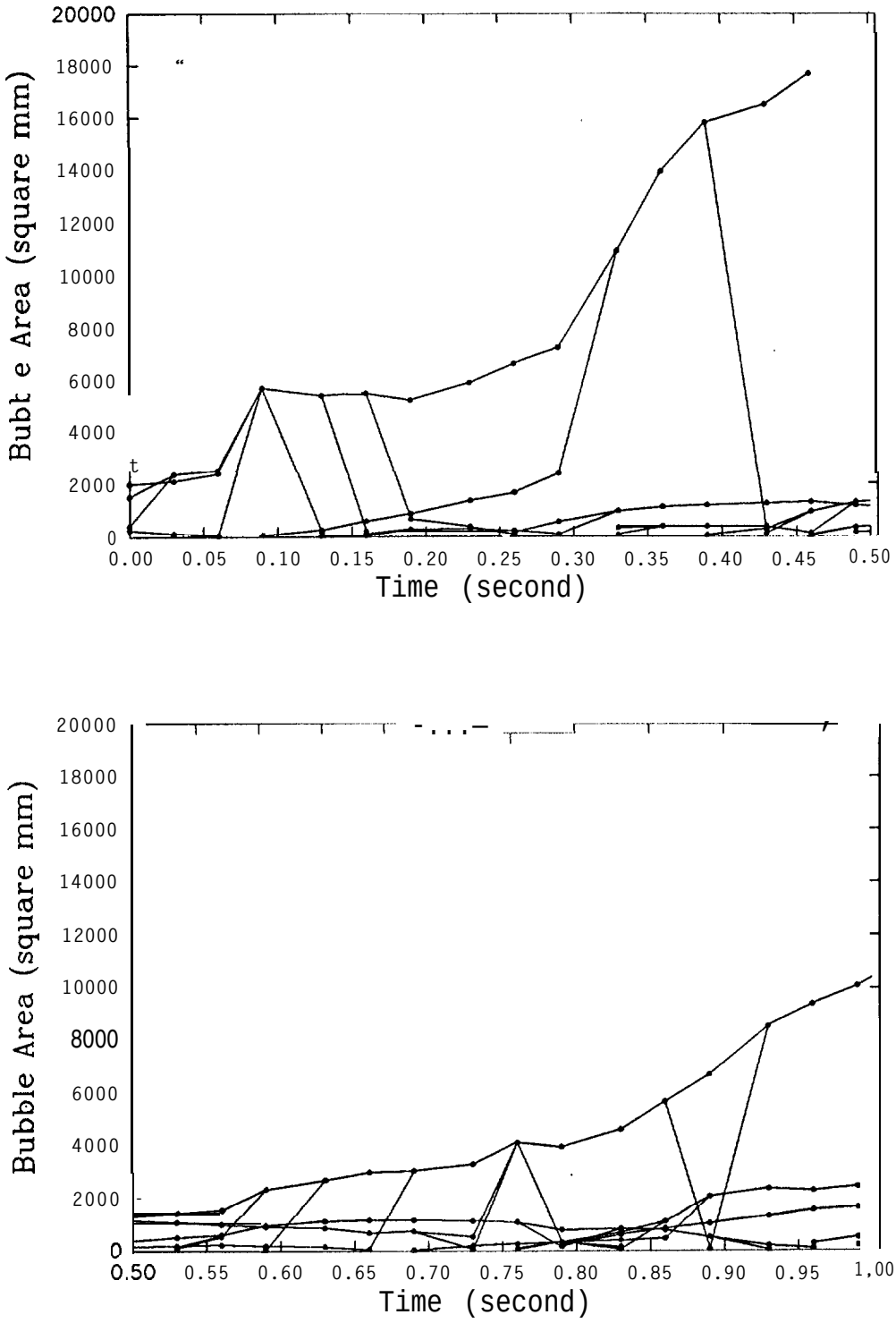

Figure 3-AI2-N1 Volume of transient bubbles vs **time** under experimental **condition** I (normal period)

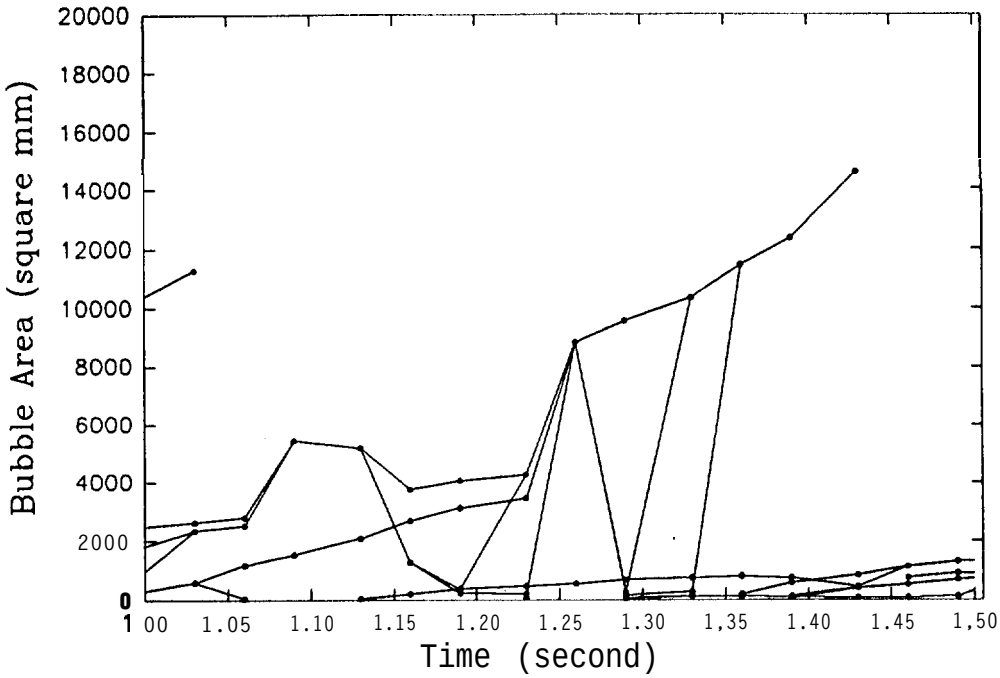

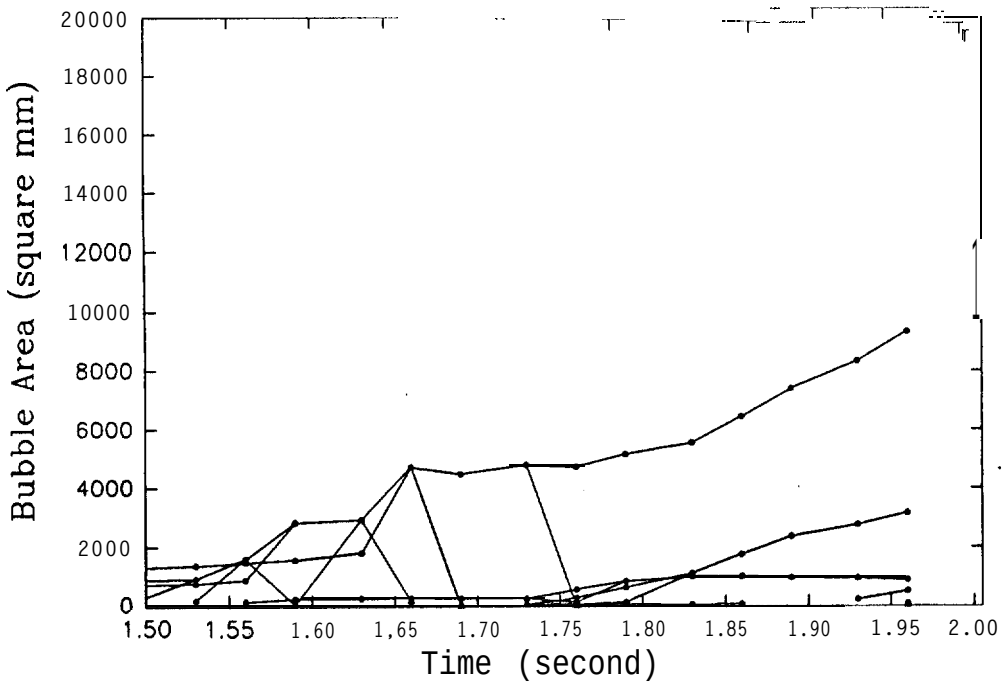

Figure 3-A12-N2 Volume of transient bubbles vs **time** under experimental condition I (normal period)

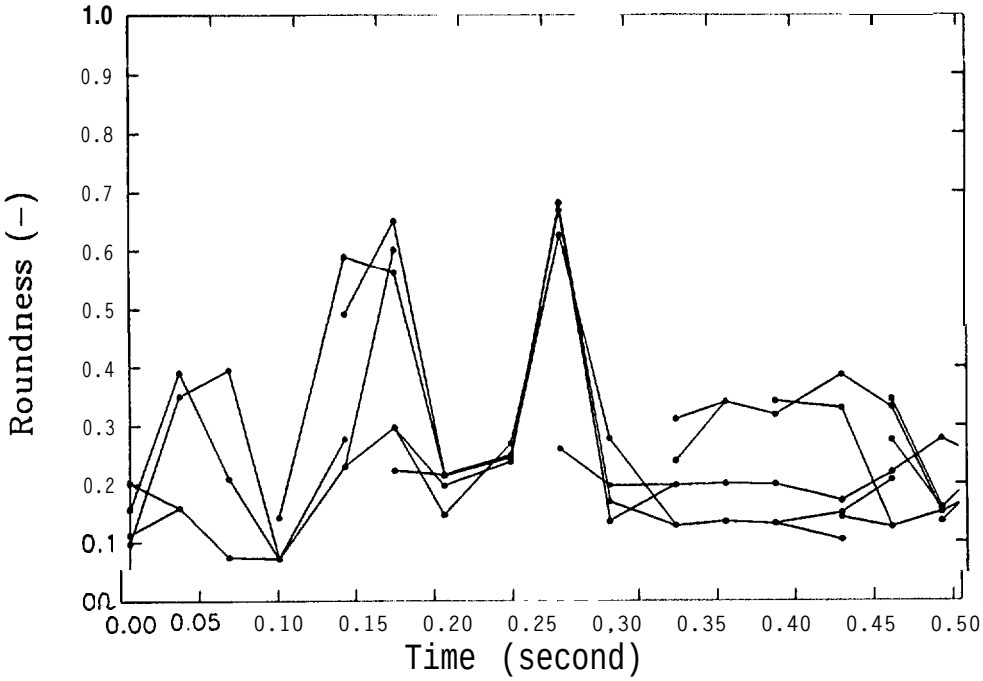

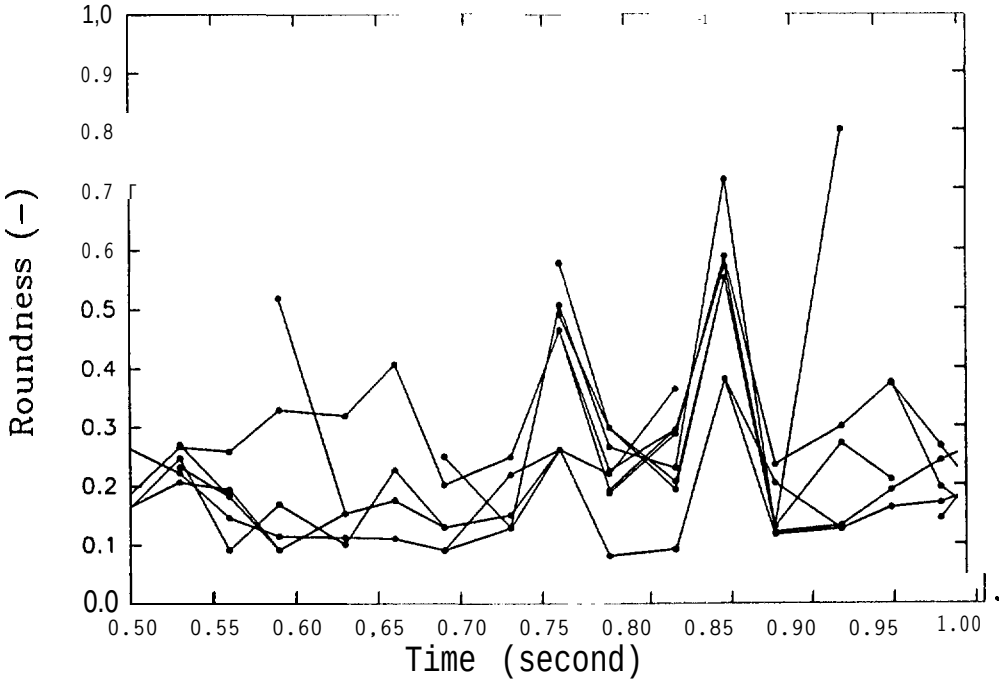

Figure 3-AI3-N1 Roundness of transient bubbles vs time under experimental condition I (normal period)

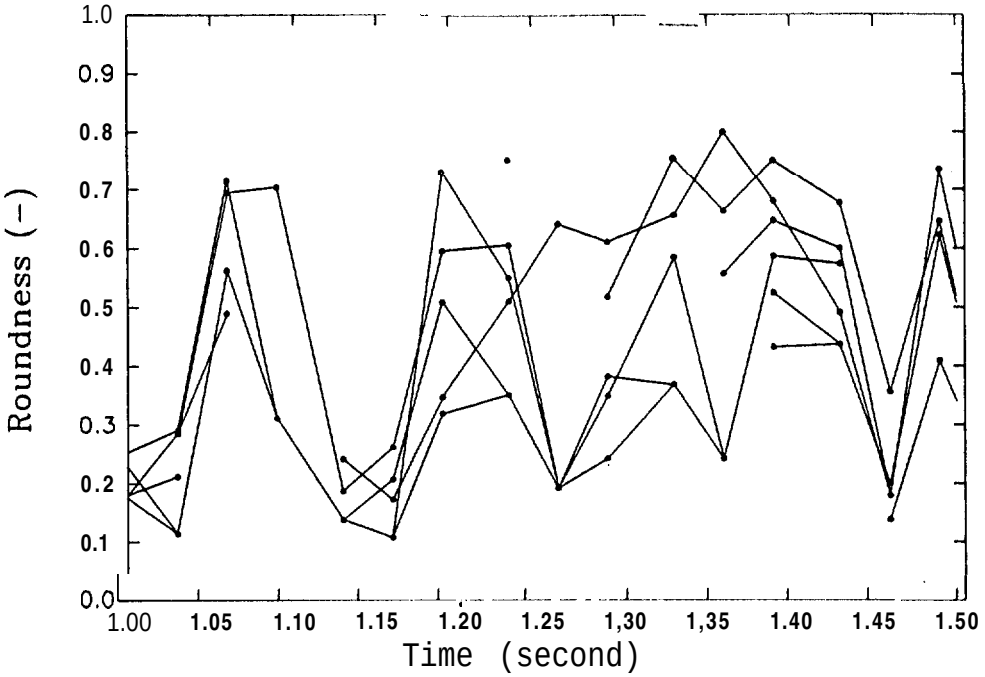

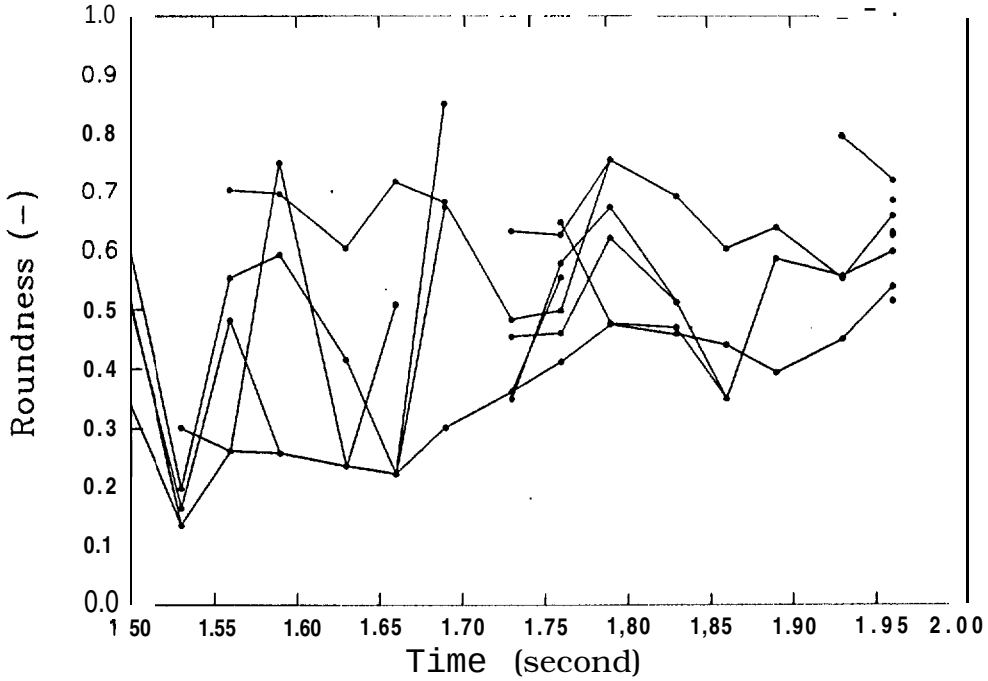

Figure 3-A13-N2 Roundness of transient bubbles vs **time** under experimental condition I (normal period)

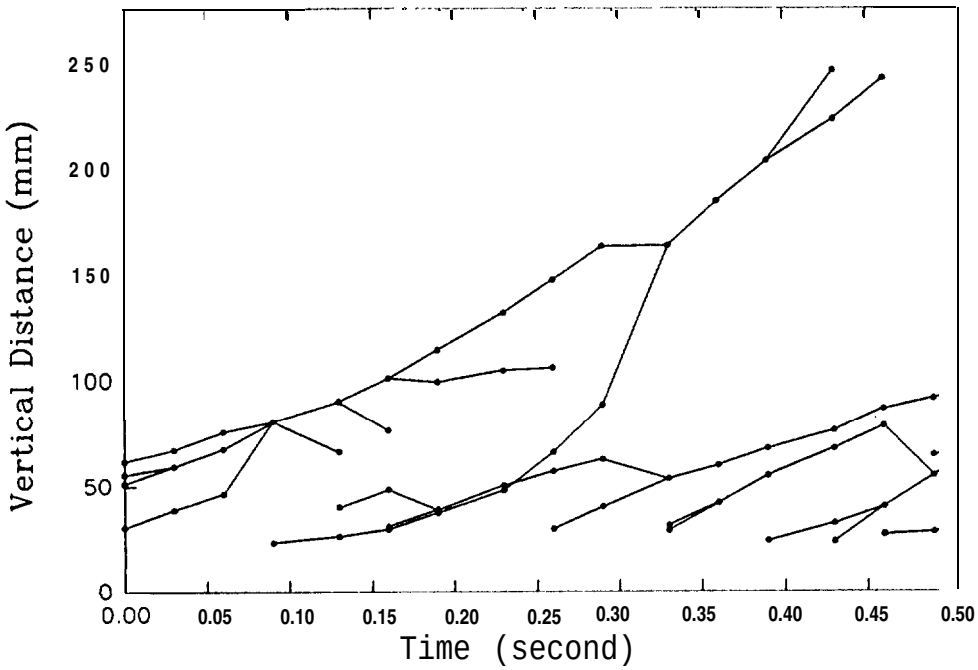

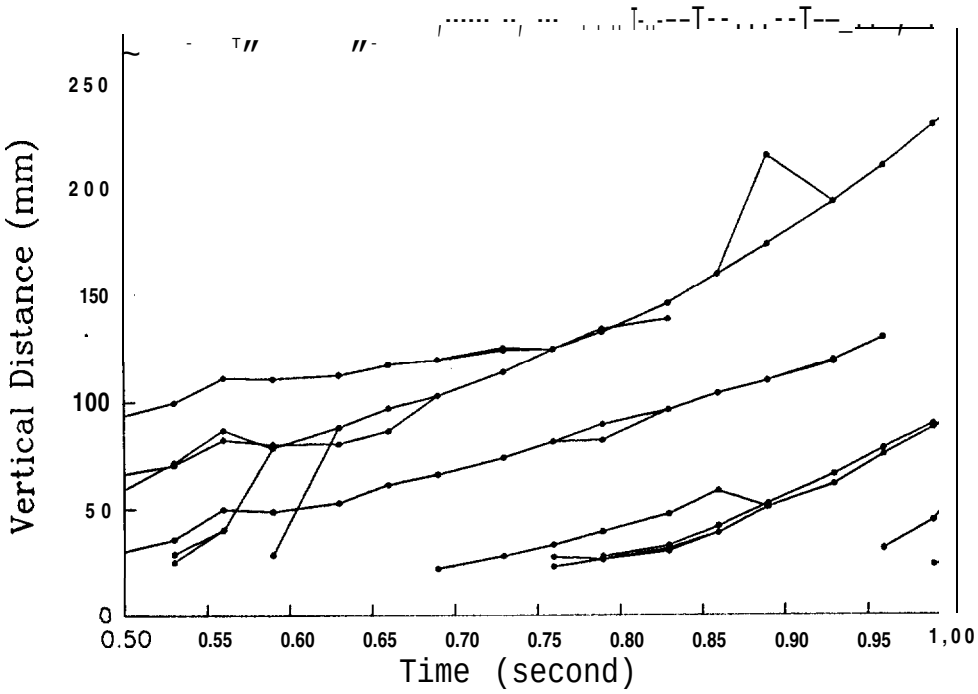

Figure 3-AI4-N1 Vertical distance of transient bubbles vs the under experimental condition I (Normal period)

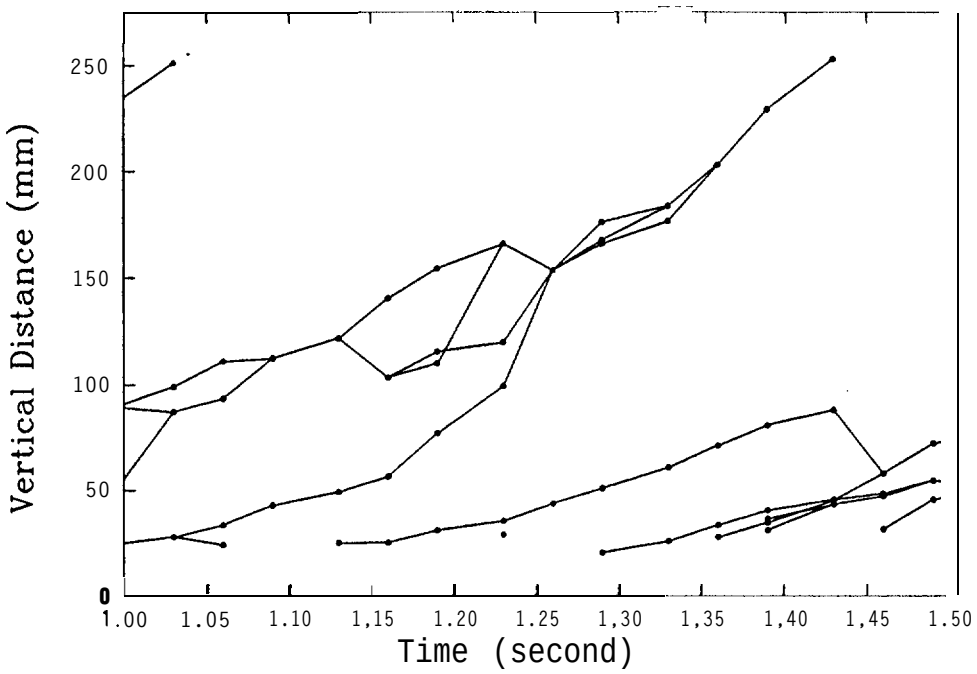

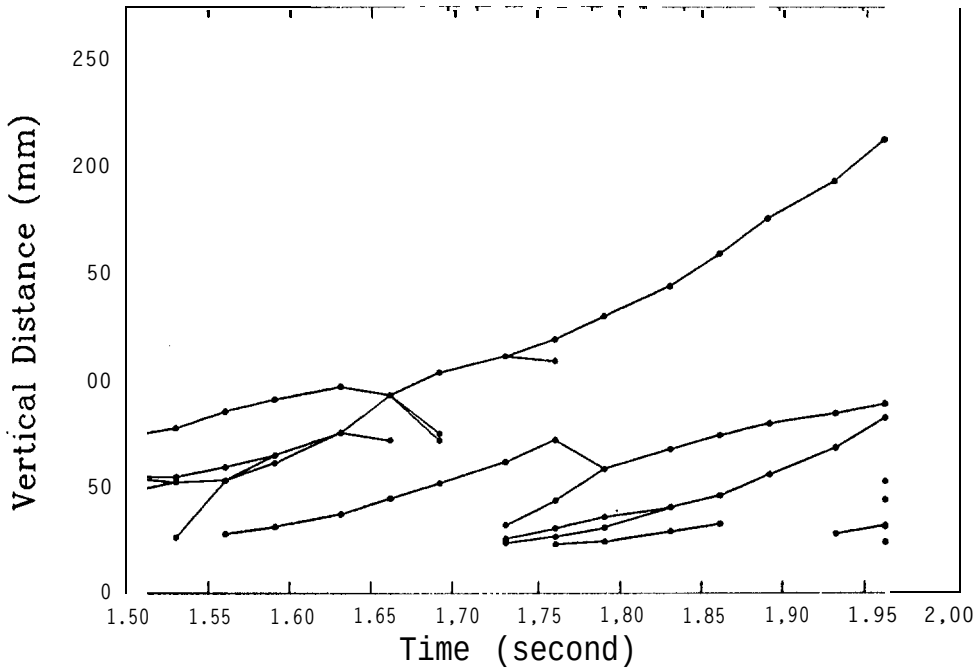

Figure 3-A14-N2 Vertical distance of transient bubbles vs **time** under experimental condition I (normal period)

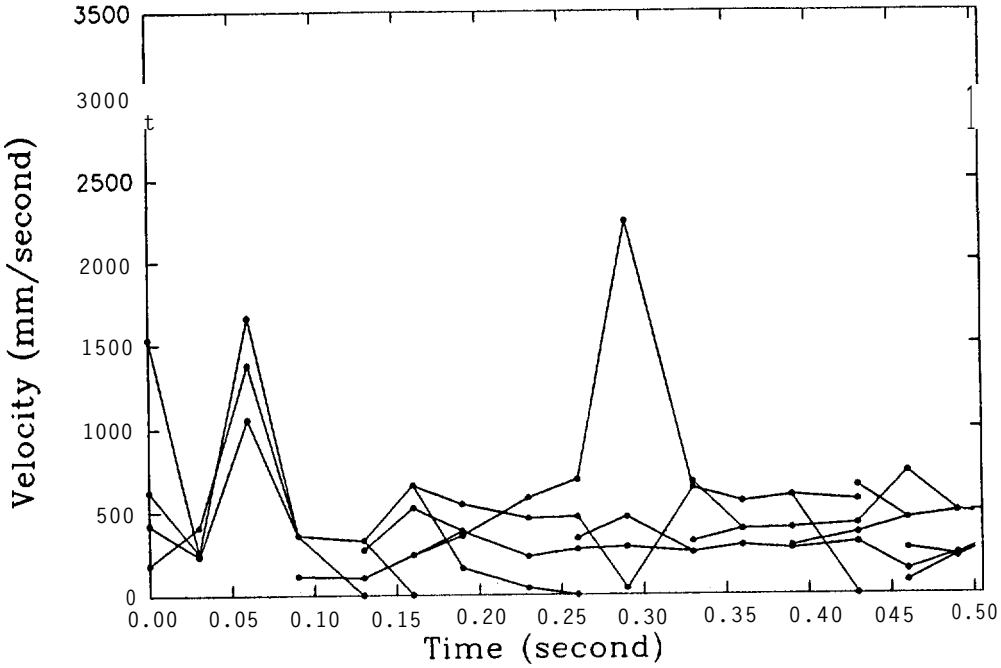

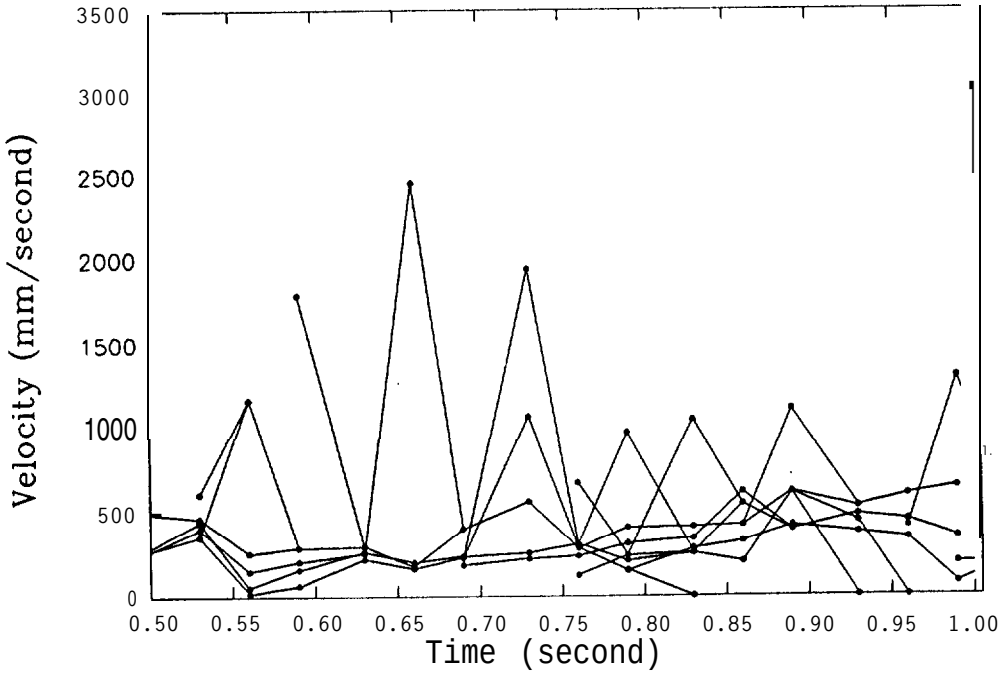

Figure **3-AI5-N1** Velocity of transient bubbles vs time under experimental condition I (normal period)

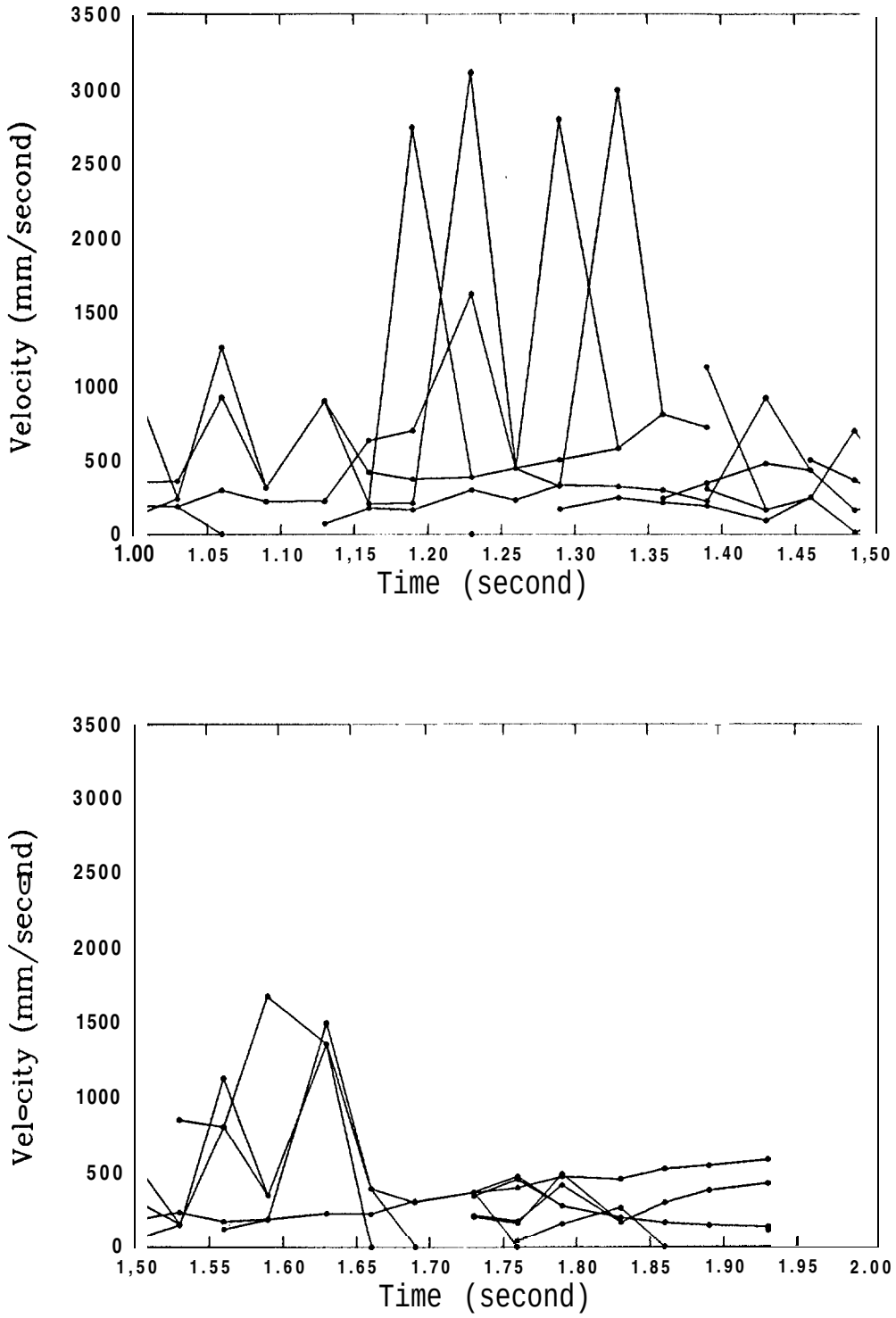

Figure 3-A15-N2 Velocity of transient bubbles vs time under experimental condition I (normal period)

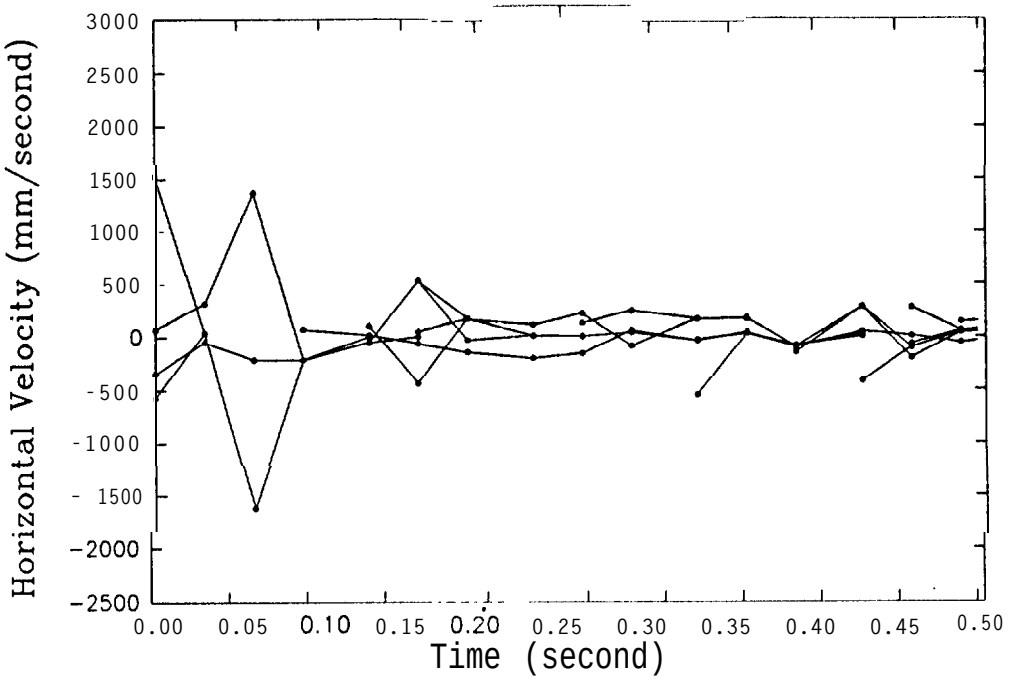

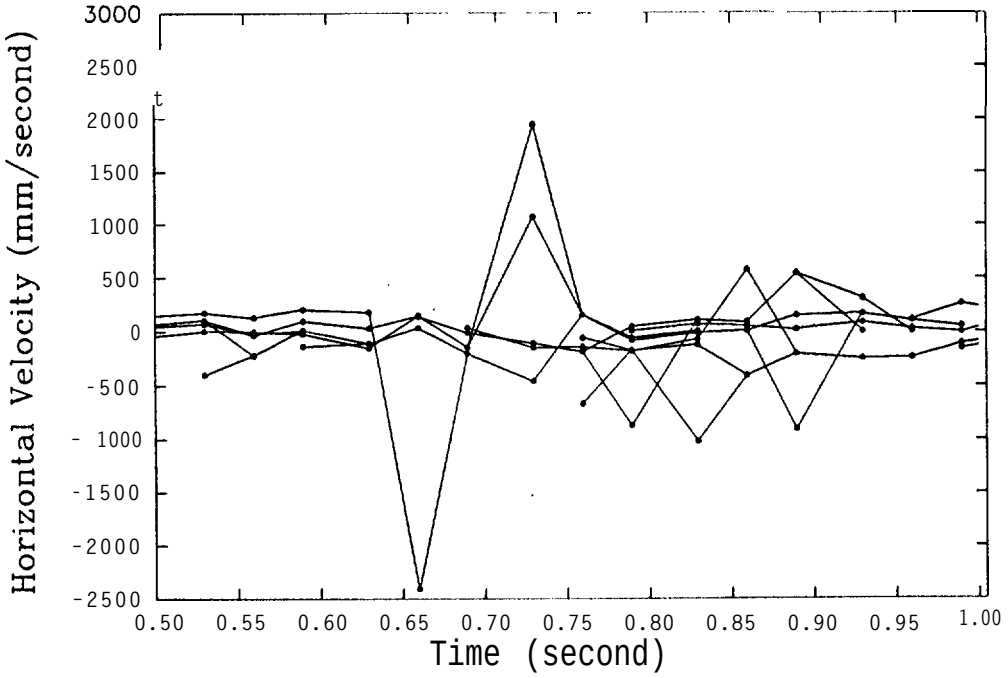

Figure 3-AI6-N1 Horizontal velocity of transient bubbles vs time under experimental condition I (normal period)

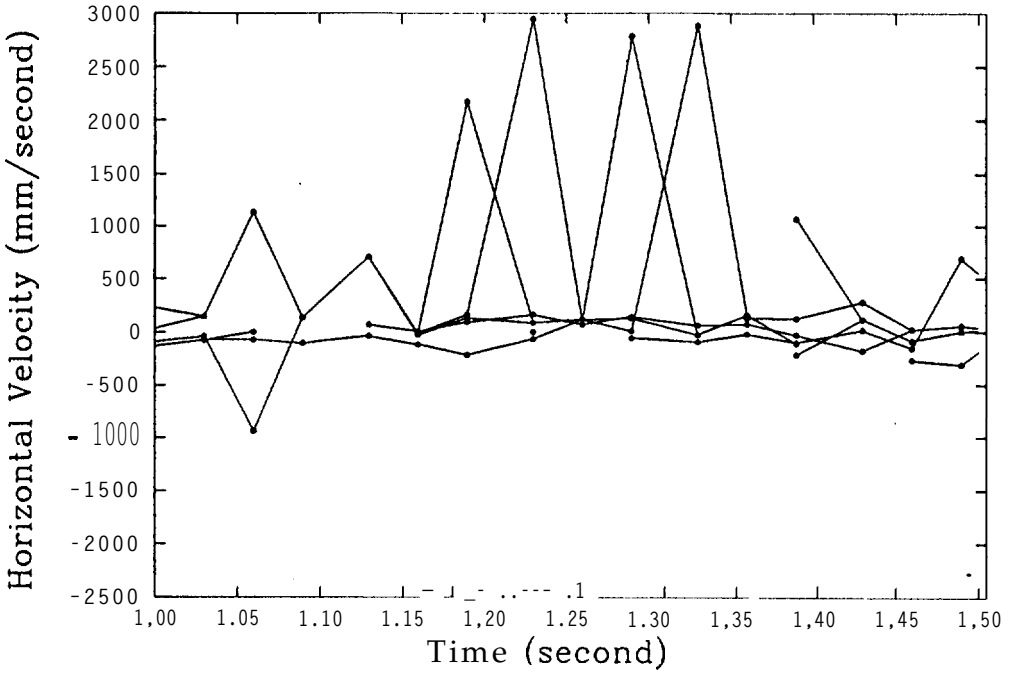

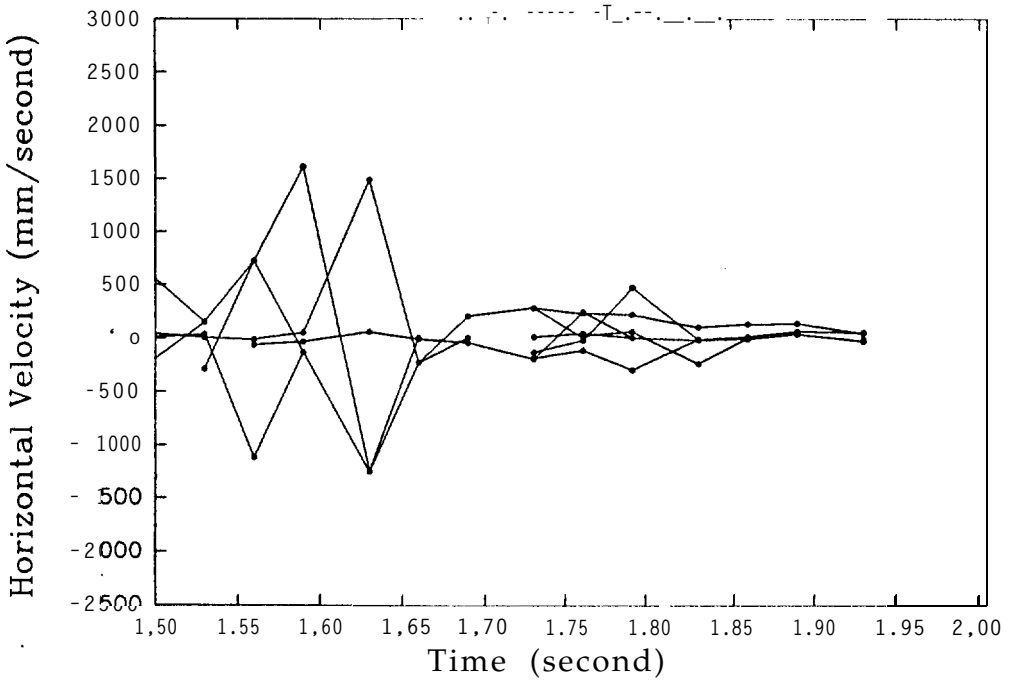

Figure 3-A16-N2 Horizontal velocity of transient bubbles vs time under experimental condition I (normal period)

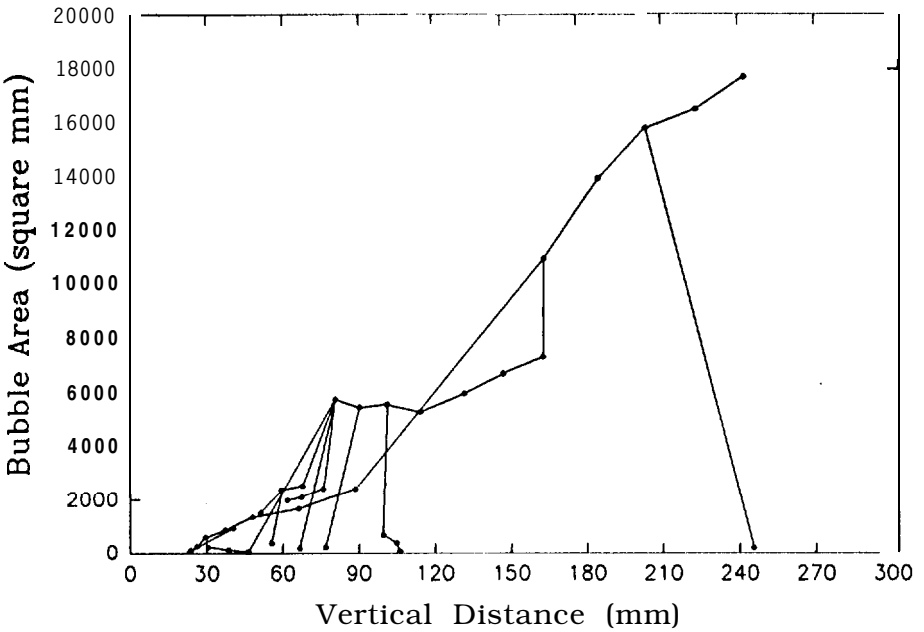

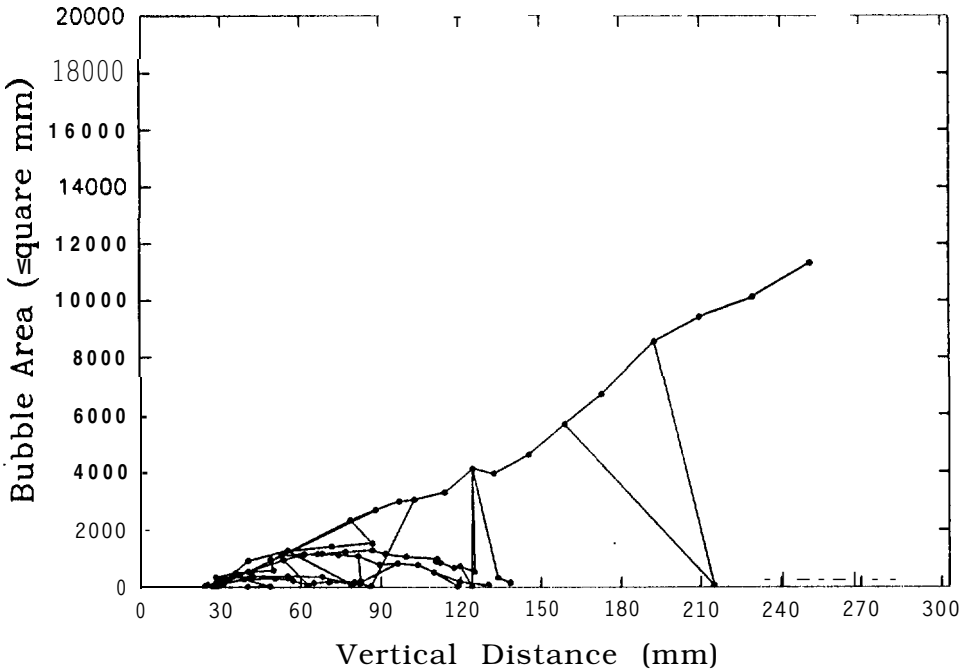

Figure 3-AI7-N1 Cross sectional area of transient bubbles vs vertical distance under experimental condition I (normal period)

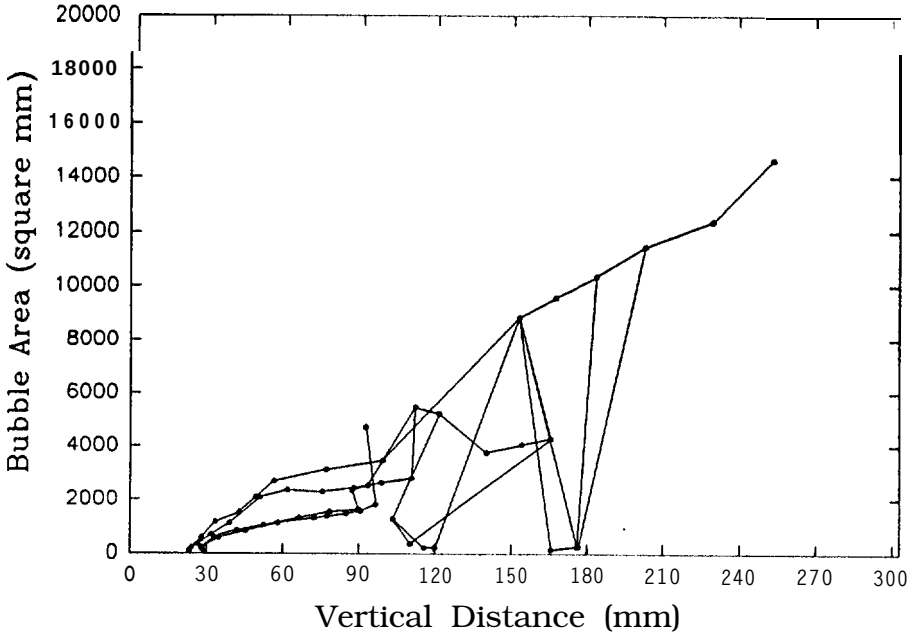

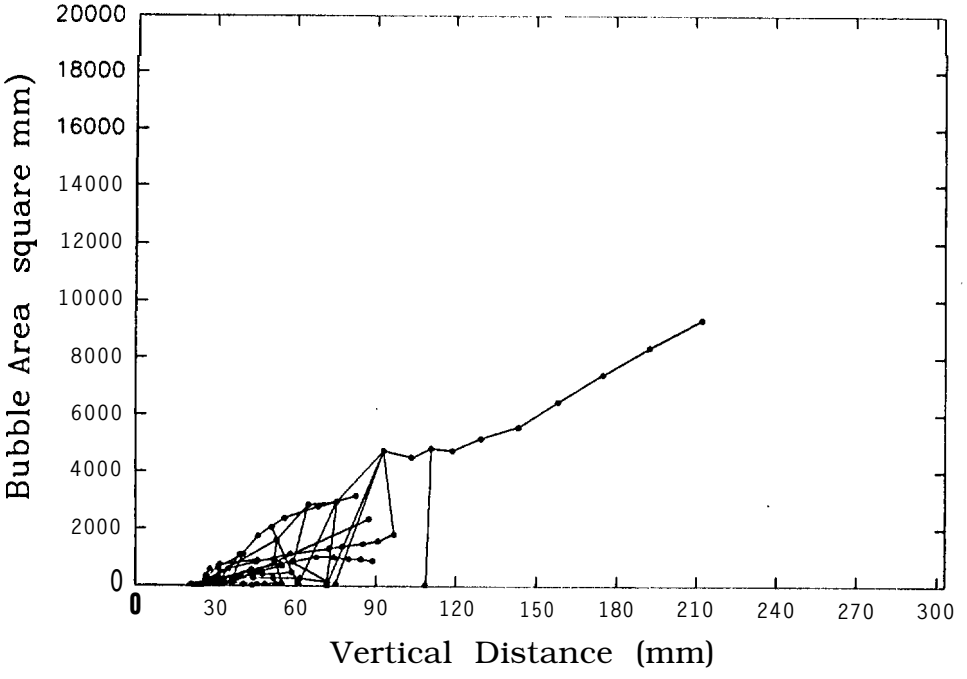

Figure 3-A17-N2 Cross sectional area of transient bubbles vs vertical distance under experimental condition I (normal period)

Time = 001.99

Time = 002.03

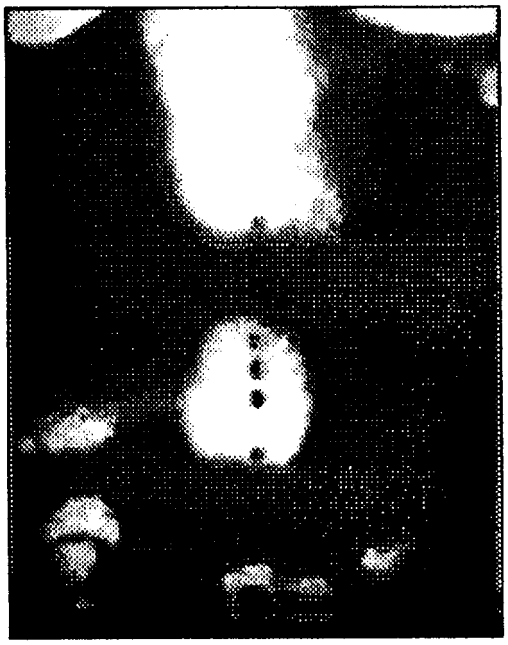

Time = 002.06

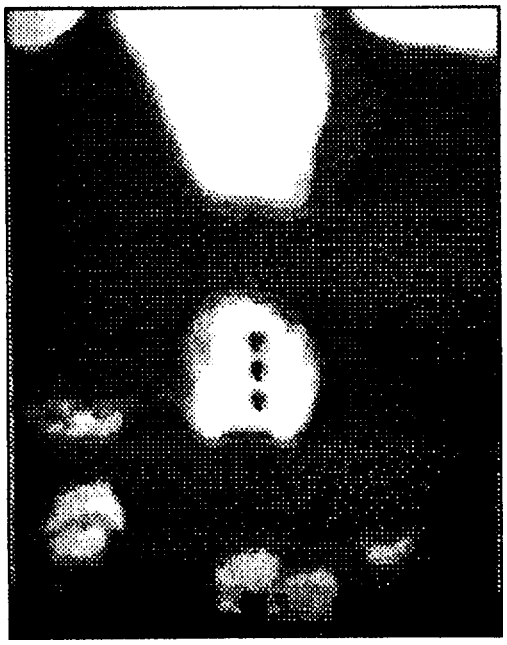

Time = 002.09

Picture 3.AI-AN-1 Transient bubble images under the experimental condition I (abnormal-period)

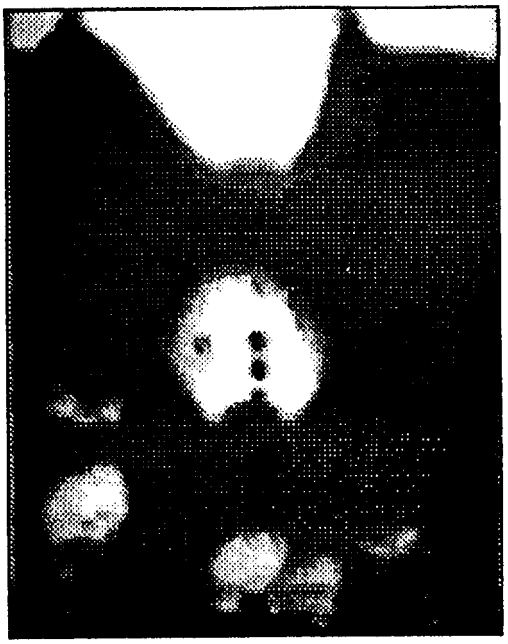

Time = 002.13

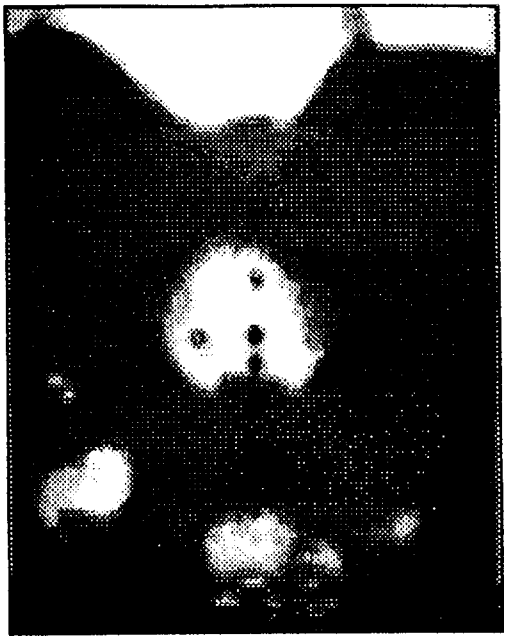

Time = 002.16

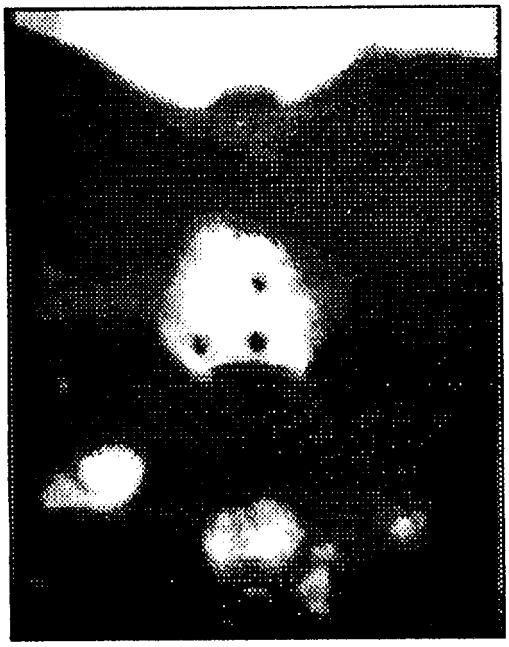

Time = 002.19

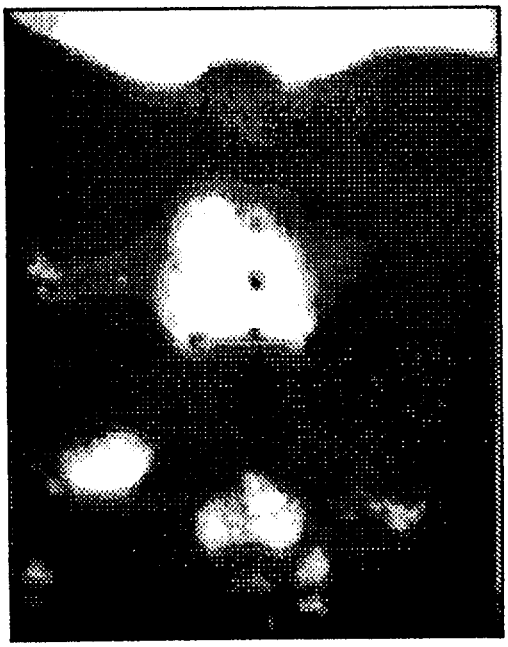

Time = 002.23

Picture 3.AI-AN-2 Transient bubble images under the experimental condition I (abnormal period)

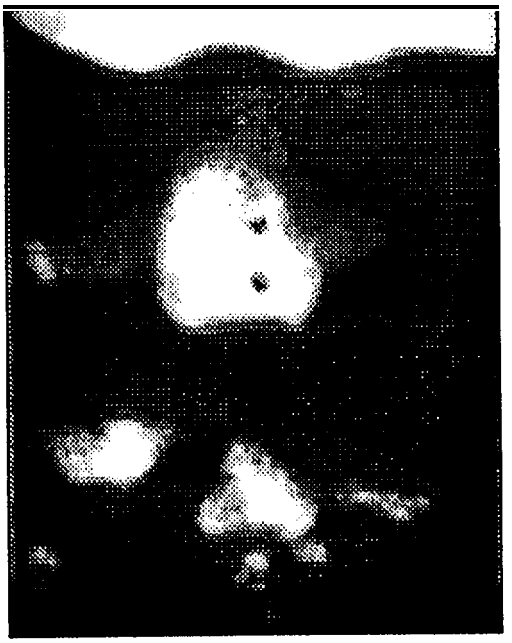

Time = 002.26

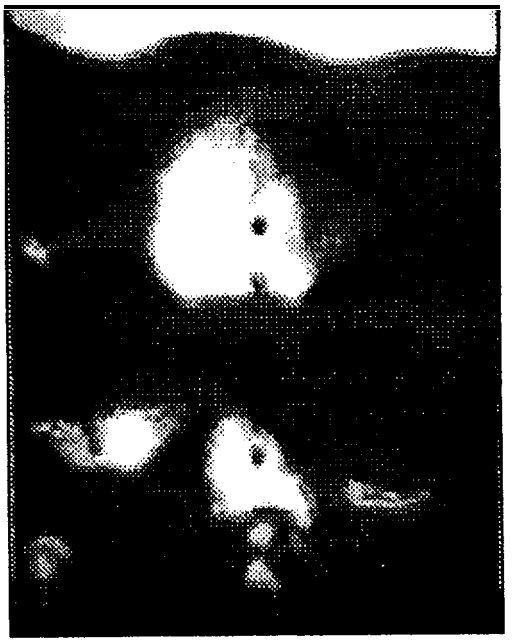

Time = 002.29

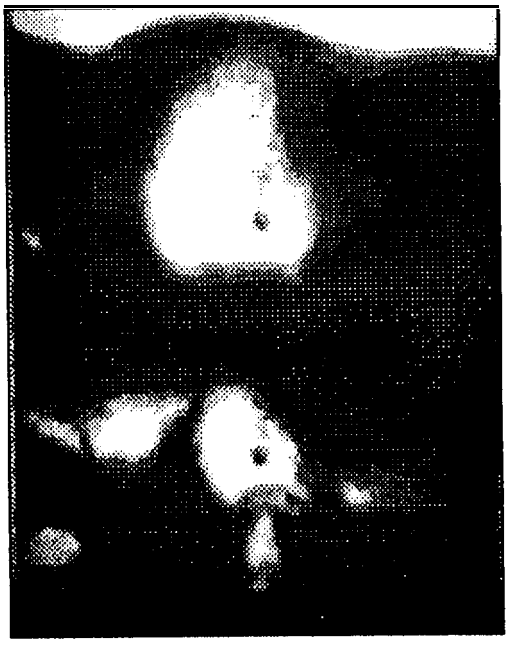

Time = 002.33

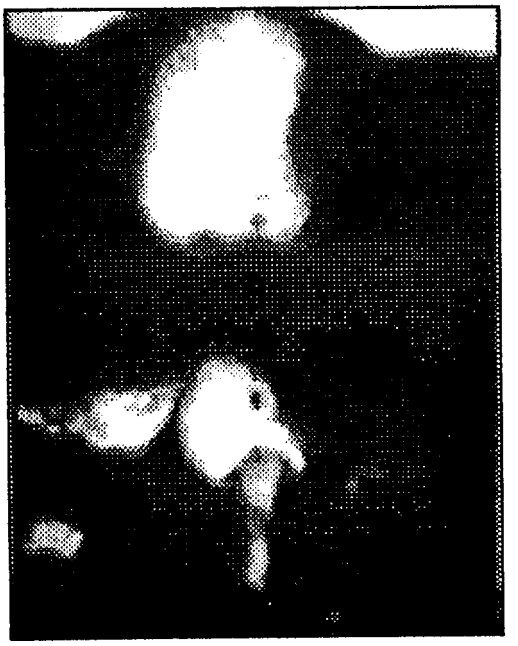

Time = 002.36

Picture 3.AI-AN-3 Transient bubble images under the experimental condition I (abnormal period)

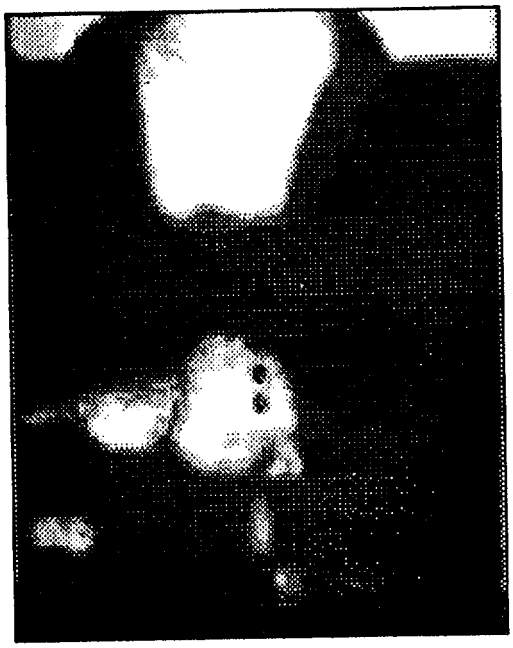

Time = 002.39

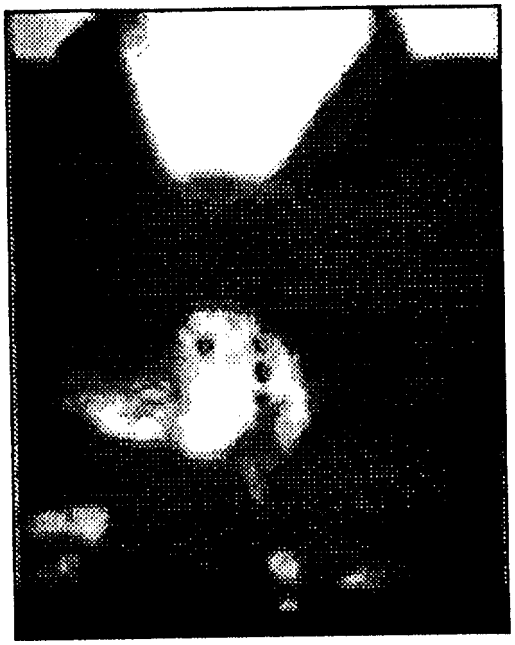

Time = 002.43

Time = 002.46

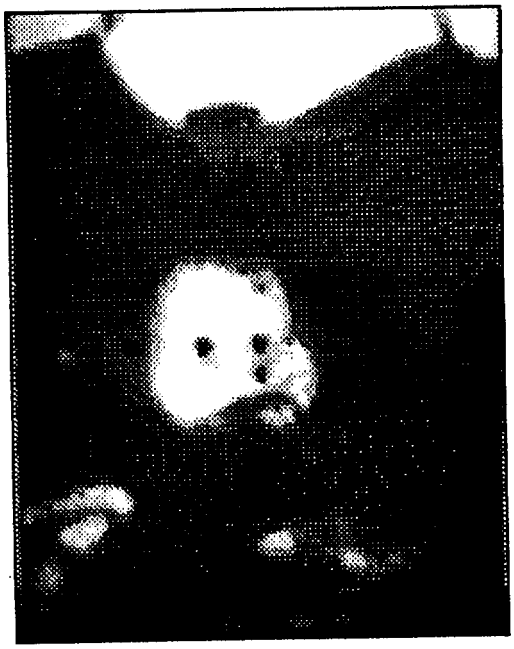

Time = 002,49

Picture 3.AI-AN-4 Transient bubble images under the experimental condition I (abnormal period)

Table 3.AI-2 Analysis results of bubbles of abnormal period (t=1.99 to 2.49 s)

Time (Sec.)	Bubble Num.	Area (sq. mm)	Centroid X (mm)	Centroid Y (mm)	Perimeter (mm)	Roundness (o-1)	Gray Avg. (0-256)
i.99	0	98.64099	186.49680	25.80304	61.84720	.32411	104.54440
1.99	1	621.66470	34.39830	36.23128	188.58270	.21971	141.08390
1.99	2	32.74750	126.89200	49.87798	29.94948	.45886	93.56667
1.99	3	27.82472	125.44580	58.02802	28.94407	.41744	83.60784
1*99	4	875.29090	23.62350	91.41013	220.96340	.22532	161.75360
1.99	5	3638.98500	118.82280	92.89096	435.34840	.24132	205.59990
1.99	6	213.89710	242.49260	286.21200	116.06550	.19955	131.73030
1.99	7	10389.11000	127.80690	231.99170	732.24430	.24352	202.66100
2.03	0	141.91630	188.43410	31.71515	47.55036	.78886	113.16600
2.03	1	669.82450	35.03491	45.20169	128.67670	.50846	154.82400
2.03	2	838.94720	26.64107	96.62968	128.56280	.63796	150.53880
2.03	3	4016.20600	120.02090	106.96290	264.30520	.72257	207.18210
2.03	4	189.91780	243.27470	291.71090	77.42519	.39816	119.99430
2.03	5	11206.38000	124.06760	255.44370	559.94260	.44921	206.44170
2.06	0	58.55061	155.64480	21.58755	34.66965	.61223	82.93458
2.06	1	236.49480	122.48710	24.93639	69.31815	.61860	120.06470
2.06	2	143.00920	190.82010	35.61913	51.33634	.68201	112.03830
2.06	3	281.48140	33.07855	35.00856	72.05490	.68142	118.73740
2.06	4	672.89660	36.54419	54.70935	126.83740	.52571	161.47700
2.06	5	30.31862	7.13575	96.29912	20.61718	.89648	81.39286
2.06	6	652.58780	33.64832	103.47700	126.91080	.50925	150.88540
2.06	7	4177.31100	121.18870	122.72060	283.38910	.65860	205.62380
2.06	8	140.42480	247.53660	292.55870	60.79832	.47744	129.72090
2.09	0	245.66480	154.40970	22.98106	132.48750	.17590	105.03340
2.09	1	567.43330	123.01210	27.78212	185.25290	.20781	148.77190
2.09	2	131.51600	195.36120	39.29529	118.66250	.11739	111.46670
2.09	3	1242.61000	36.86009	55.04765	265.52470	.22152	163.72470
2.09	4	499.76300	37.81252	108.04760	229.06460	.11971	138.07370
2.09	5	4417.66000	122.84770	135.80170	464.66550	.25715	204.21050
2.13	0	29.58362	190.81940	40.92497	48.55060	.15774	82.44444
2.13	1	62.48108	203.10310	46.73315	60.44419	.21494	102.42110
2.13	2	1235.20900	131.05960	31.71781	394.17940	.09992	148.97040
2.13	3	1369.29900	36.97557	64.15500	264.52630	.24595	174.51390
2.13	4	63.98414	48.10457	114.14920	67.60713	.17594	117.59320
2.13	5	152.19870	27.86991	115.45190	108.29760	.16310	107.66550
2.13	6	4627.93900	119.78900	149.62390	541.75520	.20102	203.81980
2.16	0	163.03710	161.15790	34.05394	113.16360	.16001	121.86580
2.16	1	110.68900	203.54590	51.62161	73.75988	.25570	105.11880
2.16	2	1160.51200	123.27270	41.17699	234.33050	.26563	177.51080
2.16	3	1417.82100	38.87778	71.95444	271.98970	.24088	191.06510
2.16	4	31.38741	22.09161	129.11330	25.56499	.60360	97.31035
2.16	5	4914.76600	118.23190	161.80210	510031950	.23908	203.36470
2.19	0	122.02670	157.77870	24.83850	91.69562	.18241	108.95960
2.19	1	50.32154	160.99980	40.96125	41.45108	.36810	108.10870
2.19	2	112.31860	202.98630	54.90533	66.53548	.31887	132.32190
2.19	3	1421.21400	124.61580	48.51559	286.02600	.21834	179.82100
2.19	4	1410.38200	43.23867	77.92780	311.37500	.18283	192.38640
2.19	5	5260.59800	117.08930	173.97590	575.34780	.20122	204.69340
2.23	0	49.95177	11.88463	29.12363	40.68551	.37929	89.65218
2.23	1	180.52080	157.20910	32.59631	92.64282	.26435	126.57580
2.23	2	192.78210	199.97240	61.51106	118.36490	.17294	110.36360
2.23	3	1701.66600	124.56990	58.46357	323.42150	.20446	181.66530
2.23	4	1381.47200	47.52448	86.75552	280.71540	.22034	194.17290
2.23	5	100.95120	16.48742	191.77290	78.32318	.20683	103.24060
2.23	6	5792.15600	114.79990	189.01170	547.81610	.24257	204.98040
2.26	0	68.26991	126.99440	32.13442	46.02678	.40503	126.89600
2.26	1	83.67880	156.50290	36.47552	67.14803	.23325	96.52287

2.26	2	65.14685	14.96861	34.54271	63.89150	.20059	91.60000
2.26	3	303.82250	194.14730	64.55558	183.25030	.11371	109.33690
2.26	4	2012.71600	126.87620	66.42049	350.13990	.20634	183.54150
2.26	5	1485.04900	51.41009	90.97196	297.62790	.21071	185.40210
2.26	6	122.50820	15.16228	191.94260	96.70100	.16466	102.37890
2.26	7	33.44233	11.98865	201.81690	49.26366	.17319	86.25806
2.26	8	6457.07600	114.67540	201.32950	520.89990	.29909	207.90740
2.29	0	136.02620	128.60540	27.10753	58.38993	.50145	123.32530
2.29	1	79.28226	15.99627	29.64279	49.41533	.40808	84.69863
2.29	2	86.86514	20.19766	41.83582	79.55359	.17251	87.90000
2.29	3	131.55940	129.74000	48.85155	64.25897	.40044	132.44810
2.29	4	381.36820	188.31060	69.29872	166.73000	.17242	112.15780
2.29	5	2286.72700	125.15400	81.60938	357.61870	.22473	196.97210
2.29	6	1615.54200	52.59044	100.10570	425.22530	.11230	172.53140
2.29	7	104.12630	12.11404	201.97980	69.21743	.27316	121.88600
2.29	8	7109.40200	113.13020	219.11460	669.29450	.19947	208.66840
2.33	0	378.96590	20.93057	41.67878	139.09680	.24618	110.59890
2.33	1	307.38910	129.47350	43.72284	105.21520	.34899	163.25040
2.33	2	148.74950	179.70460	71.17551	73.16344	.34925	137.43380
2.33	3	1551.90700	55.15605	106.28820	454.36570	.09448	181.46150
2.33	4	2673.57800	120.91170	94.09251	352.85200	.26989	200.50570
2.33	5	28.04588	9.52874	206.92860	31.74166	.34986	92.92308
2.33	6	7932.96400	111.95010	239.19110	649.22510	.23655	213.51690
2.36	0	190.04450	128.88380	33.41777	90.67992	.29048	123.44250
2.36	1	420.69380	22.87514	45.98017	165.65260	.19269	128.84900
2.36	2	68.72624	10.69582	112.64870	75.64238	.15097	99.43307
2.36	3	4848.07700	100.44270	107.23310	769.35830	.10294	190.32420
2.36	4	9330.52600	112.22820	264.82870	652.38160	.27553	214.45030
2.39	0	35.52857	139.06970	23.60970	34.33558	.37877	100.15380
2.39	1	85.13550	128.97260	51.66600	52.93396	.38188	98.69231
2.39	2	460.31880	25.20042	49.38231	175.81580	.18717	125.17690
2.39	3	55.74467	14.33155	114.86820	83.30363	.10096	85.78641
2.39	4	5208.54200	100.44450	116.15730	722.85010	.12608	190.59100
2.43	0	66.27178	176.10200	24.48978	73.35258	.15480	101.40500
2.43	1	162.85240	138.73900	31.88632	72.82904	.38589	119.18120
2.43	2	509.21500	28.85572	55.98644	192.58230	.17257	133.21960
2.43	3	5744.14800	100.65310	127.94260	823.70980	.10640	186.34860
2.46	0	96.38387	177.05620	29.11918	49.91820	.48614	109.89770
2.46	1	153.50490	136.73810	39.25116	69.77175	.39632	140.15660
2.46	2	159.68280	28.59499	42.19755	75.80862	.34923	123.01360
2.46	3	532.65140	36.39706	62.03725	261.67480	.09777	136.41390
2.46	4	6145.86100	105.93210	137.62430	711.59440	.15721	184.76190
2.49	0	29.32735	17.61994	28.44282	40.97037	.21960	73.44444
2.49	1	61.85674	174.73200	37.36067	38.54187	.52336	110.92040
2.49	2	157.82370	135.40350	46.27753	81.14355	.30126	137.40480
2.49	3	299.25510	33.82453	51.02683	161.40500	.14438	149.35390
2.49	4	463.70230	41.69198	69.17636	209.89080	.13229	149.42620
2.49	5	6023.41500	108.76020	152.35550	677.31440	.16594	202.53680

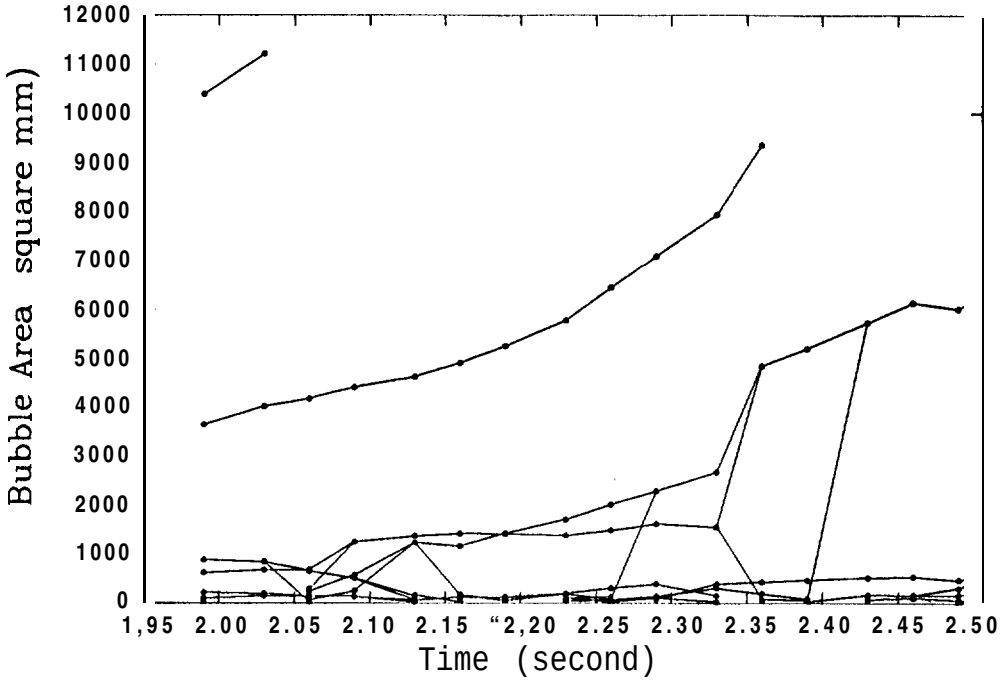

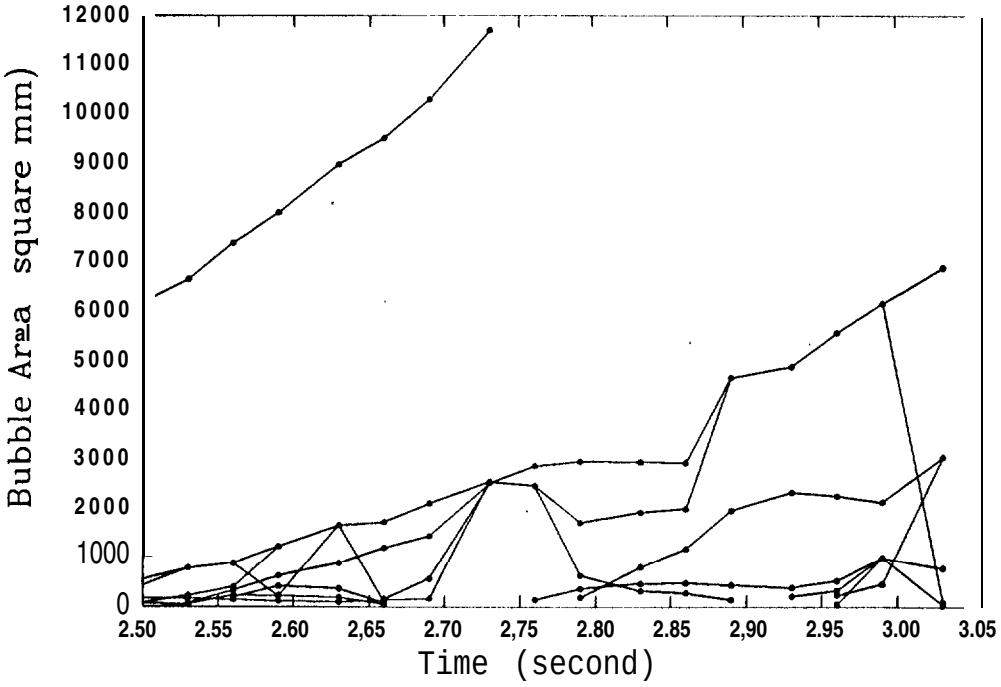

Figure 3-AI2-AN-1 Cross sectional area of transient bubbles vs **time** under experimental condition I (abnormal period)

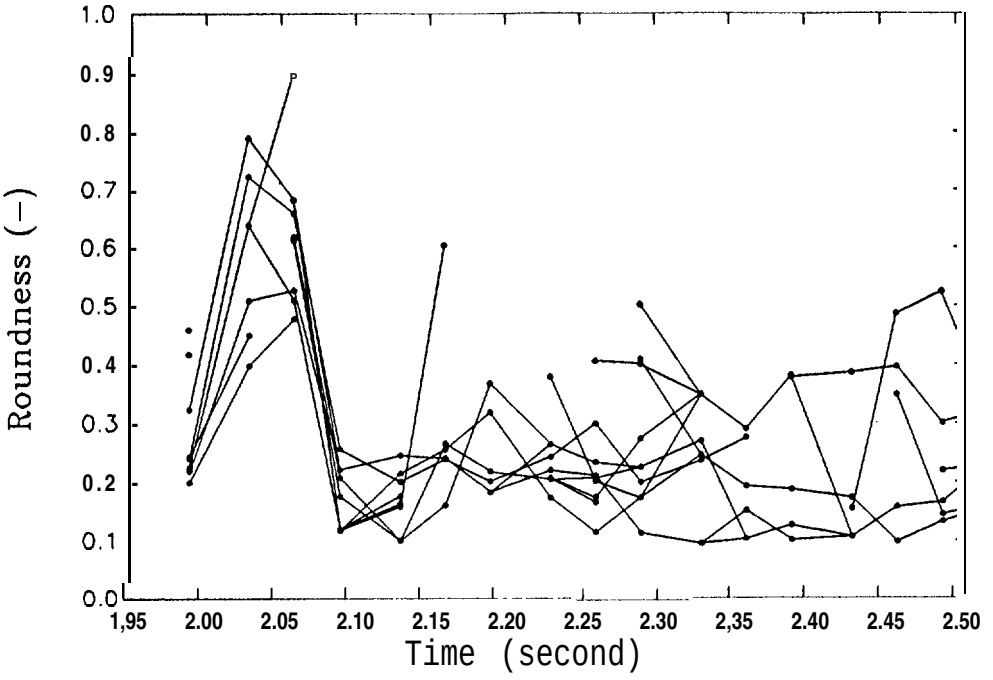

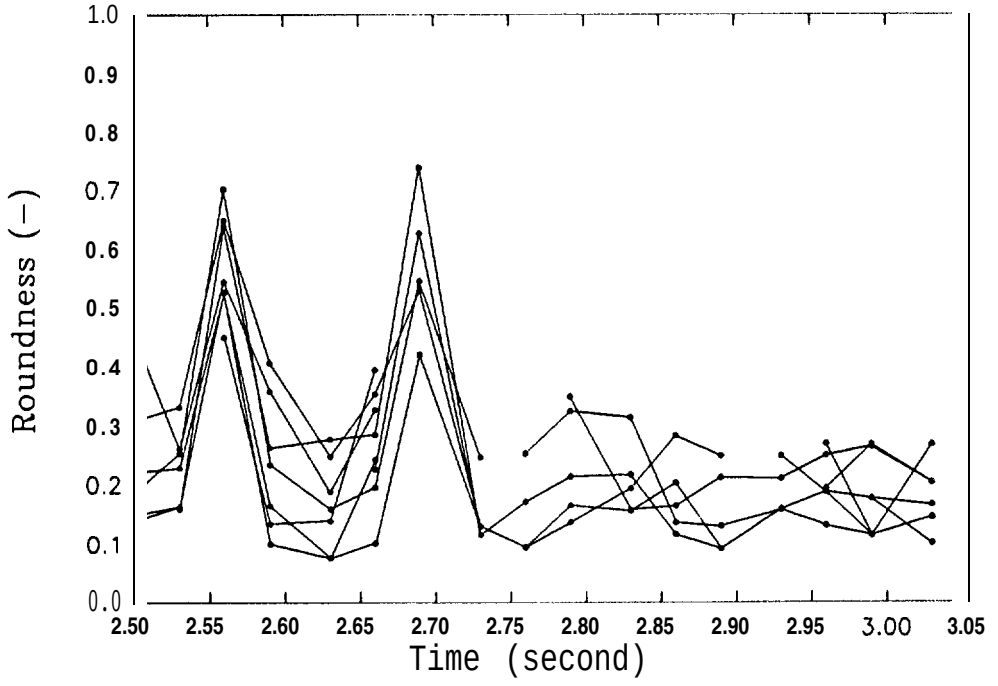

Figure 3-AI3-AN-1 Roundness of transient bubbles vs time under experimental condition I (abnormal period)

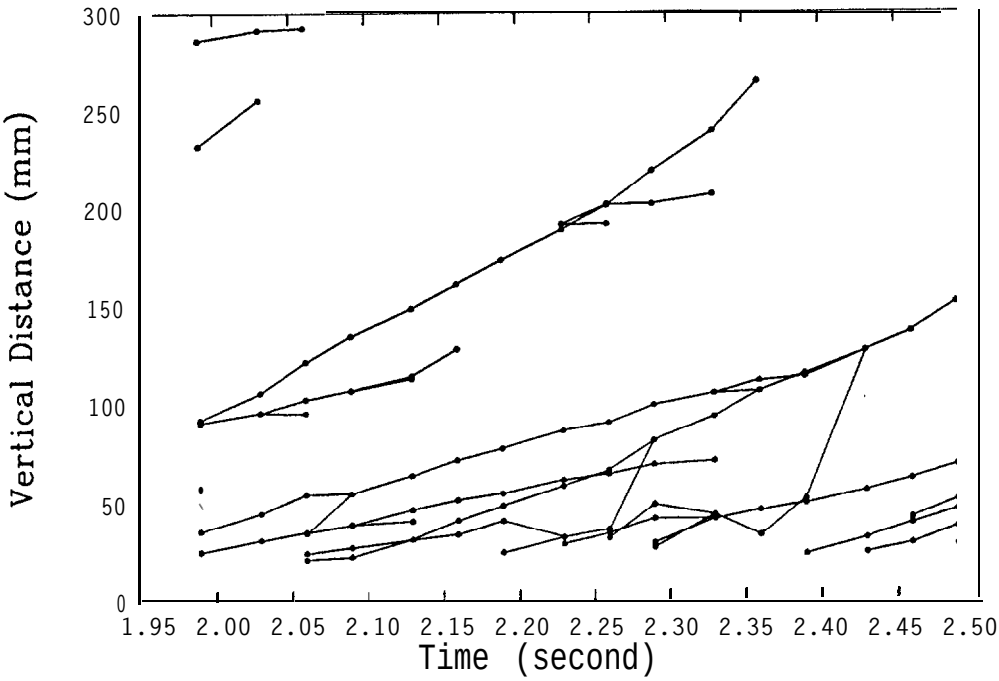

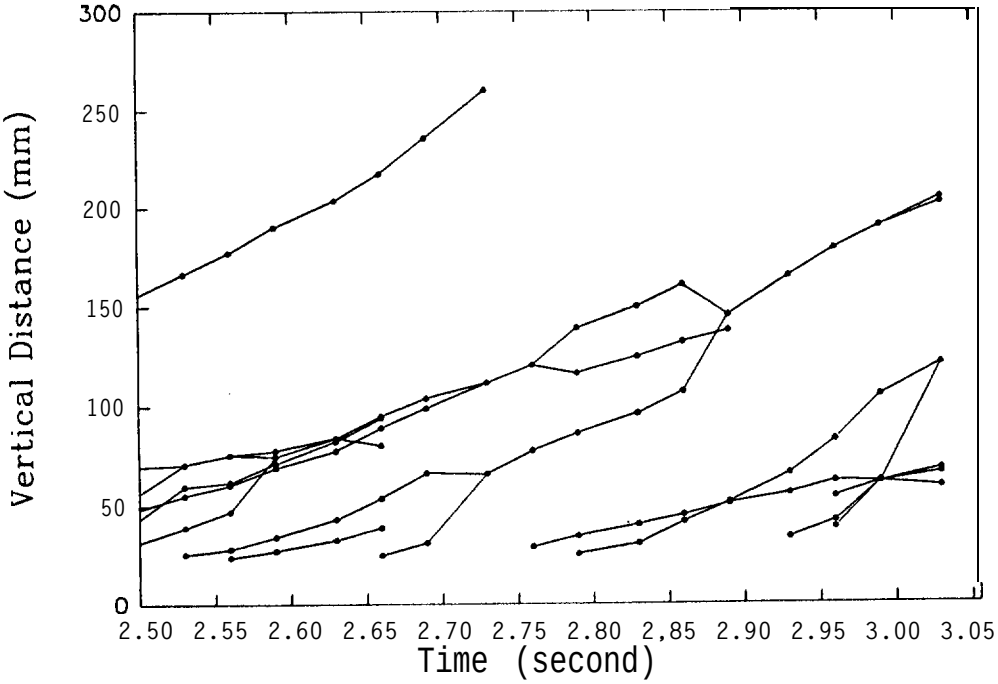

Figure 3-AI4-AN-1 Vertical distance of transient bubbles vs time under experimental condition I (abnormal period)

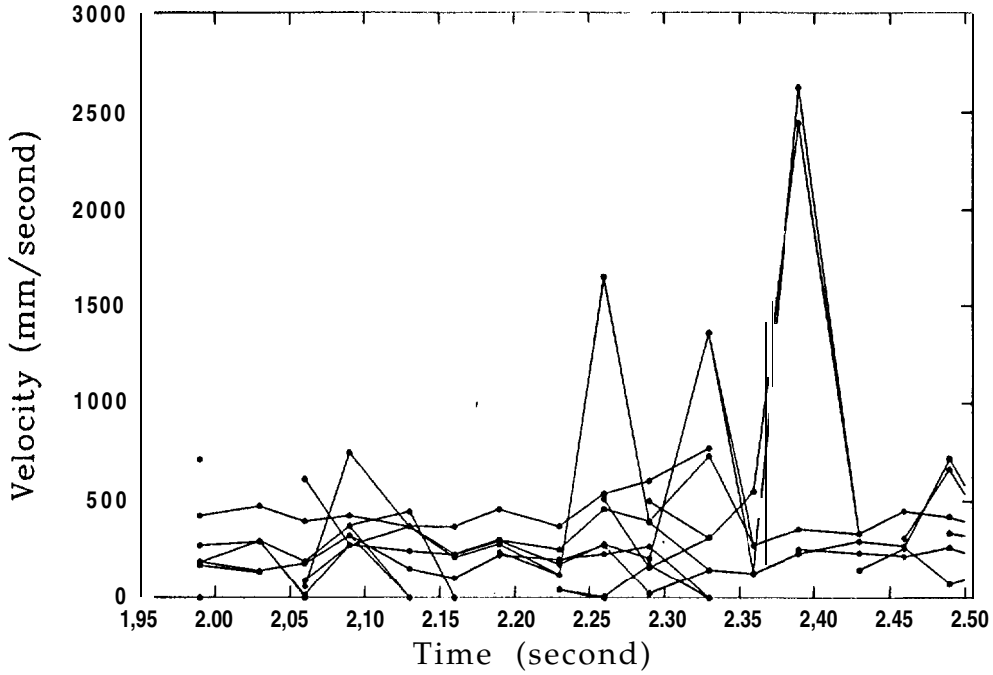

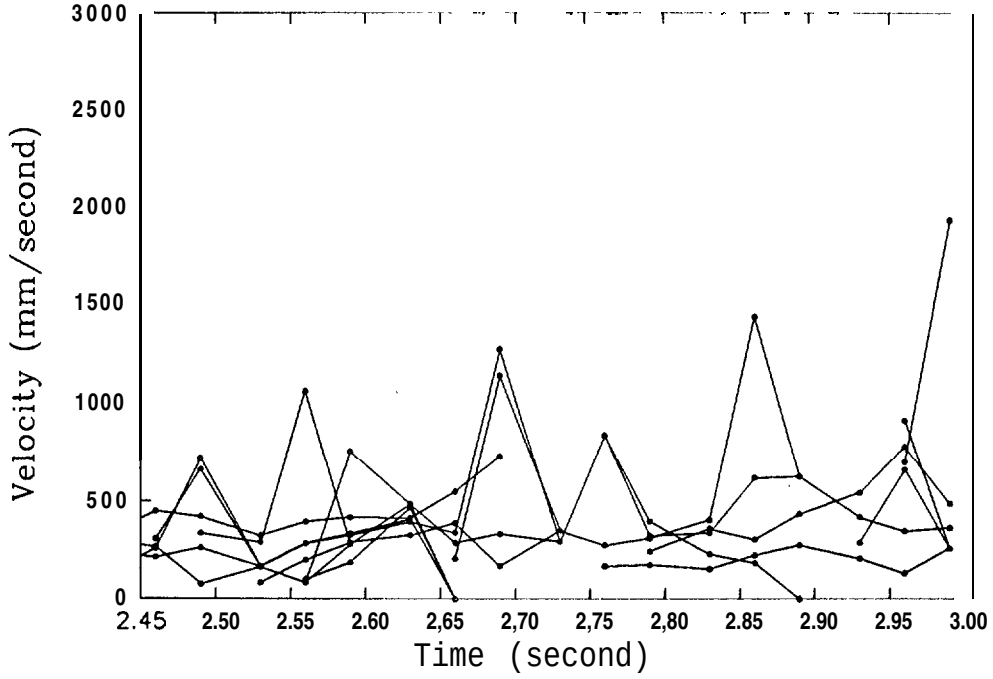

Figure 3-AI5-AN-1 Velocity of transient bubbles vs time under experimental condition I (abnormal period)

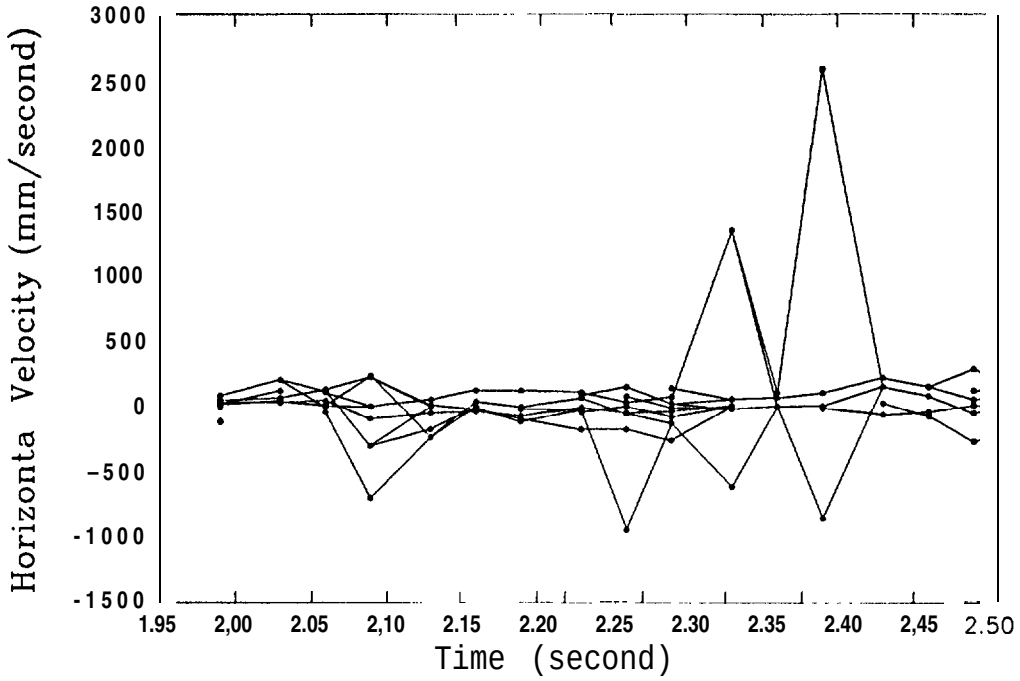

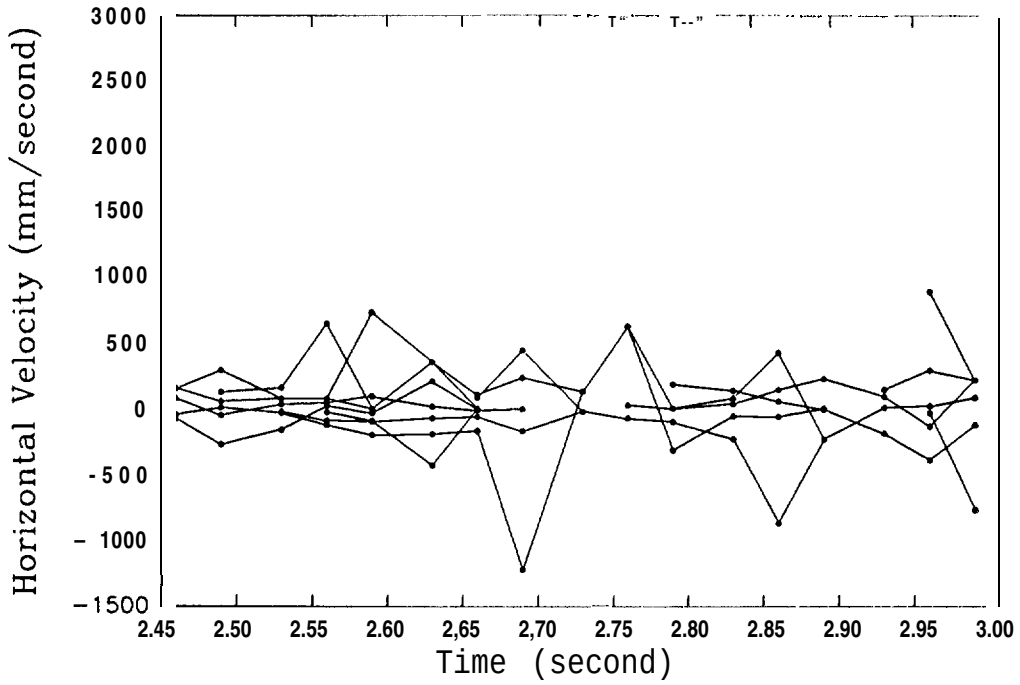

Figure 3-AI6-AN-1 Horizontal velocity of interacting bubbles under experimental condition I (abnormal period)

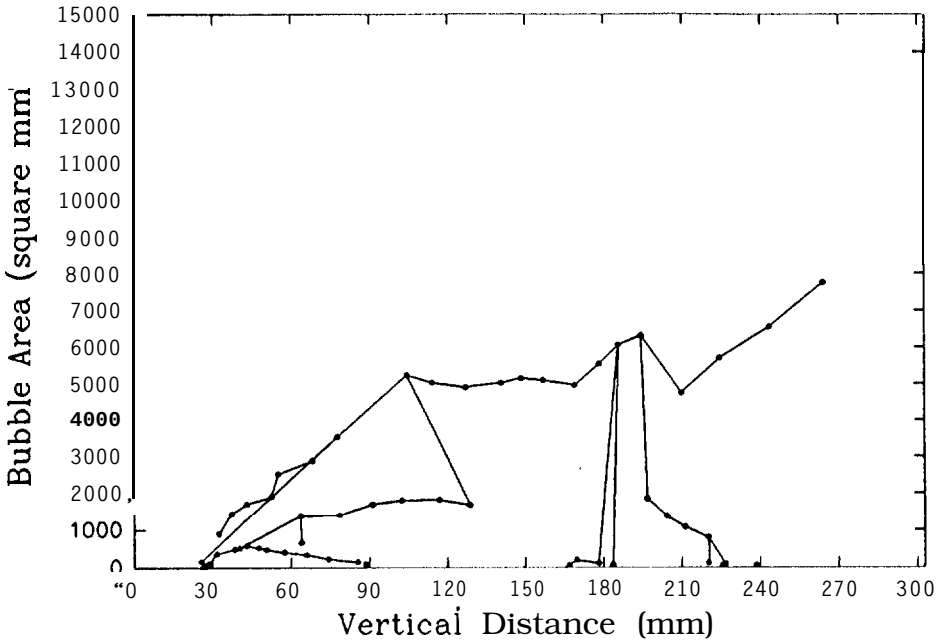

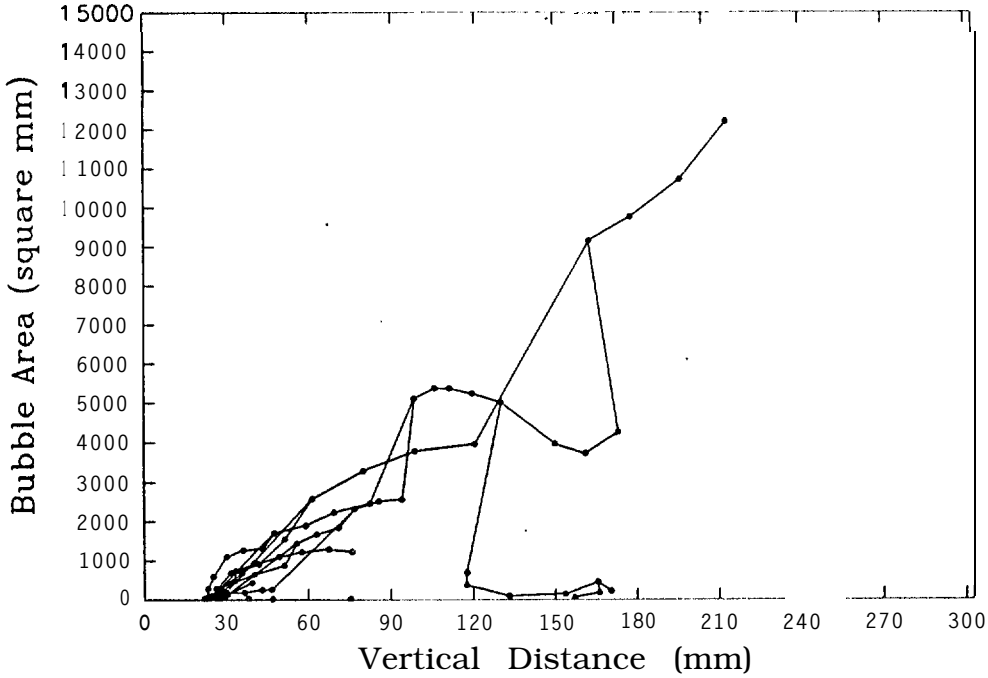

Figure 3-AI7-AN-1 Cross sectional area of transient Bubbles vs vertical distance under experiment condition **I** (abnormal period)

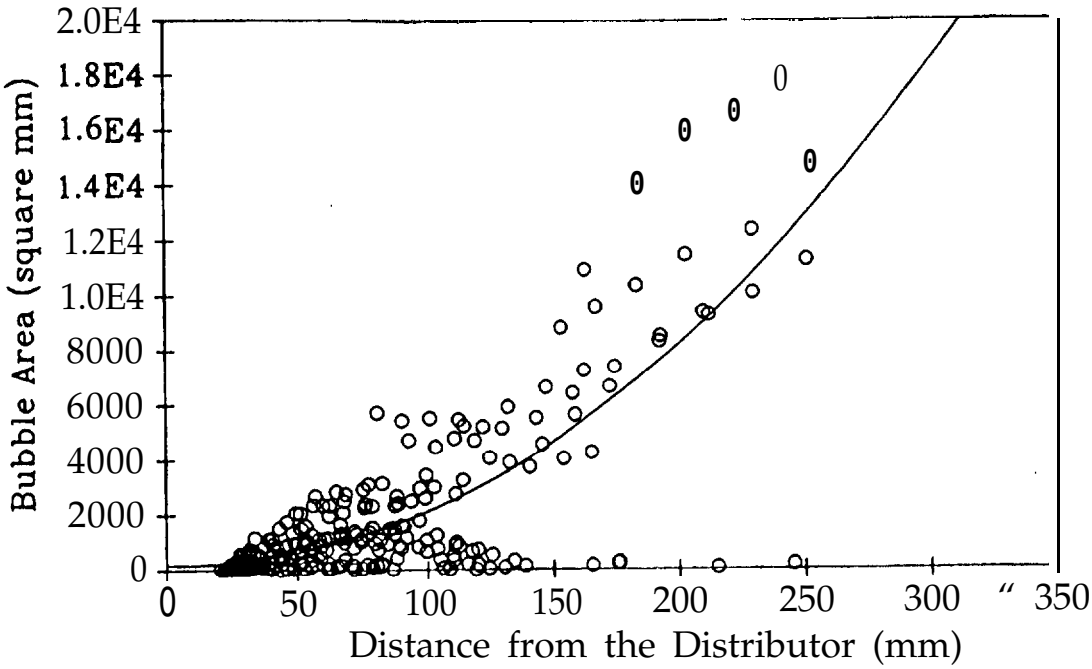

Figure 3 -A8 -N1 Cross sectional area of transient bubbles vs vertical loction (t=0 to 1.96 seconds)

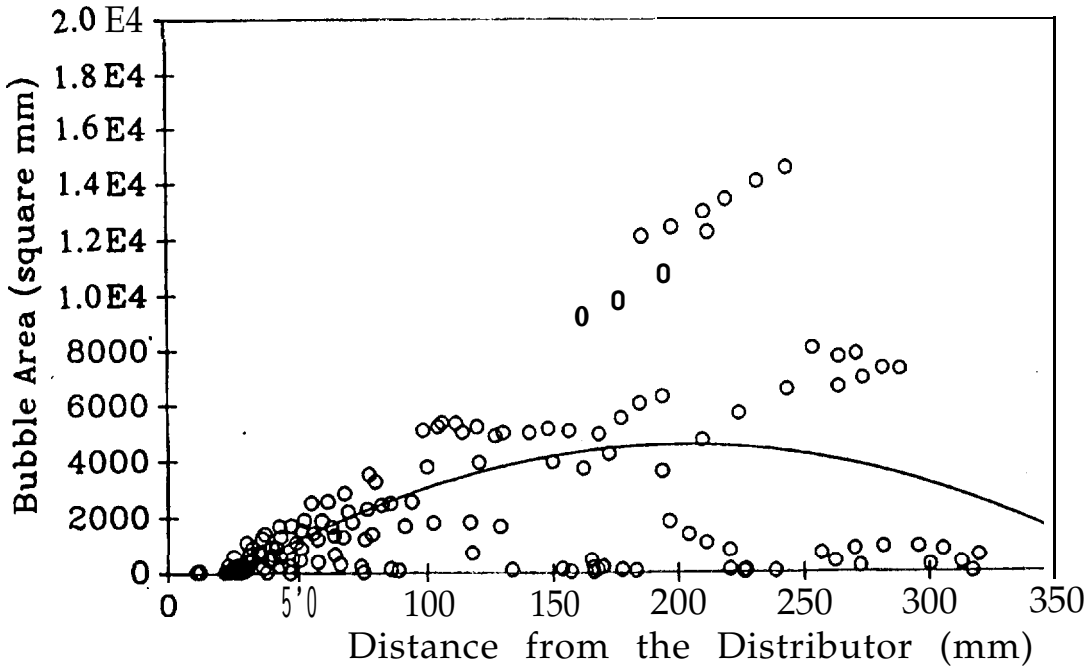

Figure 3-A8-AN Cross sectional area of transient bubbles vs vertical loction (t=13.89 to 14.92 seconds)

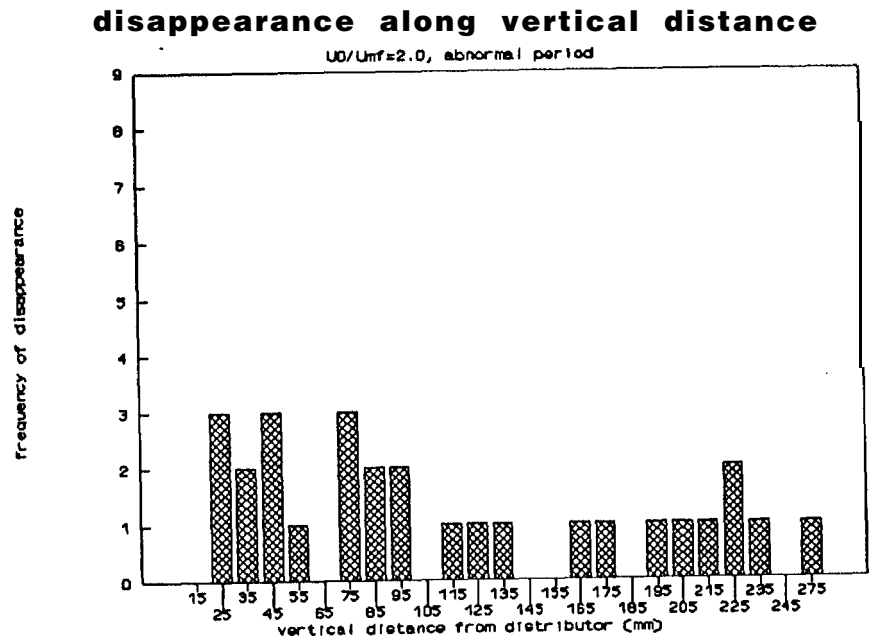

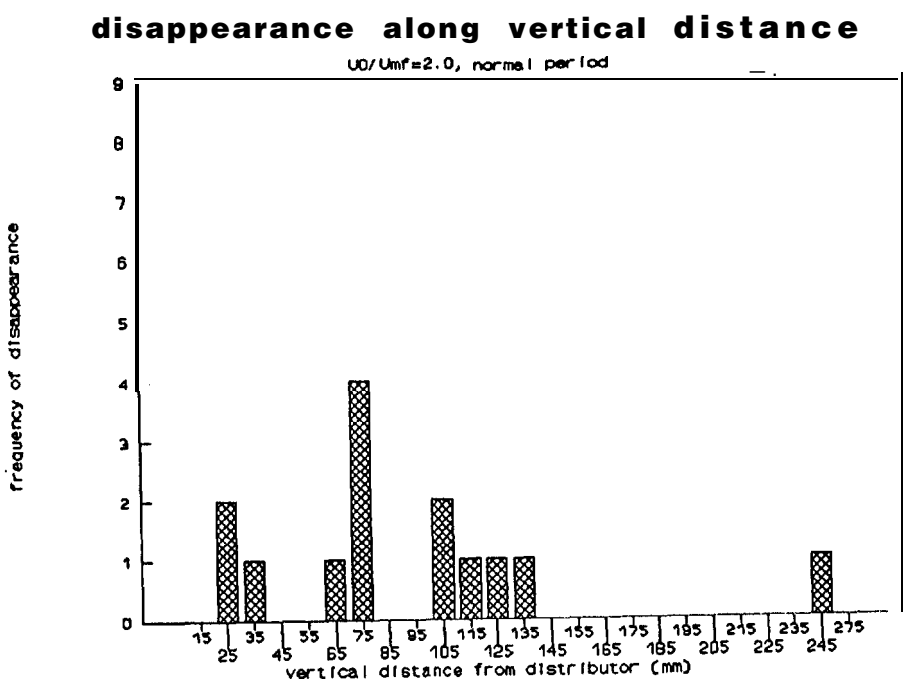

Figure 3-AI9-N&AN Disappearance along vertical distance at $U_0/U_{mf}=2.0$

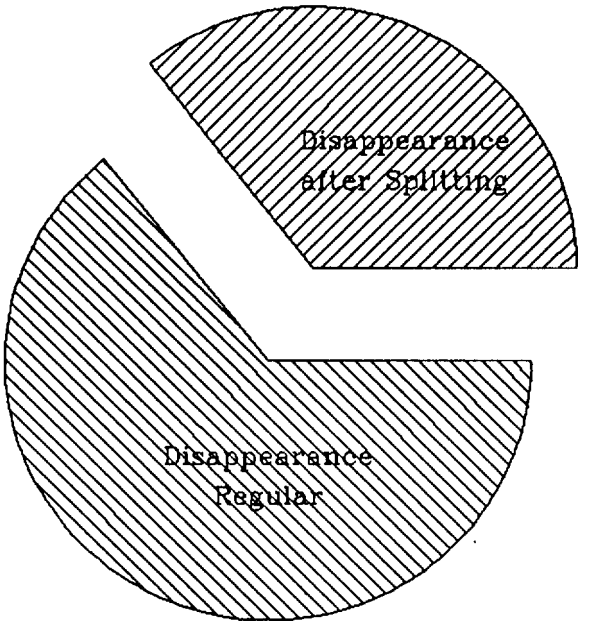

U_o / U_{mf} = 2.0 Normal Fluidization Period
Glass Beads 1 mm

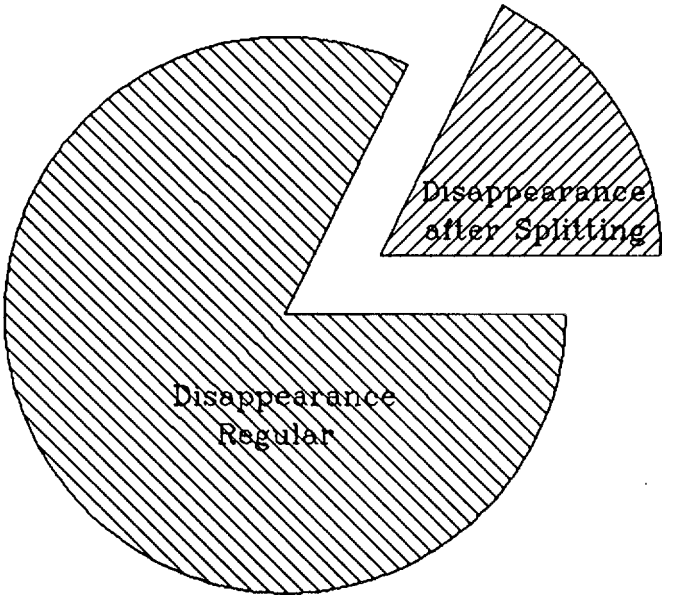

U_o / U_{mf} = 2.0 Abnormal Fluidization Period
Glass Beads 1 mm

Figure 3-AI **10-N&AN** Two **kinds** of disappearance **at** U_0/U_{mf}=2. 0

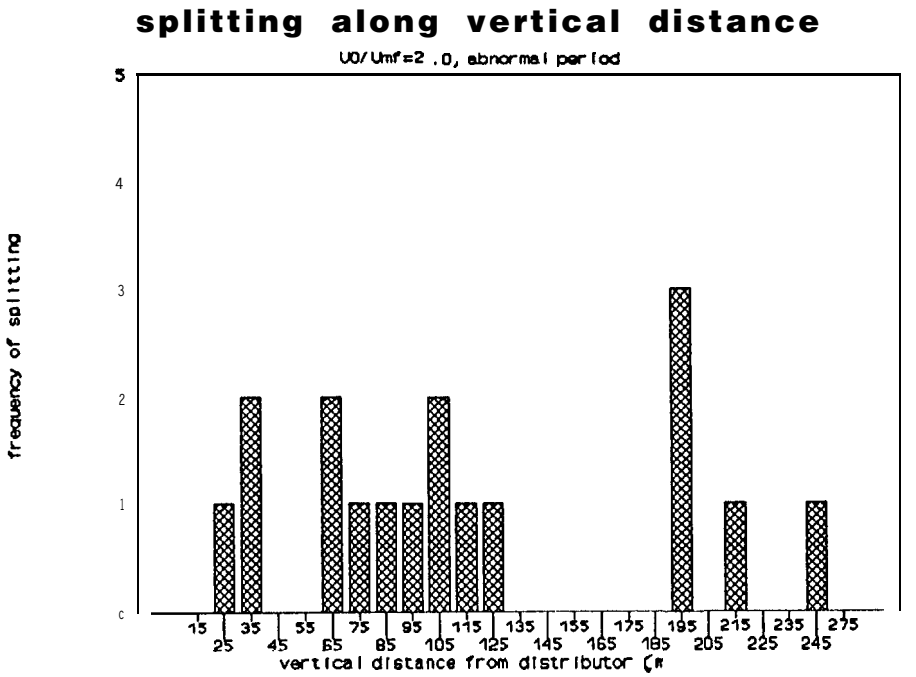

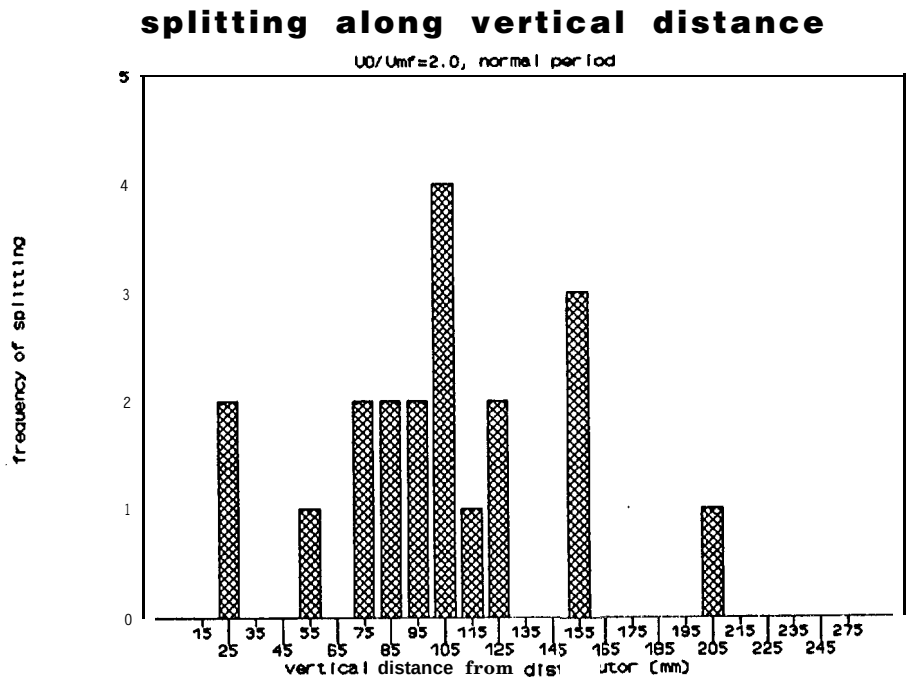

Figure 3-AI11-N&AN Splitting along vertical distance at U_0/U_{mf}=2.0

along the vertical distance at "normal" and "abnormal" fluidization period is shown in Figures 3-AI11-N AND 3-AI11-AN. All the experimental data showed that the interaction of bubble was more intensive during the abnormal fluidization period of time than that of the normal period of time. This finding of stochastically existing two types of fluidization pattern provide a new fundamental insight into fluidization.

3.AII&III Normal and abnormal fluidization at various gas velocities.

The systematic data taking was carried out under the experimental conditions of II (U_0/U_{mf}=2.3) and III (U_0/U_{mf}=1.8) in the same way as those done for the experimental condition I (U_0/U_{mf}=2.0) Namely, the transient bubbles images are shown in Pictures 3-AII-1 under experimental condition II, and Pictures 3-AIII-1 under experimental condition III. The summary of analysis results of bubbles are shown in Table 3-AII-1 under experimental condition II and Table 3-AIII-1 under experimental condition III. The data of the cross-sectional area of bubbles versus time under the experimental conditions of II and III are shown in Figure 3-AII2-N1 and Figure 3-AIII2-N1. The data of roundness of transient bubble versus time are shown in the Figure 3-AII3-N1 and 3-AIII3-N1 respectively. The vertical distance of transient bubbles as the function of time are shown in Figure 3-AII4-N1 and 3-AIII4-N1 respectively. The effective velocity and horizontal velocity of transient bubble are shown in Figures 3-AII5-N1 and 3-AIII5-N1 and Figures 3-AII6-N1 and 3-AIII6-N1 respectively. The coalescence mechanism's difference at normal and abnormal fluidization period under the experimental condition II and III are shown in Figures 3-AII7-N AND 3-AIII7-AN and Figures 3-AII8-N and 3-AIII8-AN respectively. These results showed that the coalescence of transient bubbles at normal fluidization period occurred more intensively at the lower part of the bed than those at abnormal fluidization period.

3.B. Two Dimensional Circulation Fluidized Bed

A two dimensional transparent circulating fluidized bed was installed. The fluidized bed vessel was 92 mm in width, 10 mm in thickness and 1000 mm in height. The fluidizing particles were spherical glass beads with the average diameter of 0.5 mm. The minimum fluidization velocity of this particle was 22 cm/sec. The experiments were carried out under the following velocity: U_0/U_{mf}=24.0 (U_0=5.29 m/s), 20.5 (U_0=4.51 m/s) and 17.0 (U_0=3.73 m/s) with the corresponding bed heights of 85 mm, 135 mm and 255 mm respectively. The two dimensional circulating fluidized bed equipment provided unexpectedly very clear image, showing the special characteristics of this type of fluidization. Experiments of U_0/U_{mf}=24.0 and 20.5 show typical steady circulating fluidization. The experiment of U_0/U_{mf}=17.0 shows a wave-like

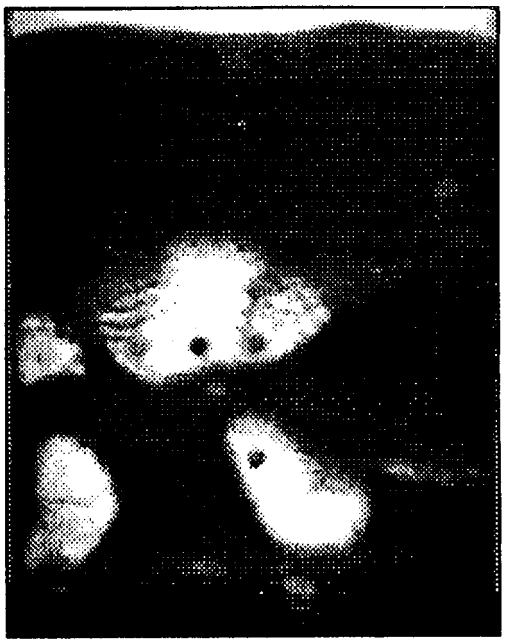

Time = 000.49

Time = 000.53

Time = 000.56

Time = 000.59

Picture 3-AII-1 Transient bubble images under the experimental condition II

Table 3-AII Analysis results of bubbles under experimental condition II (t=0.49 to 0.59 second)

Time (Sec.)	Bubble Num.	Area (sq. mm)	Centroid X (mm)	Centroid Y (mm)	Perimeter (mm)	Roundness (0-1)	Gray Avg. (0-256)
.49	0	78.26901	204.95990	84.21278	49.87733	.39542	92.65734
.49	1	2347.52400	32.05880	65.28387	238.05910	.52063	185.86960
.49	2	3373.46700	148.88070	72.96529	299.33380	.47320	200.49260
.49	3	886.88750	18.78264	147.12270	158.04760	.44625	157.64270
.49	4	6397.24400	104.25850	168.81590	439.07900	.41705	191.77240
.53	0	161.27770	156.42330	42.74915	86.73518	.26944	104.44070
.53	1	37.75367	202.85400	86.31258	46.06813	.22358	95.68116
.53	2	2704.76400	33.50809	79.01783	333.73650	.30522	204.50300
.53	3	4039.72900	136.30400	93.98793	506.02650	.19828	195.83130
.53	4	534.97510	17.42146	160.92240	143.01620	.32874	145.17980
.53	5	29.41667	200.46440	202.35790	30.80099	.38970	91.92593
.53	6	7611.54200	109.38730	186.39710	922.98370	.11229	191.20560
.53	7	33.76254	231.66330	256.46140.	32.21667	.40882	95.03226
.56	0	251.45600	139.60010	26.25151	121.04560	.21570	106.83480
.56	1	113.04390	149.07290	65.67955	81.75181	.21258	100.33820
.56	2	85.80753	180.92520	88.94839	76.17107	.18587	89.92357
.56	3	2689.83400	31.28771	86.03149	320.63900	.32884	208.80000
.56	4	392.69830	14.20274	167.07700	157.18690	.19976	123.60110
.56	5	14021.49000	115.48680	172.90280	1668.14500	.06364	186.96800
.56	6	55.52728	234.55850	269.34440	40.40245	.42751	96.19608
.59	0	60.17941	142.83800	9.30136	66.53780	.17084	97.78181
.59	1	766.68120	139.77900	35.49643	197.01110	.24826	165.56240
.59	2	2420.59700	30.79823	94.06792	323.02980	.29156	205.26140
.59	3	184.68030	10.59214	169.97100	85.05309	.32087	113.11700
.59	4	17234.49000	114.94230	190.73130	1451.81800	.10277	182.34720
.59	5	313.28130	235.14210	294.28320	198.59590	.09983	110.83330

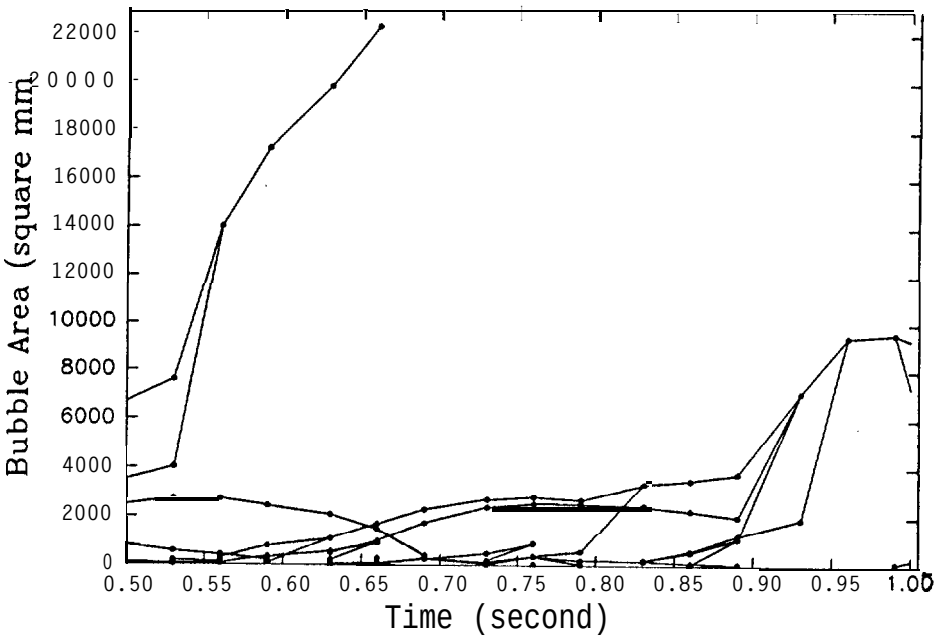

Figure 3-AII2-N1 Cross sectional area of transient bubbles vs **time** under experimental condition II

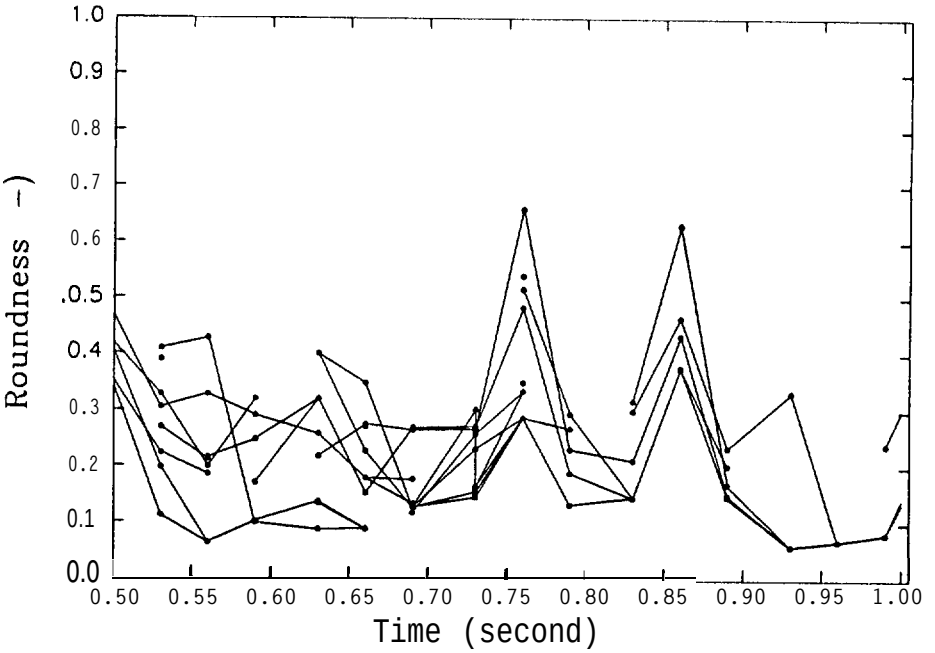

Figure 3-AII3-N1 Roundness of transient bubbles vs **time** under experimental condition II

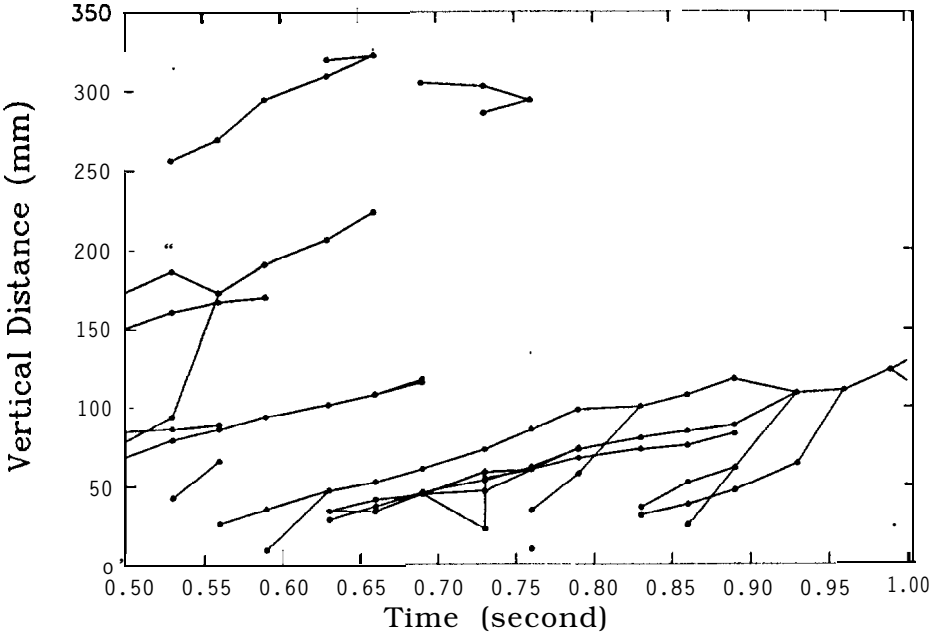

Figure 3-AII4-N1 Vertical distance of transient bubbles under experimental condition II

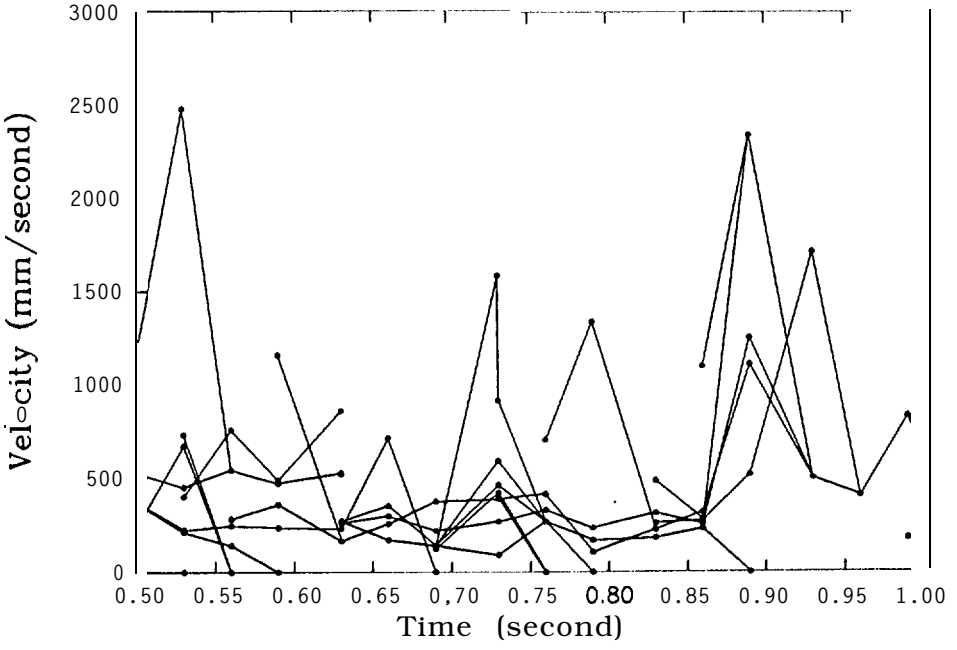

Figure **3-AII5-N1** Velocity of transient bubbles vs time under experimental condition II

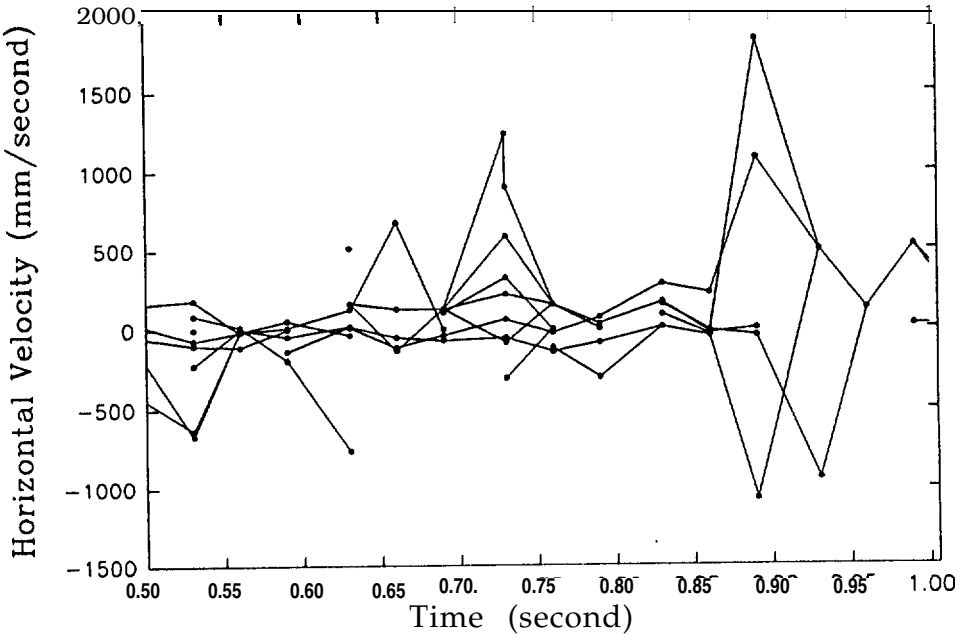

Figure 3-AII6 Horizontal velocity of transient bubbles vs time under experimental condition II

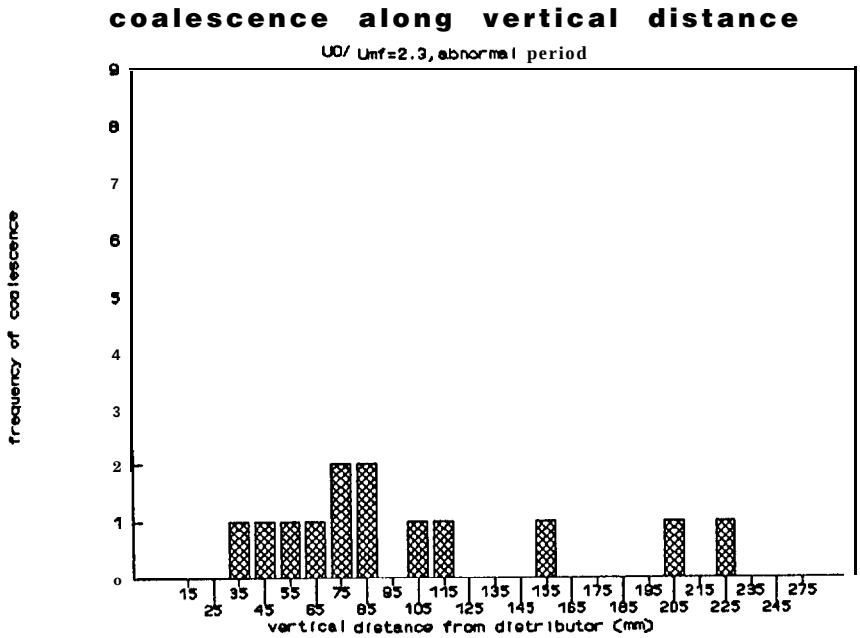

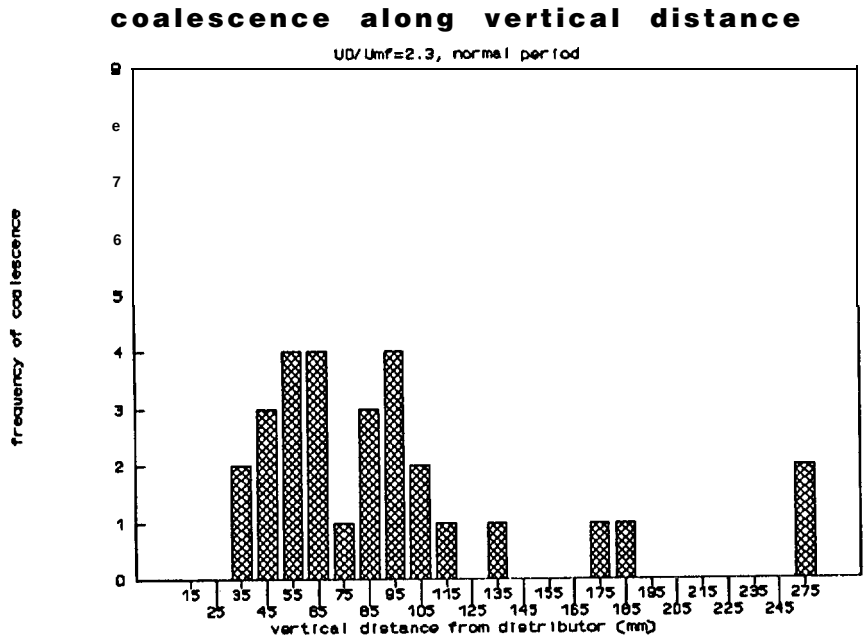

Figure 3-AII7-N&AN Coalescence along vertical distance at $U_0/U_{mf}=2.3$

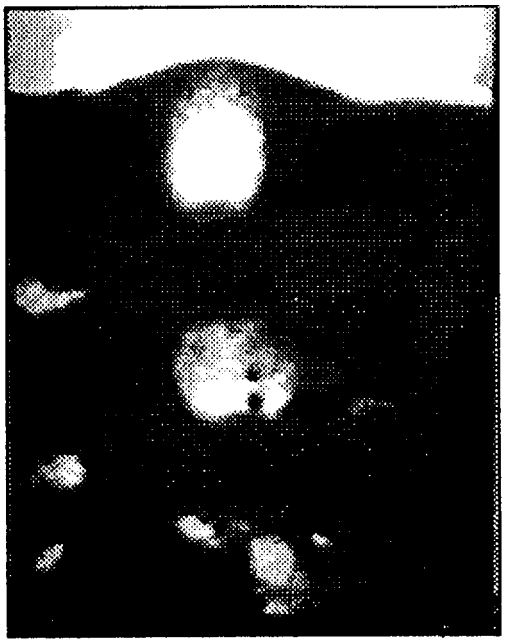

Time = 000.48

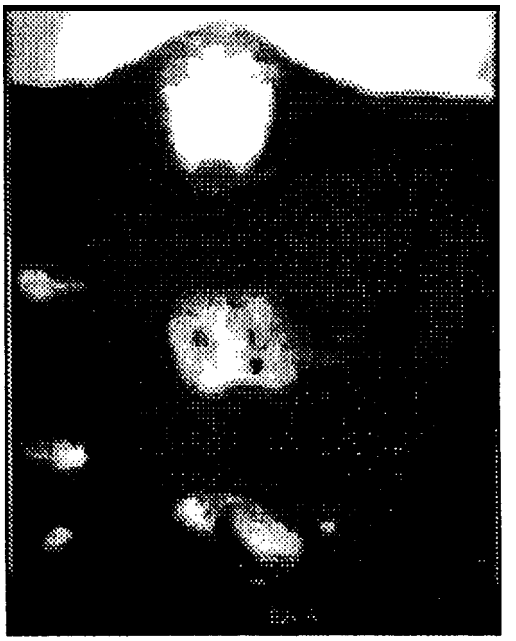

Time = 000.52

Time = 000.55

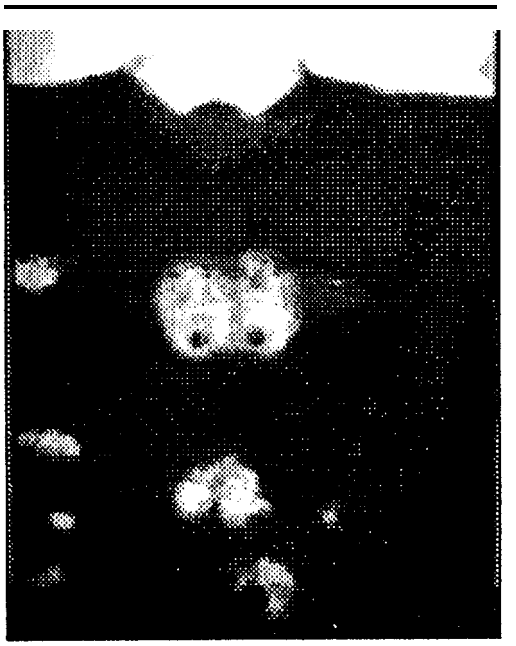

Time = 000.58

Picture 3-AIII-1 Transient bubble images under the experimental condition III

Table 3-AIII Analysis results of bubbles under experimental condition III (t=0.49 to 0.59 second)

Time (Sec.)	Bubble Num.	Area (sq. mm)	Centroid X (mm)	Centroid Y (mm)	Perimeter (mm)	Roundness (o-1)	Gray Avg. (0-256)
.49	0	99.37926	20.91567	35.34586	47.21238	.56037	93.50819
.49	1	39.92069	161.68600	46.03307	31.58971	.50279	116.02740
.49	2	555.70920	137.84910	33.85022	123.95740	.45455	145.39630
.49	3	27.82371	121.39910	53.31796	26.79902	.48692	77.09804
.49	4	227.79650	98.73789	50.72731	85.46259	.39199	145.45930
.49	5	298.82820	28.11324	81.95090	74.77041	.67182	153.45920
.49	6	2524.21600	116.11100	135.64500	241.48450	.54403	172.75920
.49	7	353.25900	16.72626	176.28580	97.75130	.46466	129.24460
.52	0	111.83800	22.34581	45.13594	64.36861	.33926	118.74760
.52	1	38.27355	162.96660	52.58002	33.75721	.42213	102.48570
.52	2	1117.71600	118.76120	53.02041	326.25110	.13198	152.57300
.52	3	310.07390	24.68243	89.69714	148.04240	.17782	151.14340
.52	4	2781.05500	112.91480	150.76210	367.26930	.25913	167.41070
.52	5	298.56400	12.58566	183.15770	173.37880	.12483	129.82280
.55	0	94.46224	24.25288	49.02662	58.22005	.35027	125.44830
.55	1	45.92910	163.89460	55.16701	44.49615	.29156	85.80952
.55	2	1238.15500	113.20720	60.65569	360.23930	.11992	155.94980
.55	3	286.71590	23.65194	91.74124	150.62820	.15883	142.75610
.55	4	3030.10100	111.67400	159.85060	363.42880	.28833	171.58180
.55	5	292.01100	11.39707	184.13520	125.00040	.23489	138.18480
.58	0	220.79720	137.25080	27.58438	68.90353	.58451	125.04950
.58	1	78.70734	26.56037	55.91574	34.09126	.85118	119.82070
.58	2	32.25636	166.49190	60.00721	26.61392	.57237	92.91525
.58	3	1235.79900	110.04550	71.14351	166.44560	.56064	182.98590
.58	4	292.05180	21.33417	97.38242	89.32969	.46000	127.20220
.58	5	295.26460	12.45105	188.51910	74.18017	.67440	122.44970
.58	6	3331.85400	113.67110	171.33940	269.51900	.57648	175.70270

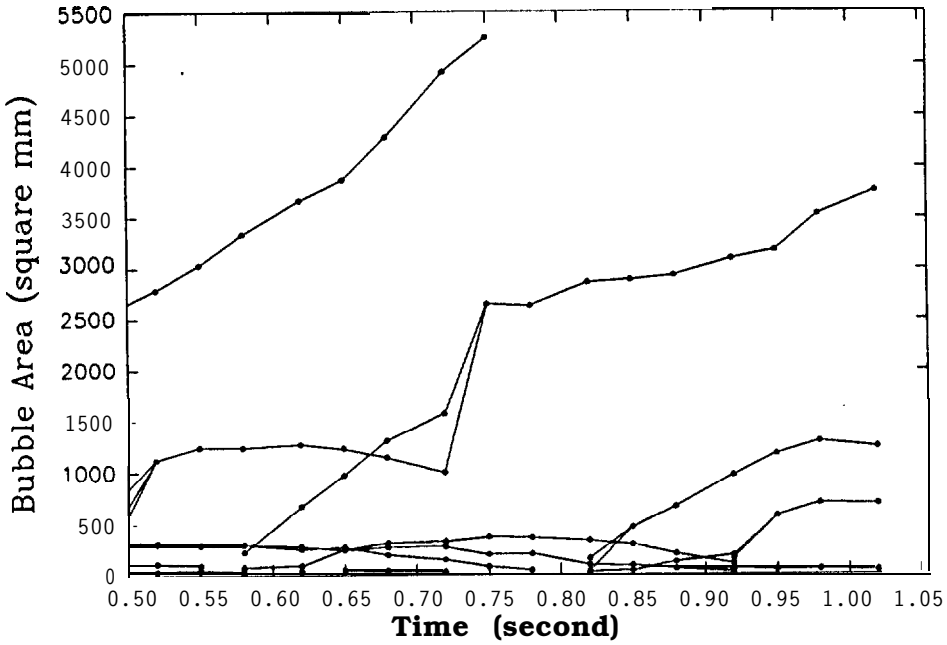

Figure **3-AIII2-N1** Cross sectional area of transient bubbles vs time under experimental condition III

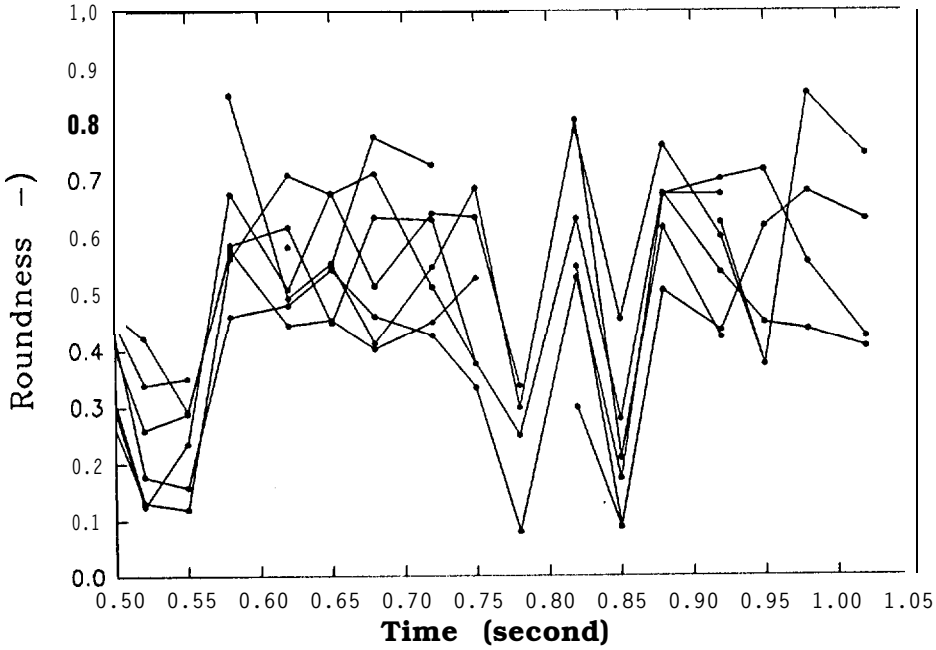

Figure **3-AIII3-N1** Roundness of transient bubbles vs time under experimental condition III

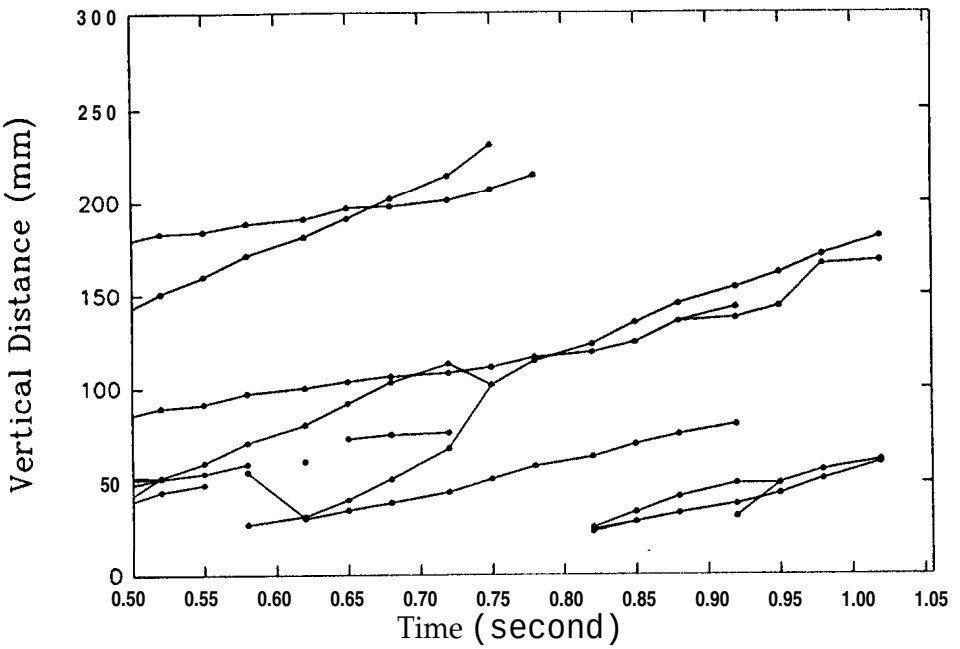

Figure **3-AIII4-N1** Vertical distance of transient bubbles under experimental condition III

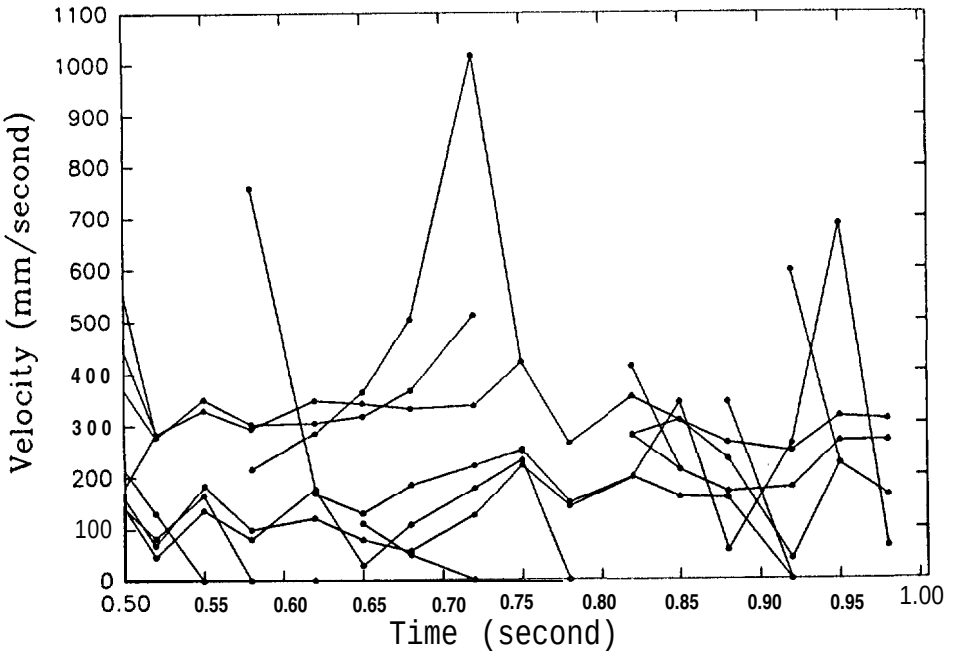

Figure **3-AIII5-N1** Velocity of transient bubbles vs time under experimental condition III

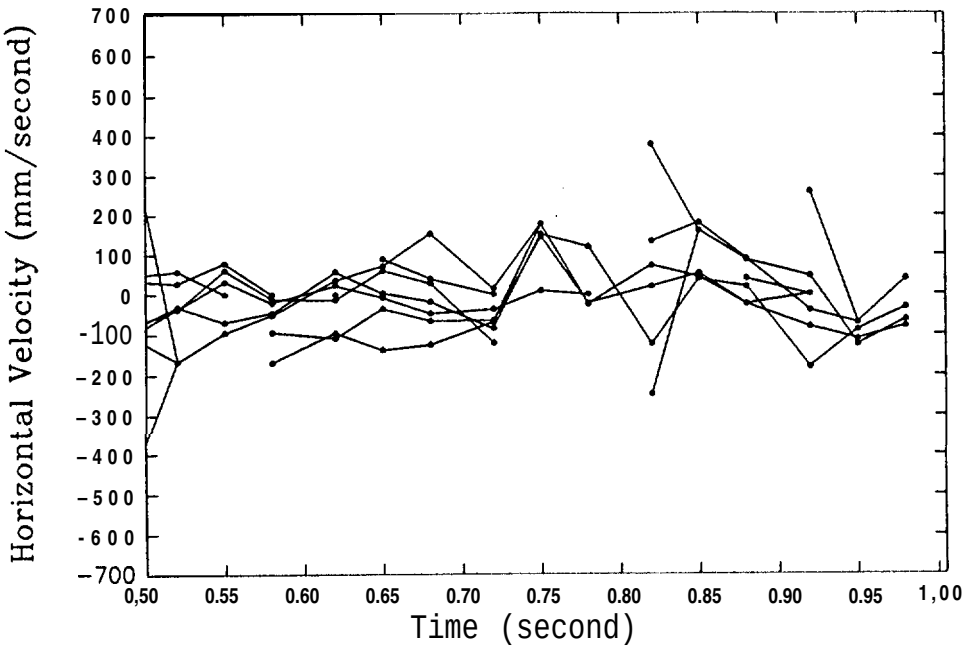

Figure 3-AI **II6-N1** Horizontal velocity of transient bubbles vs **time** under experimental condition III

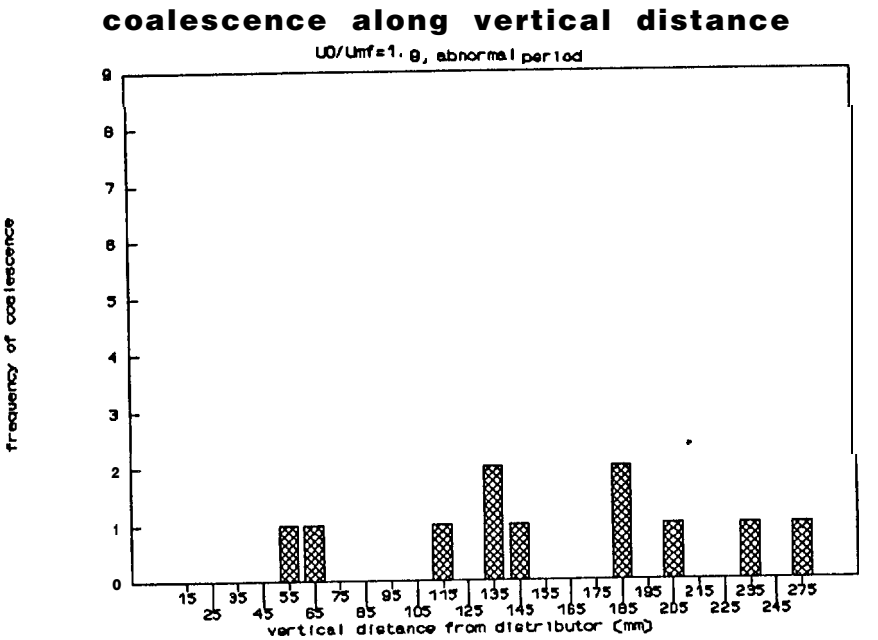

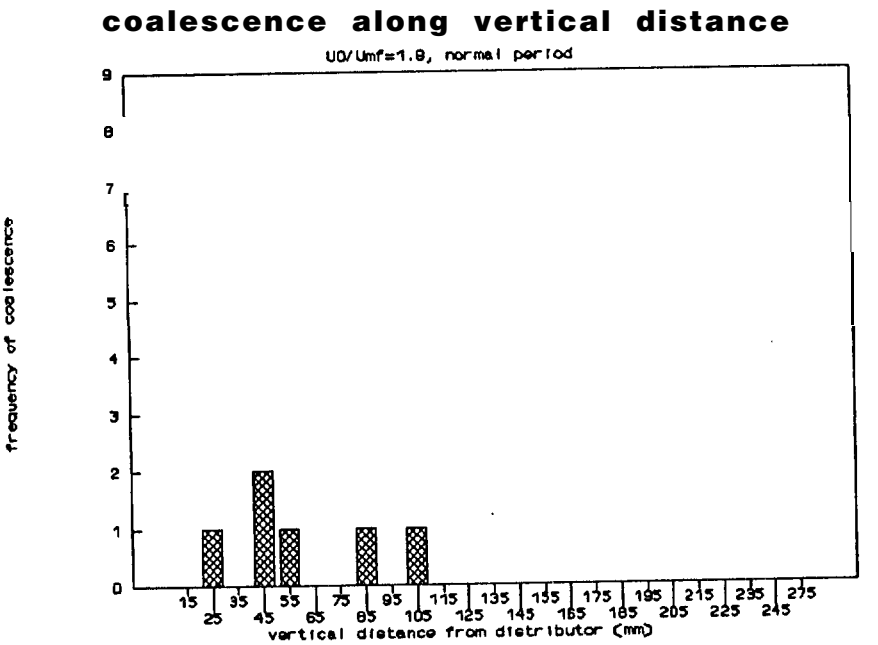

Figure 3-AIII7-N&AN coalescence along vertical distance at U_0/U_{mf}=1.8

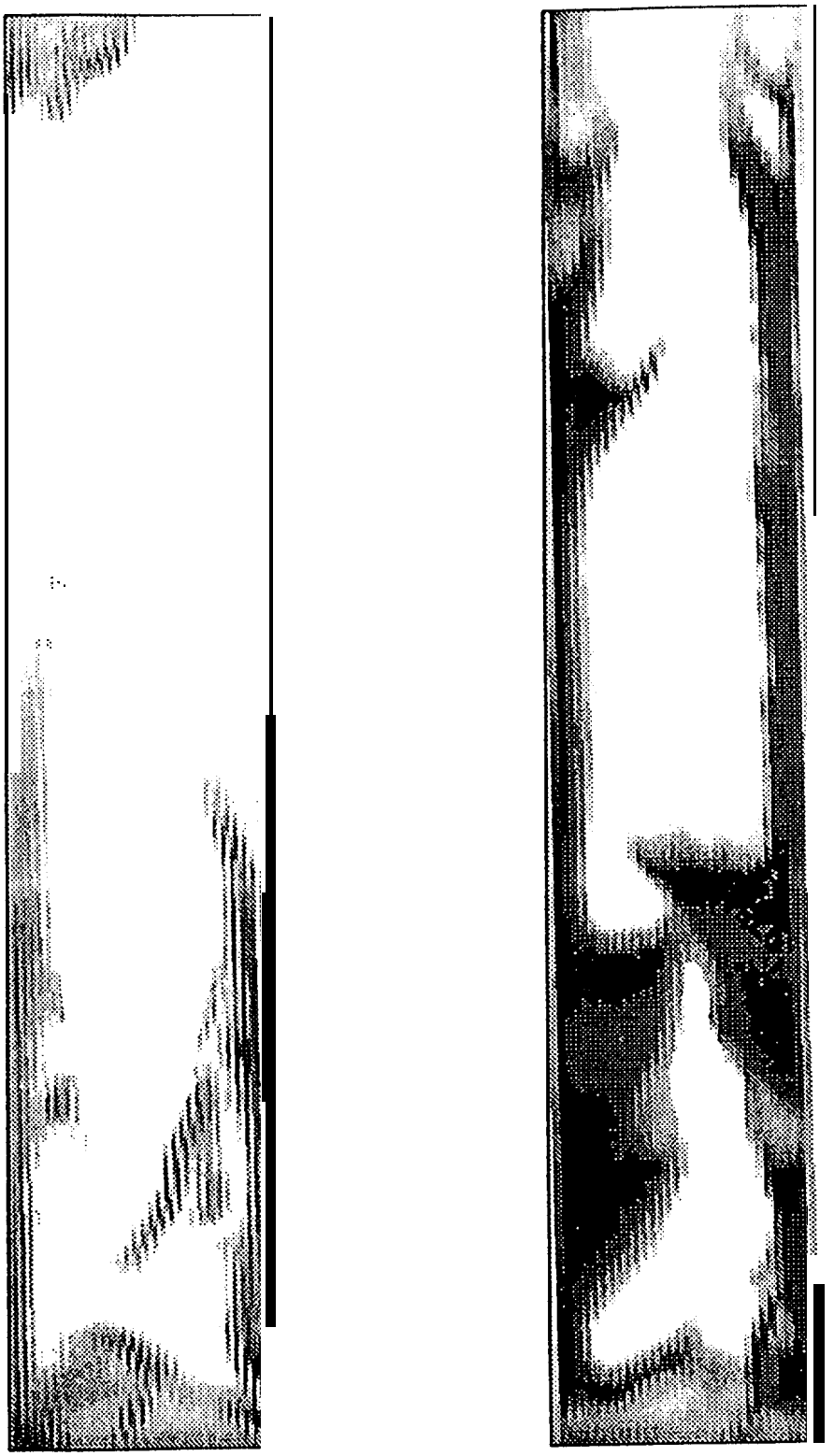

a) U_o/U_{mf}=24 .0 b) U_o/U_{mf}=17 .0

Figure 3.B.1 Images of circulating fluidized bed at different gas velocity

a) T=0.62 Sec. b) T=0.65 Sec. c) T=0.68 Sec.

Figure 3.B.2 Images of circulating fluidized bed at different time sequence

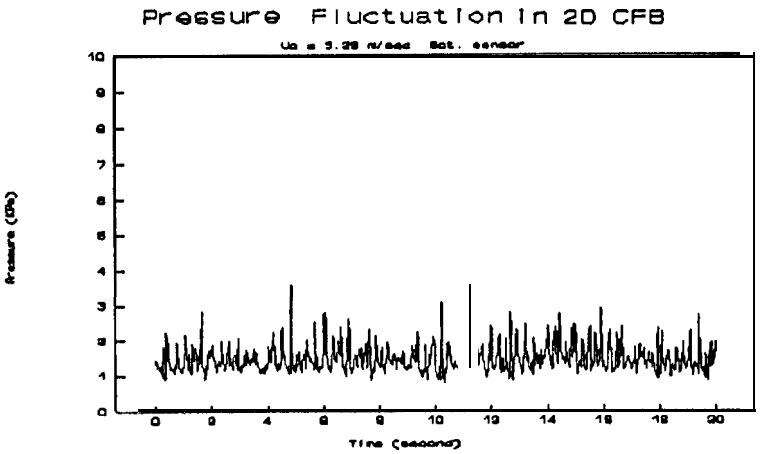

(a) bottom sensor

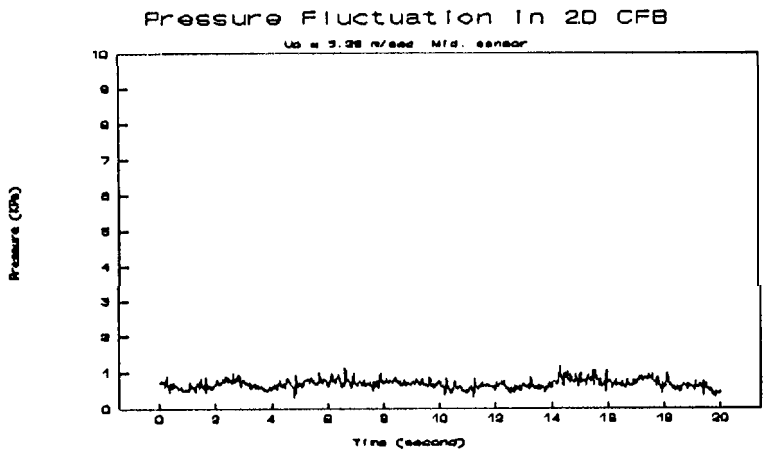

(b) middle sensor

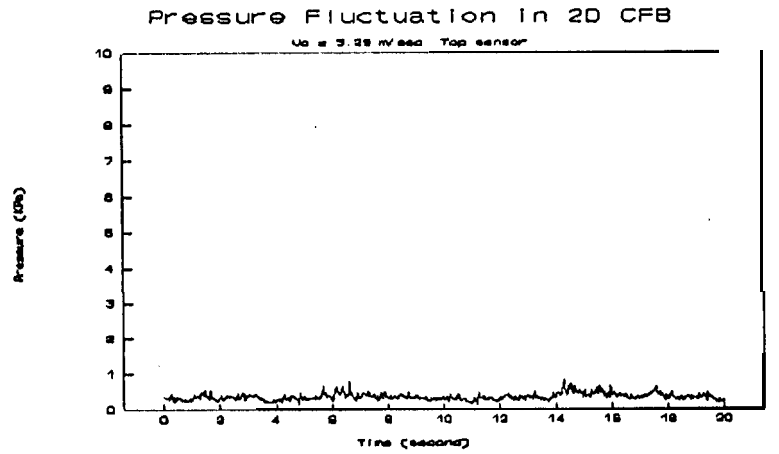

(c) top sensor

Figure 3.B.1 Pressure fluctuation at U_0=5.29 m/s

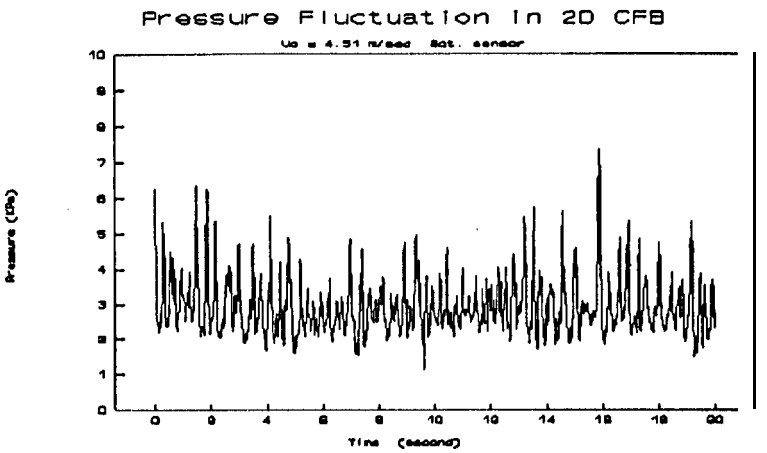

(a) bottom sensor

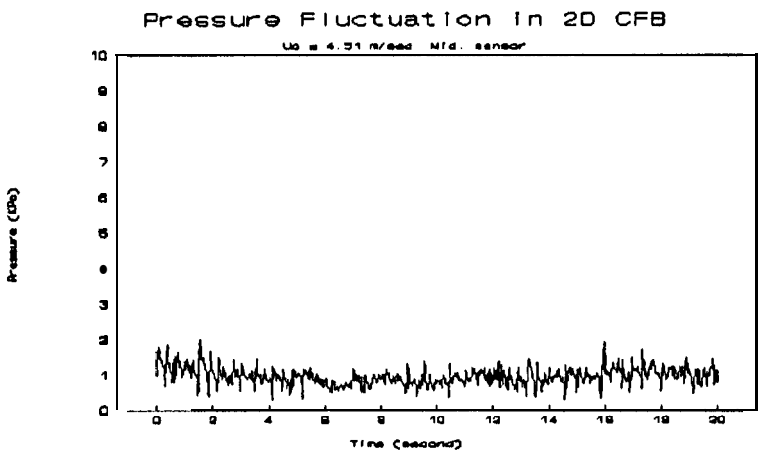

(b) middle sensor

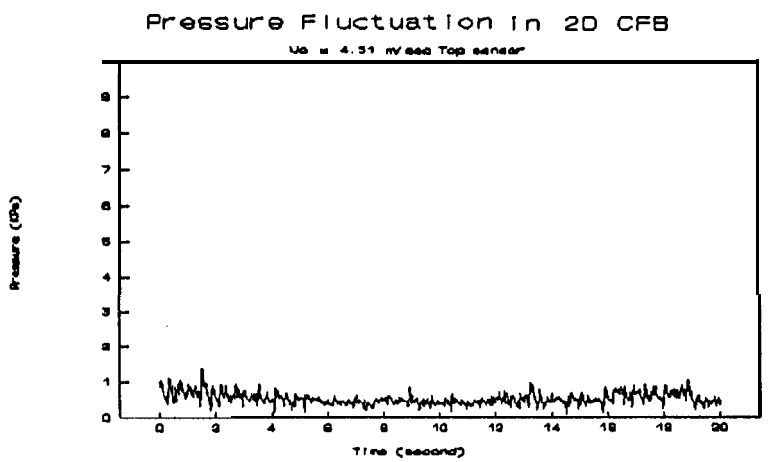

(c) top sensor

Figure 3.B.2 Pressure fluctuation at U_0=4.51 m/s

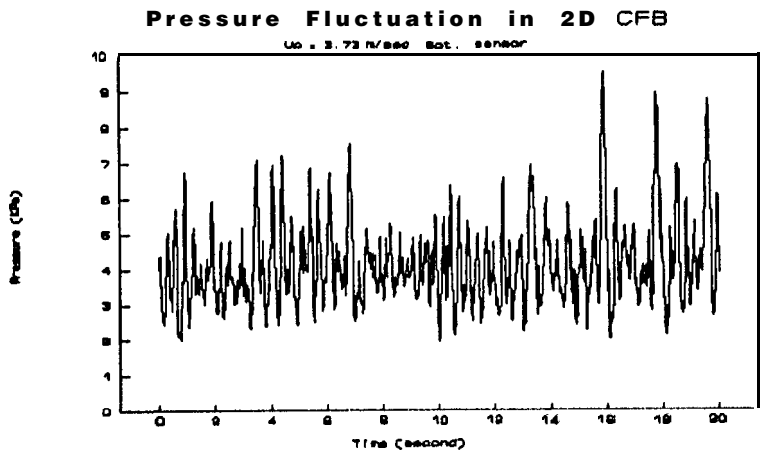

(a) bottom sensor

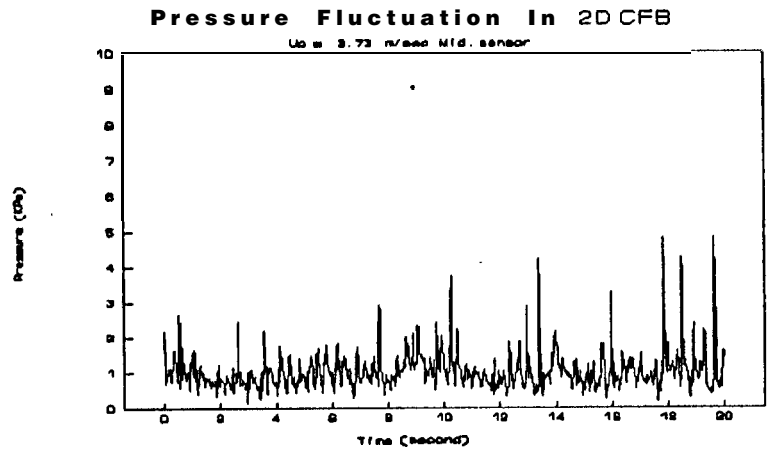

(b) middle sensor

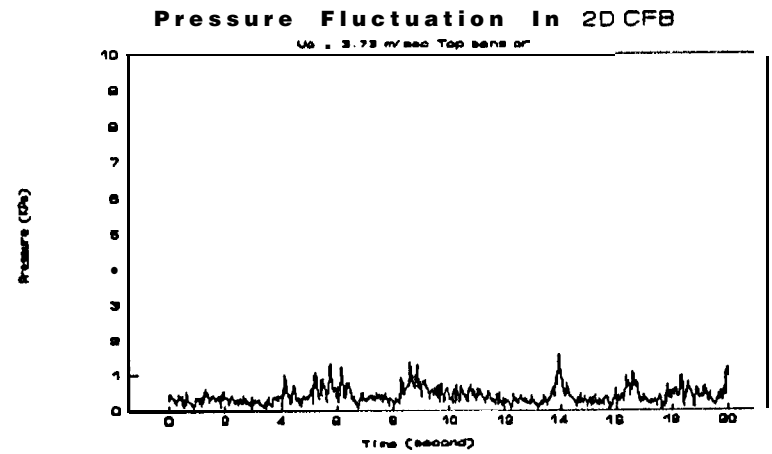

(c) top sensor

Figure 3.B.3 Pressure fluctuation at U_0=3.73 m/s

circulation. As shown in Picture 3. B.1, the emulsion phase was pretty much diluted at gas velocity of $U_0/U_{mf}=24.0$. No bubbles are observed. Circulating was not continuous but in a wave-like manner. For gas velocity of $U_0/U_{mf}=17.0$, typical bubbles were observed. Picture 3.B.2 shows typical images obtained at gas velocity of $U_0/U_{mf}=20.5$ at the time interval of 0.0333 second. While keeping the steady circulating fluidization, bubbles can still be observed at lower region of the fluidized bed. The residence time of particle in the fluidized bed seems to be in the range of 2 to 9 seconds under the fluidization velocity of 3.5 to 5.5 m/s, using the 0.5 mm glass beads as the fluidized particles. Although many papers have been published in relation to circulating fluidized beds, these sets of pictures have not been seen in the past literature.

To characterize the fluidization condition, we measured the transient gas pressure fluctuation at various locations of the two dimensional fluidized beds. Three sensors were used. The pressure from the three sensors were simultaneously measured and synchronized with video image using TTL signal. The results are given as follows (refer to Figures 3.B.1, 3.B.2 and 3.B.3):

(a) The gas pressure fluctuation $(\Delta\Delta P)_g$ increases from the top of the bed towards the bottom of the bed. In other words, the higher the concentration of particles of a specific location, the higher the $(\Delta\Delta P)_g$.

(b) With respect to the gas velocity, the higher the gas velocity, the lower the $(\Delta\Delta P)_g$. It is interesting that the circulating fluidized bed can be stabilized by increasing the gas velocity, judging from the values of $(\Delta\Delta P)_g$. Furthermore, the circulating fluidized beds will be more stabilized by using fine particles.

(c) The average circulation rate and residence time for the above experiments are:

At $U_0=5.29$ m/s, circulation rate is 2.84 kg/rein, residence time is 1.74 seconds.

At $U_0=4.51$ m/s, circulation rate is 2.60 kg/rein, residence time is 4.47 seconds.

At $U_0=3.37$ m/s, circulation rate is 2.48 kg/rein, residence time is 8.01 seconds.

The pressure signals were further analyzed by Power Spectrum of Frequencies. Discrete Fourier Transform of binary pressure data (in volts) were computed with a fast Fourier transform algorithm. The power spectral density, a measurement of the energy at various frequencies was also computed for these pressure signals. Results show that the power density has higher values at low frequencies (< 5). The powder density curve appears to have a peak at a low frequency (around 2 to 3) for the signals from bottom sensor. But for the signals obtained from the top sensor, the peak of the power

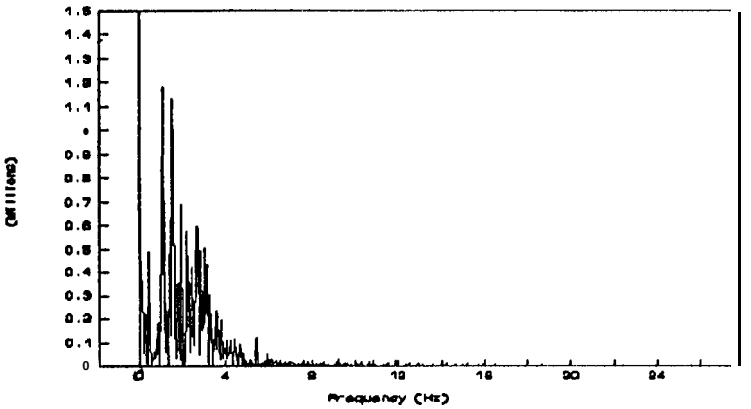

(a) bottom sensor

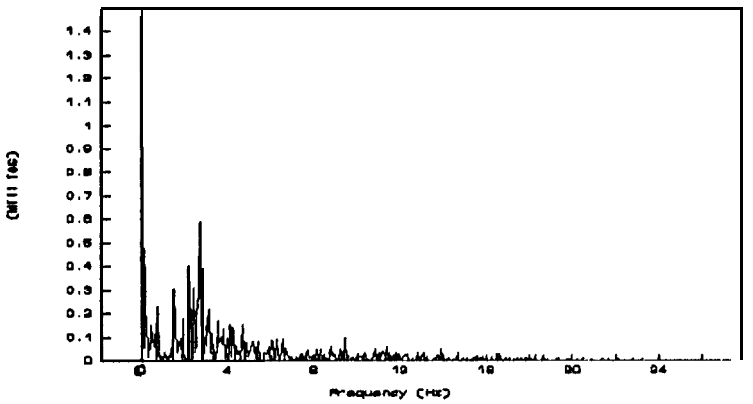

(b) middle sensor

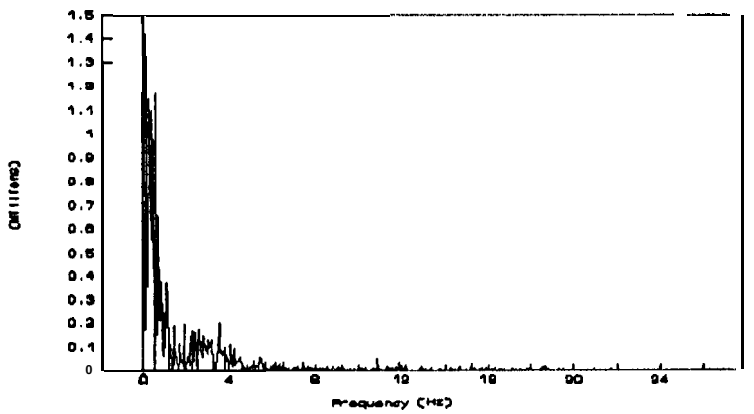

(c) top sensor

Figure 3.B.4 Power spectrum of frequency at U_0=5.29 m/s

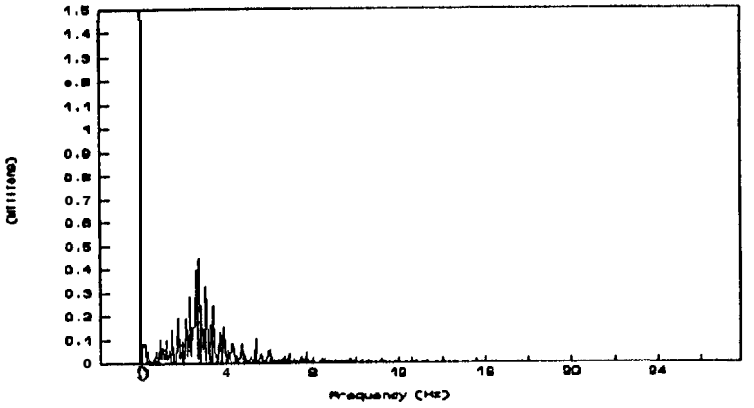

(a) bottom sensor

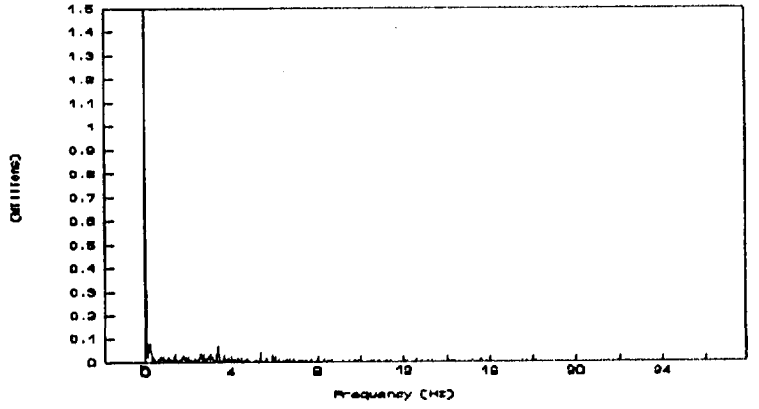

(b) middle sensor

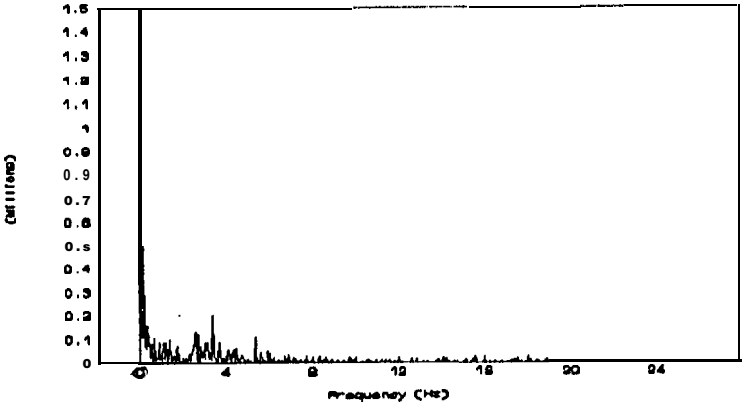

(c) top sensor

Figure 3.B.5 Power spectrum of frequency at U_0=4.51 m/s

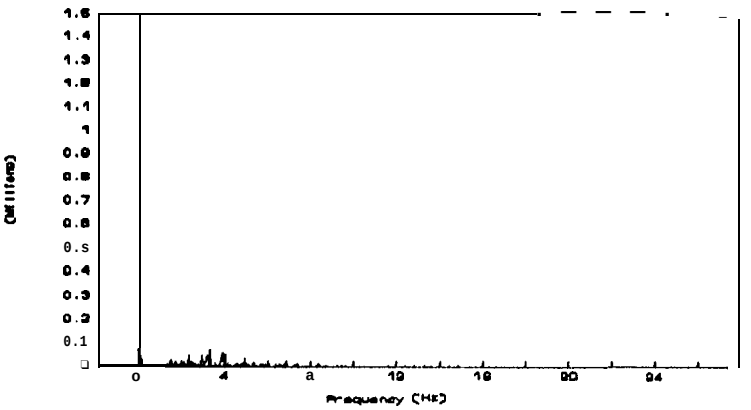

(a) bottom sensor

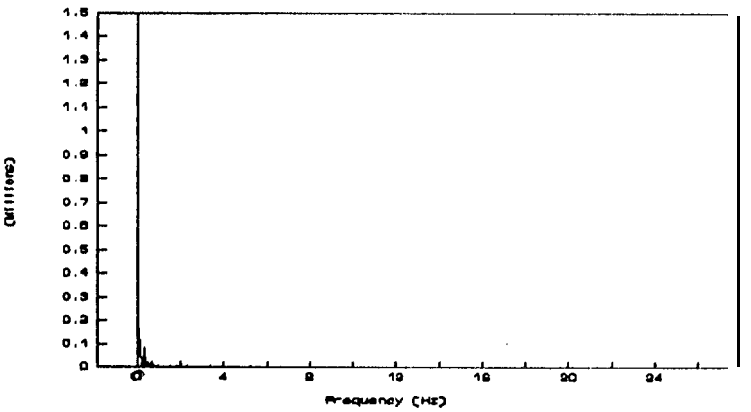

(b) middle sensor

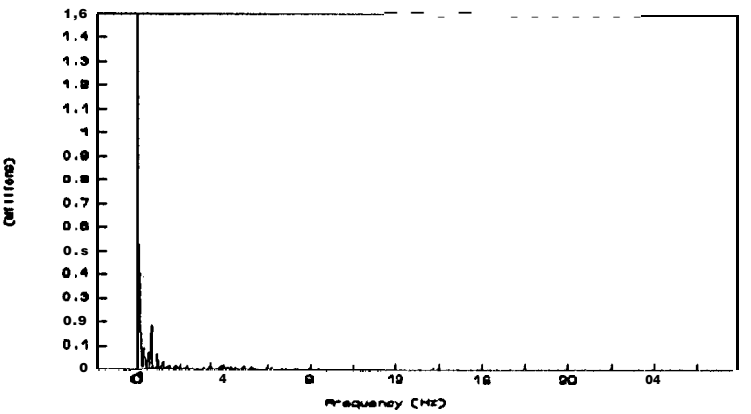

(c) top sensor

Figure **3.B.6** Power spectrum of frequency at U_0=**3.73** m/s

density curve moved very close to zero (See Figures 3. B.4, 3.B.5 and 3. B. 6).

3.C Fluidization Pressure Effect on the Transient Behaviors

Transient bubble motion in pressurized fluidized bed was investigated by measuring the stochastic gas phase pressure transient fluctuation in the bed. A two dimensional fluidized bed unit (100 mm X 500 mm X 12 mm) was installed in a pressurized vessel to accomplish a pressurized fluidization. The fluidized particles are 1 mm glass beads. The gas distributor is the same as the one used for ambient pressure two dimensional fluidized bed. The fluidization conditions were maintained under the following conditions:

U_0/U_{mf}=1.8, 200, 2.3
P=1 to 4 atm
Bed aspect ratio=1.0

glass beads with diameter of 0.5. were used, which have the U_{mf} as follows:

0.46 m/s at 1 atm
0.38 m/s at 2 atm
0.33 m/s at 4 atm

Because a lot of experimental data of transient pressure fluctuations and images have also been accumulated for ambient pressure conditions, transient bubble motion under pressurized conditions be predicted by comparing the pressure fluctuations at the experimental condition with the corresponding ones at ambient pressure. Figure 3.C.1 gives the pressure fluctuations under different operating pressures at U_0/U_{mf}=2.0. It can be seen that the pressure fluctuation under the pressurized conditions and also under the same fluidization condition (U_0/U_{mf}=2), the bigger the pressure fluctuation $(\Delta\Delta P)_g$, the higher the pressure. The motion of the solid particles got better in higher operation pressure. The pressure effect on the gas pressure fluctuation could be observed from Figure 3.C.1.

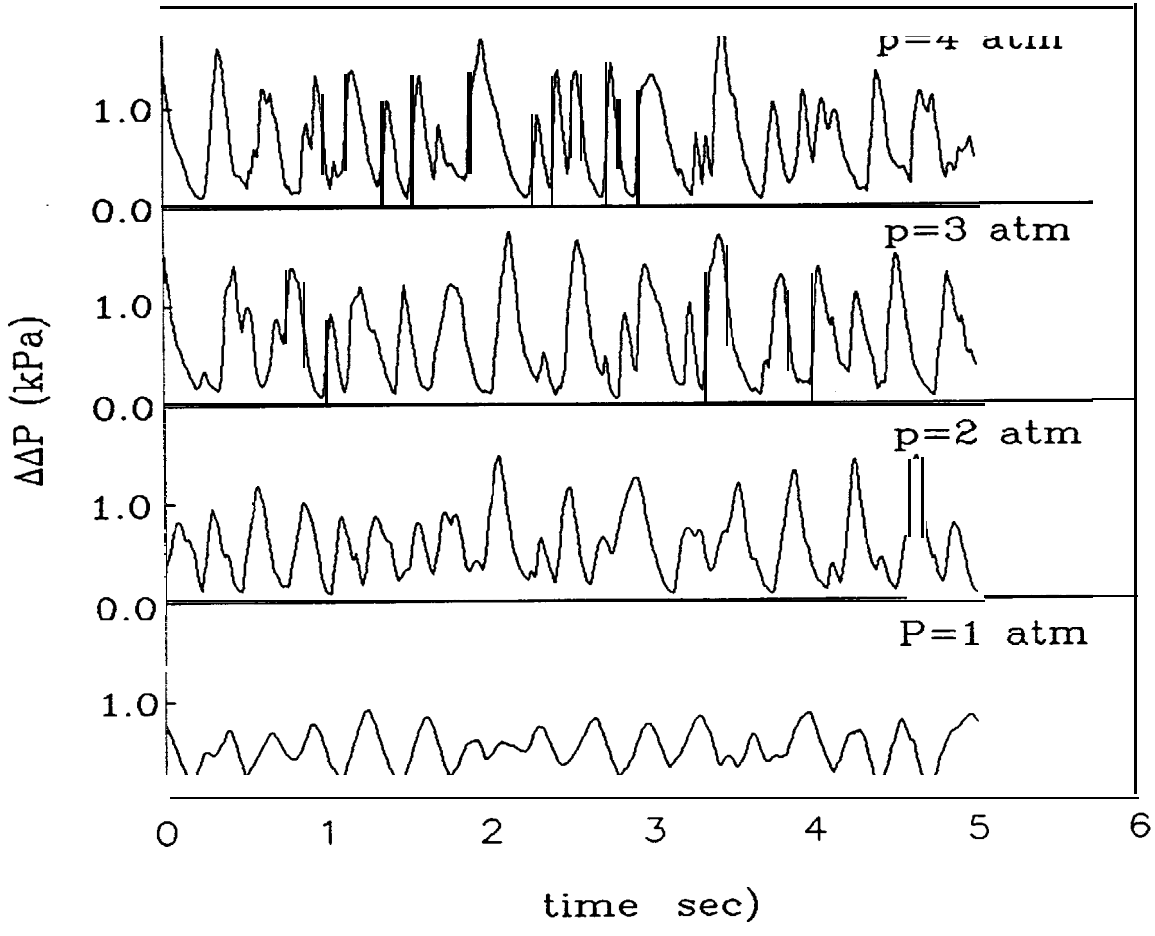

Figure 3.C.1 Pressure fluctuations at different operating pressure

3.D Comparison of Two and Three Dimensional Fluidized Beds

3.D.1 Comparison of two and three dimensional fluidized beds

The discussions of two and three dimensional fluidized bed have a pretty long history, and frequently two dimensional fluidized bed was criticized due to its wall effect. However, there has been no quantitative conclusion. Through the study of this work, we found a very interesting index of fluidization, i.e., transient gas stress in the emulsion phase $(\Delta\Delta P)^{\#}$, which was defined the transient pressure difference between two points horizontally located. The theoretical meaning of $(\Delta\Delta P)^{\#}$ can be interpreted as the intensity of transient bubble interaction. When a few gas bubble are injected into an incipient fluidized bed, the $\Delta\Delta P^{\#}$ should be zero. ($\Delta\Delta P^{\#}=0$ is the assumed oversimplified condition of classical two phase flow theory.)

Now $(\Delta\Delta P)^{\#}$ was experimentally measured in three dimensional fluidized bed (0.10m I.D.) and in a two dimensional fluidized bed (height 1.00m x width 0.254m x thickness 0.012m). The $\Delta\Delta P^{\#}$ in three dimensional fluidized bed is shown in Figure 3.D.1 and the $\Delta\Delta P^{\#}$ in the two dimensional fluidized bed is shown in Figure 3.D.2 and Figure 3.D.3. In case of three dimensional fluidized bed, the pressure difference between the center and wall of the vessel was defined as $(\Delta\Delta P^{\#})$, and in case of two dimensional fluidized beds, (P_4-P_1) and (P_4-P_5) were defined in Figure 2.3.2. Although some wall effects were observed in two dimensional fluidized beds, the basic behavior of $\Delta\Delta P^{\#}$ seems to be substantially comparable for the cases under which the experiment was conducted. Judging from those three figure's results, the transient bubble interaction intensity was found to be not much different each other so that the wall effect of two dimensional fluidized bed should not be very critical.

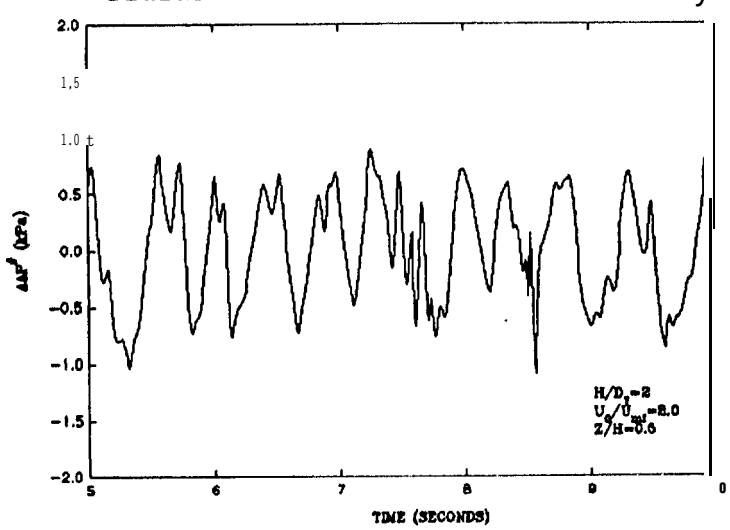

Figure 3.D.1 Pressure difference between two horizontal points

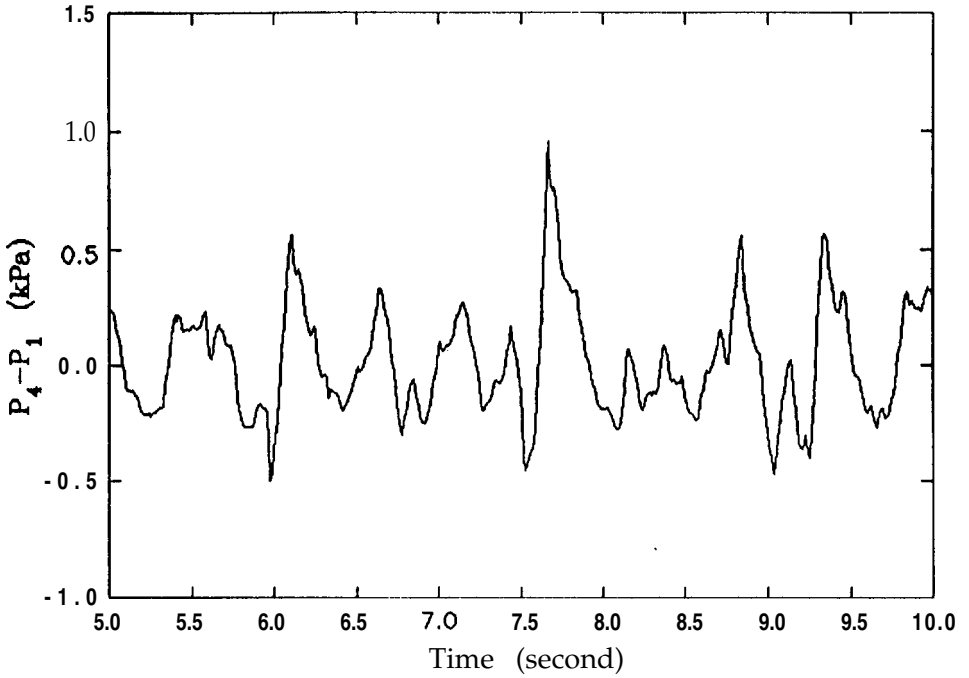

Figure 3.D.2 Pressure difference between P_4 and P_1 vs time

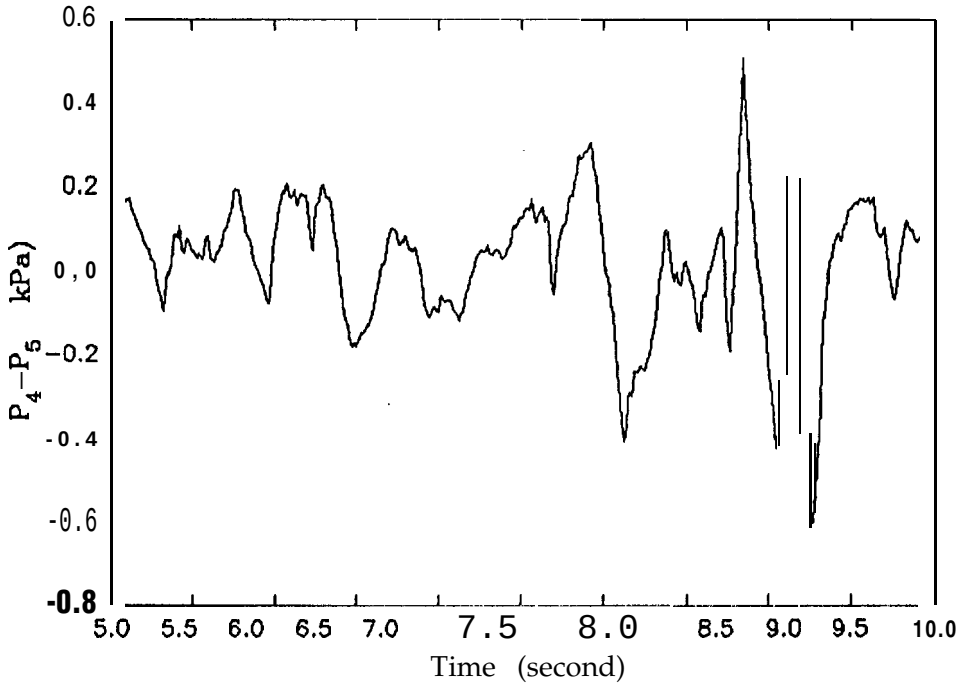

Figure 3.D.3 Pressure difference between P_4 and P_5 vs time

3.D.2 Relation between $(\Delta\Delta P)_{max}$ AND $(\Delta\Delta P)^{\#}_{max}$

As the physical meaning of (Ml?) # was clarified in the preceding section, the physical meaning of gas phase pressure fluctuation between bed center against outside atmosphere $\Delta\Delta P$ should also be defined.

A cylindrical fluidized bed with a diameter of 108 mm and height of 1500 mm was used. A sintered plate with average hole opening of 150 μm was located at the bottom of the bed as the gas distributor. Air is introduced through the porous distributor as fluidizing gas. The fluidized particles used was glass beads of averaged diameter of 1 mm (particle density: 2.49 g/cm^3; minimum fluidization velocity: 0.46 m/s).

Pressure fluctuation was taken by differential pressure transducer (Validyne P305D) which had two input channels and produces an output voltages proportional to the pressure difference between the two input channels. During the measurement, pressure probes were inserted into the specific locations of interested. Then pressure fluctuation signals were sent through the pressure transducer and A/D convertor into computer for storage and analysis. An IBM PC computer was used for pressure fluctuation data acquisition and processing. The data acquisition system has the capability of storing up to 20,000 data points at any sampling rate between 10 to 28,000 Hz. It could store the data to a floppy disk. The maximum response frequency of the transducer used in this study was 200 Hz. From preliminary experiment measurement, the appropriate sampling rate was 100 Hz and sampling time was 60 second in order to get reproducible and representative data.

Two methods taking pressure fluctuation were used during the experiment. One method was to detect the pressure fluctuation at a single point, e.g. , at center of the cross section of the fluidized bed. The other method was to measure two horizontal points pressure difference, e.g., between the center point of the cross section of the bed and the point at wall. Then the analyzed results obtained by these two methods were compared. Two vertical positions were used to measure the pressure fluctuation described above. One position was at the bottom of the bed, i.e., close to the gas distributor (Z/H=0) . The other position was at the middle of the height of the fluidized bed (Z/H=0.5). The bed aspect ratios (H/D) were chosen as follows: 1.0, 2.0 and 3.0. The gas velocities (U_0/U_{mf}) used are: 1.3, 2.0 and 2.4.

Figure 3.D.4 shows the pressure fluctuations of two horizontal points at wall and center of the cross sectional area. The experimental conditions were the bed aspect ratio of 2 and measured at the middle position of the bed height (Z/H=0.5). We could see that the intensity of pressure fluctuation increased as the superficial gas velocity increased.

Previously Kono (Kono et al., 1989) developed a novel technique using transient pressure fluctuation to correlate the maximum transient forces in fluidized beds. Using fracture sensitive sensor particles, the relationship was found between the maximum transient force and the maximum pressure fluctuation. The maximum of transient gas pressure fluctuation MP, which represented the intensity of pressure fluctuation or the transient solid particle force, could be calculated taking the difference between transient highest gas pressure and transient lowest gas pressure following the above highest pressure. Figures 3.D.5 and 3.d.6 show the superficial gas velocity effect on maximum pressure fluctuation. It could be seen clearly that for different bed aspect ratios the higher the gas velocity the higher the maximum pressure fluctuation. Figure 3.D.5 is for case of two horizontal points. Figure 3.D.6 is for the case of single point measurement, which shows the same tendency as Figure 3.D.5. Figures 3.D.7 and 3.D.8 present the bed aspect ratios effect on the maximum pressure fluctuation for both single point and two horizontal point measurement at different superficial gas velocity. Like the gas velocity effect, the bed aspect ratio had the same effect on the maximum pressure fluctuation. When high bed aspect ratio was used, the higher maximum pressure fluctuation was observed and hence the higher transient solid particle force was prevailing in the fluidized bed.

Results of maximum pressure fluctuation measured by two different methods, i.e., single point measurement and two horizontalpoint measurement, are shown in Figure 3.D.9. The horizontal pressure fluctuation was very significant. The maximum pressure fluctuation by two horizontal point measurement was found to be approximately 1/2 of the maximum pressure fluctuation by single point pressure fluctuation.

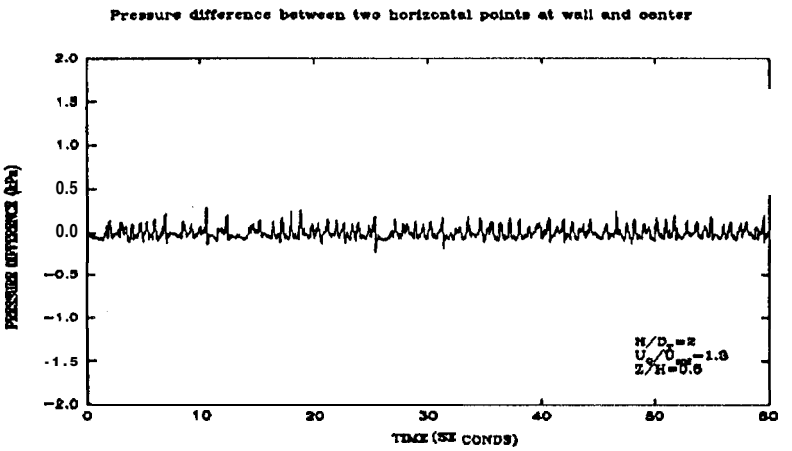

(a) U_0/U_{mf}=1. 3

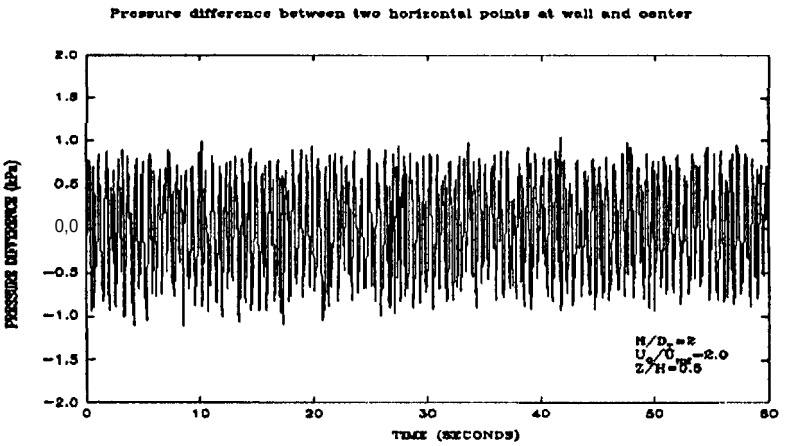

(b) U_0/U_{mf}=2.0

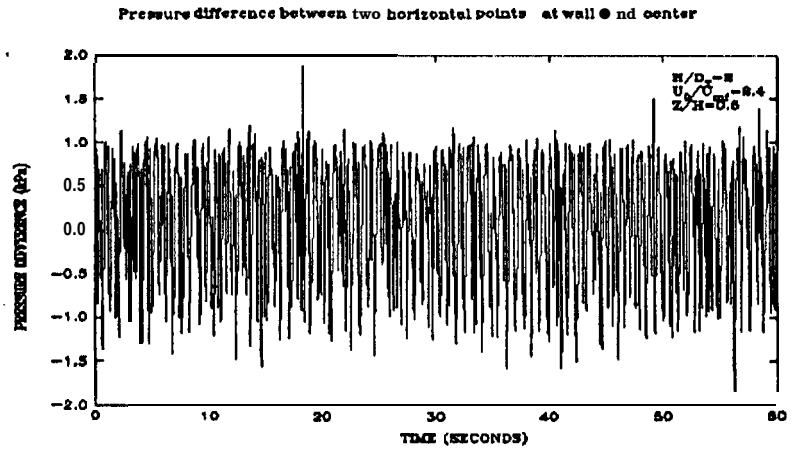

(c) U_0/U_{mf}=2 .4

Figure 3 .D. 4 Pressure fluctuation for three dimensional bed

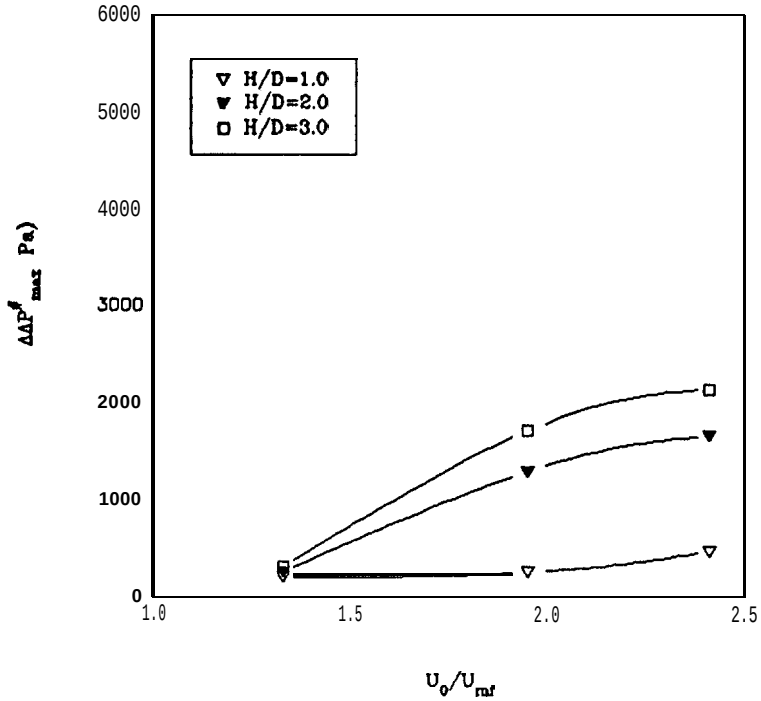

Figure 3.D.5 $\Delta\Delta P^{\#}$ vs gas velocity for two horizontal points (Z/H=0.5)

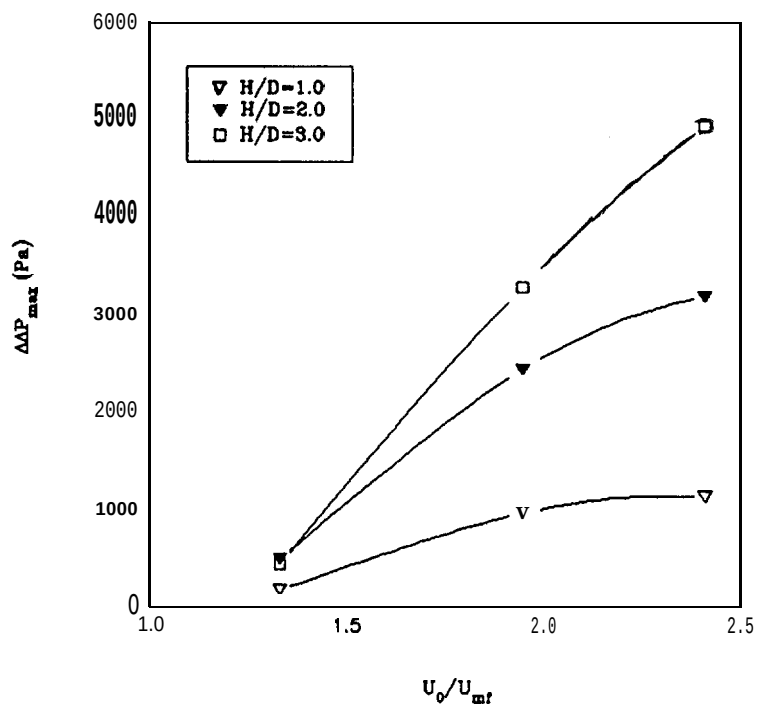

Figure 3.D.6 $\Delta\Delta P_{max}$ vs. gas velocity for single point (Z/H=0.5)

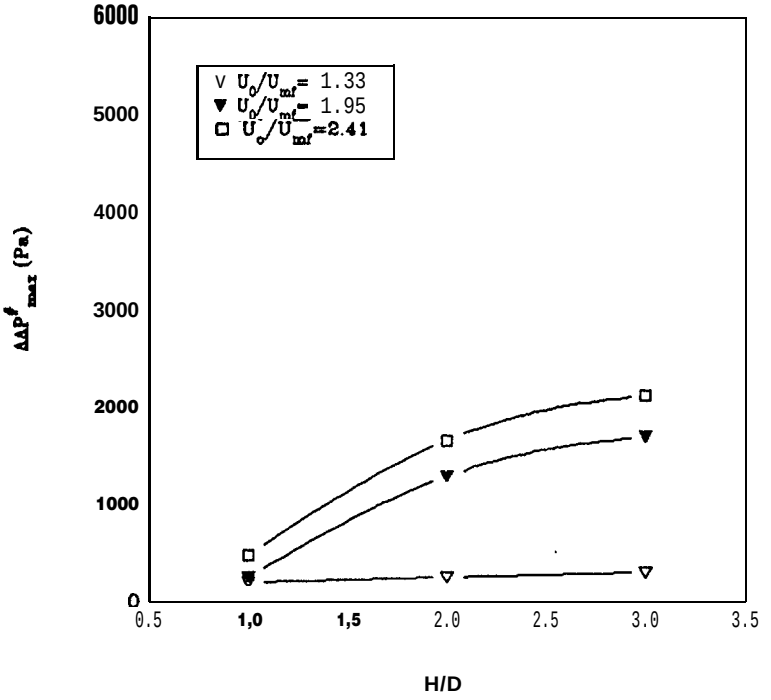

Figure 3.D.7 $\Delta\Delta P^{\#}$ vs bed height for two horizontal points (Z/H=0.5)

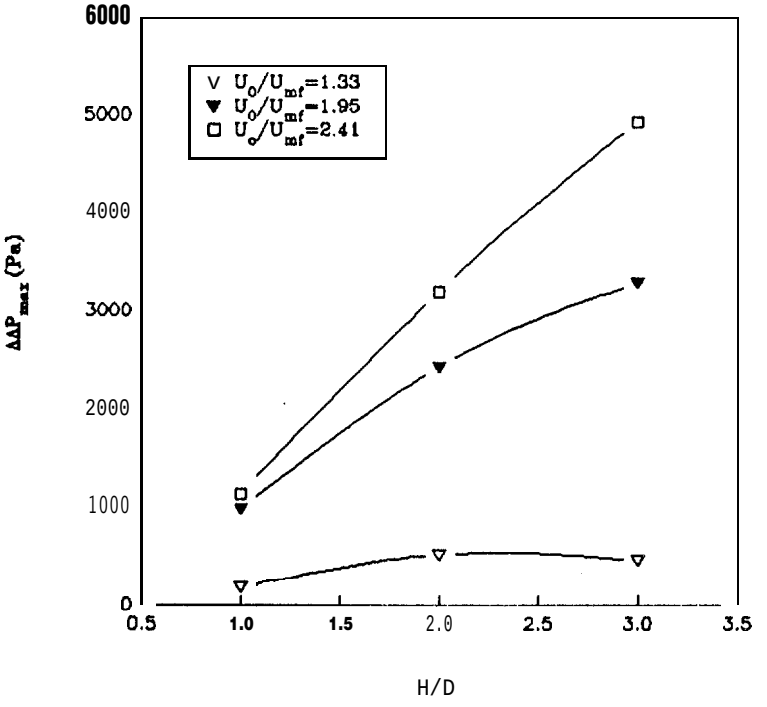

Figure 3.D.8 $\Delta\Delta P_{max}$ vs. bed height for single point (Z/H=0.5)

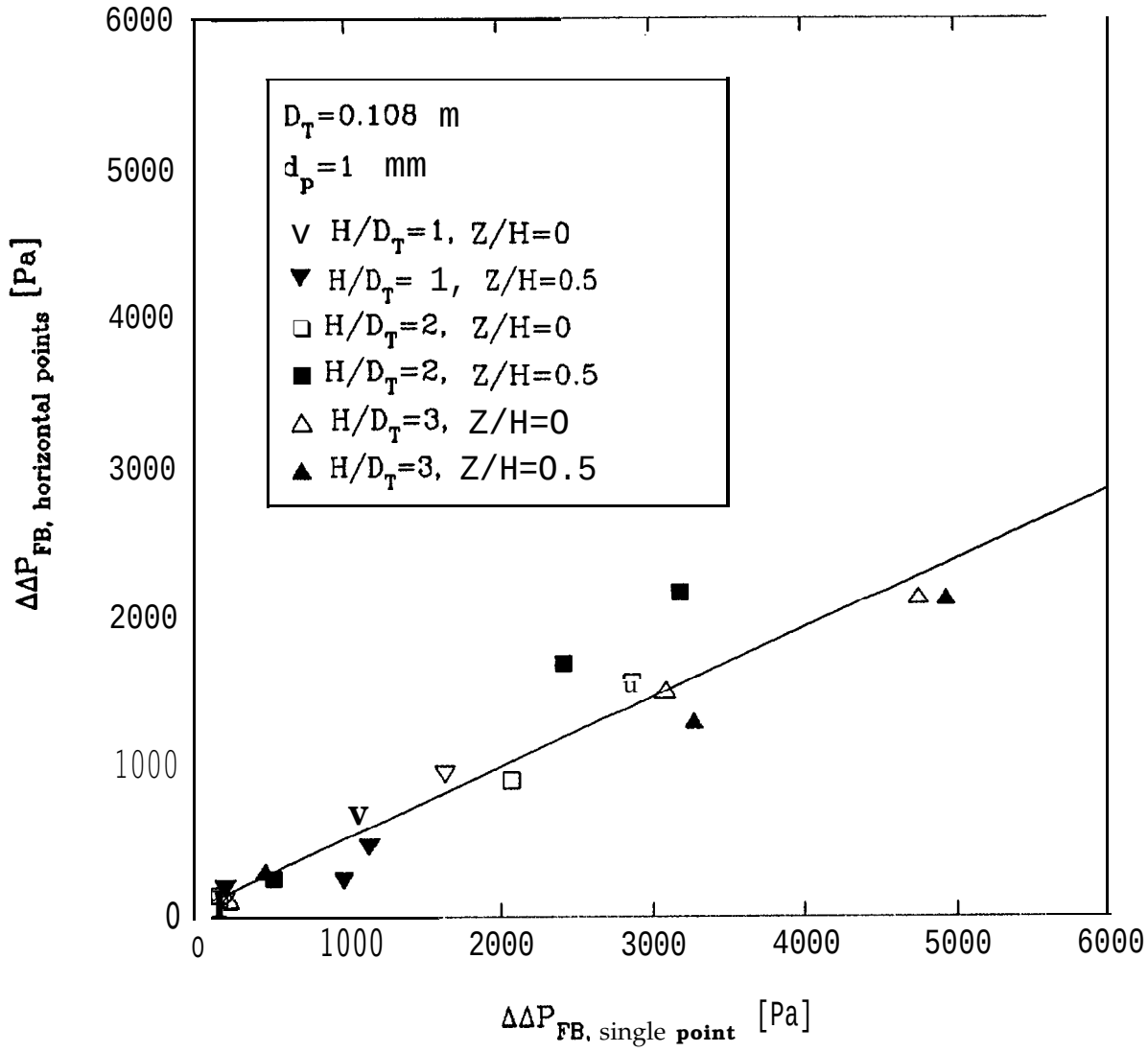

Figure 3.D.9 Comparison of single point $\Delta\Delta P_{max}$ vs two points $\Delta\Delta P^{\#}_{max}$

4. EROSION: AN INDEX TO THE TRANSIENT MOTION OF SOLIDS IN FLUIDIZED BEDS

4.1 Introduction

One of the important aspects of fluidization is its stochastic nature: the behavior of gas and solid particles in fluidized beds is fully transient. These transient characteristics are most important to describe the basic features of fluidized beds which have not been taken into consideration in past classical fluidization research. A vital consequence of the transient solid particles motion is the so-called erosion phenomena which has frequently been a major operational problem.

As is well accepted, the assessment and prevention of the erosion of in-bed tubes is a critical engineering problem especially for the design of fluidized bed combustors. However, there has been no practical answer nor quick remedy for this problem. On the other hand, in view of engineering science research, the erosion phenomenon is interesting because it can provide a very important picture of intrinsic fluidization mechanisms.

The objective of this study was to develop a predictive model for the erosion rates of different in-bed tube materials in fluidized beds. The approach consists of the following three major steps: (1) development of a working model by assuming that the erosion rates, defined as erosion index (I) , should be a function of the maximum forces of solid particles which are in transient motion in the fluidized bed and the mechanical properties of tube material and the fluidized particles, (2) measurement of both the erosion rates of several different in-bed tubes under various fluidization conditions and the maximum force of solid particles; (in these experiments, the mechanical properties of the test tubes and fluidized particles are intentionally changed by selecting different materials), (3) introduction of an erosion rate equation with a dimensionless erosion characterization number based upon the principles of solid state fracture theory, (4) The effect of elevated temperature on the errosion rate, i.e., first by the change of properties of materials and secondly by the change of the maximum force prevailing due to the change of temperature.

In general, the removal of materials from a solid surface by the action of hitting solid particles is termed as erosion. Therefore, erosion rates of in-bed tubes are affected by: 1) the properties of the in-bed tube material such as tensile strength, modulus of elasticity, etc; 2) the properties of fluidized particles such as particle size and size distribution, shape factor, etc.; 3) operating conditions such as fluidizing velocity, temperature and pressure.

In the early stages of the development of fluidized bed

technology, researchers did not pay too much attention to erosion. However, as larger scale equipment and larger capacities handling coarse solid particles were utilized, a severe wear of in-bed tubes was encountered. Thus, detailed studies on erosion became necessary particularly in relation to fluidized bed combustors. Some researchers (Lyczkowski and Bouillard, 1991; Ding and Lyczkowski, 1992; Nesic and Postlethwaite, 1991) proposed erosion models that aimed to describe both solids and gas transient motions. Others (Levy et al., 1992 and Finnie, 1972) approached the problem experimentally by measuring the erosion rates of in-bed tubes under certain operating conditions with specific scale and configuration.

Despite the voluminous published literature, it has still been impossible to at least explain the erosion phenomenon completely. As a consequence, it is difficult for engineers to design a fluidized bed with minimized erosion problem.

In this study, a unique characterization method was developed to assess the erosion rates of in-bed tubes. Unlike the conventional erosion measurement methods that consider only weight loss or diameter change and operating time, this method defines an erosion rate index considering surface area, weight loss of in-bed tubes and operating time.

The characterization method of the maximum transient forces of solid particles in fluidized beds was first developed by Kono et al. (1987). They presented that there is a correlation between the maximum of gas pressure fluctuation and the maximum force prevailing in a fluidized bed. Here, that method was further improved for the erosion study. The maximum force concept was refined to take frequency into account. In other words, the average of the top five maximum forces, which takes both the maximum and the frequency into account, was used for the assessment of the transient forces of solid particles as an index for erosion.

Systematic studies were carried out in a 4" rectangular fluidized bed to study the relationship between erosion rates and the peaks of the transient forces of solid particles in fluidized beds. Three different kinds of metal tubes with well defined tensile strength (σ_t) and modulus of elasticity (E) were used. They are copper, aluminum (alloy) and stainless steel. By considering the tensile strength and modulus of elasticity together with the peaks of the transient forces of solid particles, a characteristic erosion function was introduced. This function was found to have a good correlation with the erosion index. Consequently, the prediction of in-bed tube erosion rates was achieved when the peaks of the transient forces of solid particles and tube material properties are known.

To investigate the effect of fluidization particles on the

erosion index, two different particles were used, silica sand (d_p=1.1 mm) and glass beads (d_p=1.0 mm). As a result, silica sand particles caused more intense erosion than glass beads. This conclusion was included in the predictive equation qualitatively by considering the material properties and geometrical factors of fluidized particles.

The maximum forces in the peripheral direction around the surface of the in-bed tube were also measured and analyzed. The position of the probe on the tube surface in the radial direction were changed from 0° to 180° in increments of 45°. At each of the five probe locations (0°, 45°, 90°, 135° and 180°) the peaks of the transient maximum forces were measured under different fluidization conditions. Results show that the maximum forces (expressed as the average of top five maximum forces) reached the maximum value at 135°.

The erosion rate distribution along the longitudinal direction of the in-bed tube was also measured. Accordingly, the maximum erosion occurred at a point close to the center of the tube. Both edges experienced lesser erosion.

These conclusions indicated that the local erosion rate could be predicted by measuring the local maximum forces. Furthermore, the transient motion of solid particles in fluidized beds was found to be important for the assessment of maximum forces.

4.2 Literature Review

Fluidized beds commonly contain immersed materials such as heat transfer tubes, dip legs, probes, etc. Due to the transient forces of solid particles caused by the bubble and particle motion, these immersed objects experience severe wastage especially under continuous operations.

Forces on immersed objects in fluidized beds were studied by several investigators. Bordet and coworkers (1968) measured the kinetic energy of particles and the collision frequency against a wall by a small piezo-electric crystal microphone immersed in the liquid fluidized bed. Their experimental results were used to explain some wall mass transfer properties in fluidized beds. However, this method was reported to have some technical difficulties as applied in gas-solid fluidized beds.

Nguyen and Grace (1978) reported that the net buoyancy force imposed on an immersed object in a fluidized bed can be estimated by taking the particulate phase density equal to the bed density at minimum fluidization. By synchronizing the photographic films and pressure fluctuations on the surface of submerged tubes, they also concluded that the bubbles passing immersed objects cause transient forces leading to tube vibrations.

Kennedy, Donovan and Trigas (1981) used strain-gauge local cell to measure the external forces imparted by the bed material on tubes in a fluidized bed pertinent to the structural design of heat-exchanger tube systems. They reported that the load cell data support the view that the force pulses on the tubes are produced by the passage of bubbles. They also suggested that the forces on the tubes are the result of an impulse caused by the transfer of the momentum of a body of solids in the wake of the bubble striking the tube.

Grace and Hosny (1985) measured vertical and horizontal forces using externally-mounted strain-gauge force transducers for three bare tubes and one finned tube in fluidized beds. They concluded that static forces dominated at low gas flow rates, while bubble-induced pulses become dominant at high flow rates. Vertical forces tend to be much larger than horizontal forces. They also proposed a simple mechanistic model for the prediction of the root-mean-square forces and of the variation of these forces with superficial gas velocity, tube size, and particle properties.

Meijer and coworkers (1986) used a liquid fluidized bed to study particle impact against bed column. They reported that the Maxwell-Boltzmann velocity distribution appeared not to be valid when the values of comparatively low velocity impacts were included. They also reported that the mean perpendicular velocity at impact was about a factor 10 times lower than the superficial fluid velocity at a porosity of 0.8.

In the work of Nieh et al. (1991), the in-bed tube erosion was studied experimentally by using wax cylinders. The usage of erosion-prone tubes permitted to obtain erosion data in a short time period. They investigated the effects of tube arrangement and flow conditions. As a result, they concluded that under the same conditions, the weight loss of horizontal tubes is maximum, followed by inclined tubes and vertical tubes. They also showed that when the tube is placed close to the distributor, the erosion rate increases rapidly due to high velocity jets.

Some researchers concentrated on developing models both for the hydrodynamics and erosion in fluidized beds (Bouillard and Lyczkowski, (1991); Ding and Lyczkowski, (1992)). In these" detail models, however, only the fluidizing conditions were taken into account. The mechanical properties of the in-bed materials were disregarded. Nevertheless, the predictions were compared with limited experimental data and a fairly good agreements were obtained.

A novel approach came from Kono et al. (1987, 1990) in which three experimental methods were developed to measure the transient forces of solid particles in fluidized beds. In a recent study by the same group (1990), the effect of bed configuration on the transient forces were also presented. The most important conclusion

of these studies is that the transient forces of solid particles in fluidized beds which are solely responsible for the erosion phenomenon can be evaluated through the measurement of pressure Fluctuations.

4.3 Experimental

4.3.1 Evaluation of the force

Conventionally, erosion rates of in-bed tubes have been measured by placing the tube in a fluidized bed for a long time under the defined conditions. Accordingly, the application of-these results are rather limited and restricted to the specific experimental conditions.

Kono et al. (1987) described an experimental technique for measuring the transient forces of solid particles in gas-solid fluidized beds. The measurement of these forces was accomplished by the use of fracture sensitive tracer particles of known mechanical strength. Then, the maximum of the measured forces (F_{max}) was correlated to the maximum of the pressure fluctuations ($\Delta\Delta P_{max}$) as shown in Figure 4.3.1. This correlation suggests that through the measurement of pressure fluctuations at a point in a fluidized bed, one can evaluate the maximum force prevailing at that location. The correlation equation was given as:

$$\frac{F_{max}}{Mg} = 1.2842 \left(\frac{\Delta\Delta P_{max}\, d_p^2}{Mg} \right)^{0.7088} \qquad (1)$$

To apply this technique to the erosion rate study, the maximum force concept was further elaborated by taking the frequency of the maximum forces into account. It is assumed-that there e-xists a threshold of transient forces that determines the erosion rate. The transient forces exceeding this threshold should cause wastage. Then, the top five maximum pressure fluctuations were measured at a specific location in the bed and averaged. This value is assumed to be the force (through Figure 4.3.1) responsible for material wastage.

4.3.2. Erosion rate index

Erosion rates are generally reported as weight loss (or the diameter change of the in-bed tube) per hour in the literature. To generalize the erosion results, the erosion rate index as a function of weight loss, area and time was defined in this study as:

$$I = \frac{\Delta w}{At} \qquad (2)$$

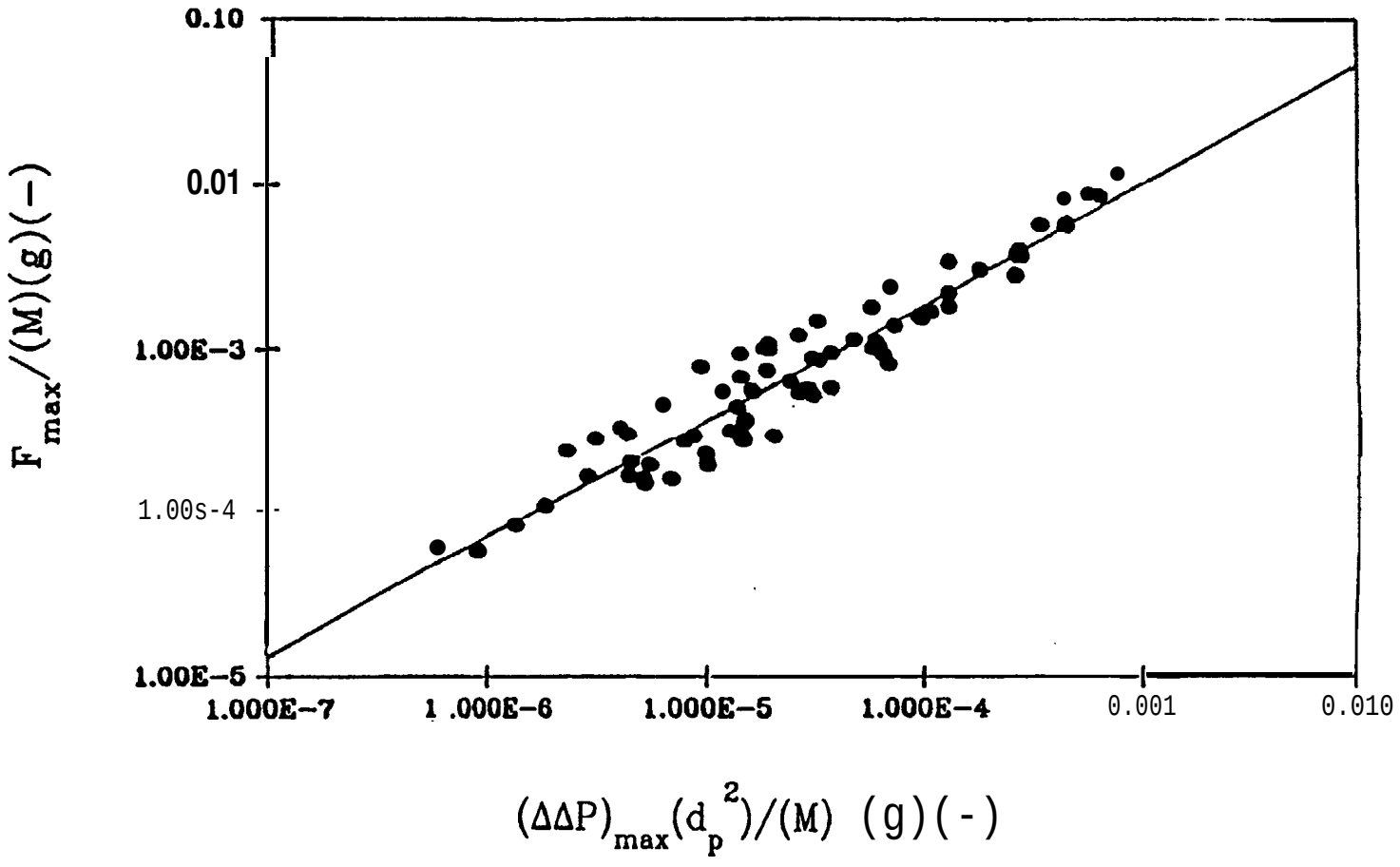

Figure 4.3.1 Correlation between the maximum pressure fluctuations and the maximum force (Kono et al., 1987)

where I has the units of $(kg/m^2/hr)$.

Since erosion is a fracture process occurring on the tube surface caused by the collision of solid particles that are in transient motion in the bed, it follows that the erosion index is a function of: (1) the mechanical properties of the in-bed tube such as its tensile strength and modulus of elasticity, (2) the properties of fluidized particles such as particle size, shape factor, tensile strength, etc., (3) the operating condition of the fluidized bed such as gas velocity, temperature, pressure, etc. Consequently, by changing these parameters experimentally, it is possible to investigate the erosion phenomena.

To cover a wide range of mechanical properties, three tubes (aluminum alloy, copper and stainless steel) were selected. These test tubes are 1/2" in diameter and 4" in length. The mechanical properties of aluminium alloy, copper 122, and 304 stainless steel were summarized in Tables 4.3.0a to 4.3.0c. These tubes were used for elevated temperature tests.

Table 4.3.0a Tensile Strength and Young's Modulus for Aluminum Alloy 6061-T6 at Different Temps

Temperatures ("F)	Tensile Strength	Young's Modulus
75	$310.2 * 10^3$ kPa	$74.5 * 10^6$ kPa
200	$268.0 * 10^3$	$71.7 * 10^6$
300	$234.4 * 10^3$	$70.3 * 10^6$
400	$131.0 * 10^3$	$68.9 * 10^6$
500	$51.7 * 10^3$	$67.6 * 10^6$
600	$31.0 * 10^3$	$66.2 * 10^6$
700	$20.7 * 10^3$	$62.7 * 10^6$
800		$58.6 * 10^6$

Table 4.3.0b Tensile Strength and Young's Modulus for Cooper 122 at Different Temps

Temperatures (“F)	Tensile Strength	Young's Modulus
75	228.6 $*10^3$ kPa	114.4 $*10^6$ kPa
212	202.7 $*10^3$	118.6 $*10^6$
300	189.1 $*10^3$	108.2 $*10^6$
400	173.6 $*10^3$	102.0 $*10^6$
550	149.3 $*10^3$	89.6 $*10^6$
700	121.0 $*10^3$	74.5 $*10^6$
850	90.9 $*10^3$	55.2 $*10^6$
925	76.5 $*10^3$	
1000	56.1 $*10^3$	
1100	43.2 $*10^3$	

Table 4.3.0c Tensile Strength and Young's Modulus for 304 Stainless Steel at Different Temps

Temperatures (“F)	Tensile Strength	Young's Modulus
85	586 $*10^3$ kPa	199.9 $*10^6$ kPa
300	489 $*10^3$	190.5 $*10^6$
600	427 $*10^3$	175.9 $*10^6$
750	414 $*10^3$	169.6 $*10^6$
900	392 $*10^3$	162.7 $*10^6$
1000	371 $*10^3$	158.6 $*10^6$
1100	336 $*10^3$	153.7 $*10^6$

To change the properties of fluidized particles, silica sand and glass beads were used. Silica sand is very irregularly shaped and has a mean diameter of 1.1 mm. Glass beads, on the other hand, are spherical with a diameter of 1 mm. The minimum fluidization velocities of silica sand and glass beads are 0.76 and 0.46 m/s, respectively. Size distribution of particles were checked after each experiment so that constant average particle diameter could be maintained. The results showed that attrition and loss of particles were minimal.

The operating condition of the fluidized bed was changed by using different superficial gas velocities. In most of the experiments U_o/U_{mf} values were 1.5, 2.0, 2.5, and 3.0. In assessing the fluidization particle effect, however, U_o/U_{mf} values were 1.50, 2.00, 2.21, 2.94, 3.68, and 4.42. The temperature was changed in the range of 25 to 400 "C.

The experimental apparatus is shown in Figure 4.3.2. It mainly consists of a 4" x 4" plexi-glass fluidized bed with a porous (200 μm) metal distributor plate, an immersed thin pipe for the measurement of pressure fluctuations, a Validyne (Model P305D) pressure sensor, an A/D converter and a desk-top computer for data acquisition and storing. For elevated temperature experiment, 4" cylindrical quartz fluidized beds were used.

Nitrogen was used as a fluidizing medium to avoid the metal surface oxidation. It was supplied to the system by a compressor via flowmeter.

4.4. Experimental Results and Discussions

4.4.1. Effect of tube material

One of the important factors in the erosion phenomenon is the mechanical properties of in-bed tubes. To investigate this effect, three different in-bed tubes (aluminum alloy, copper, stainless steel; each 1/2" in diameter) were tested under the following experimental conditions: 4" x 4" square fluidized bed, U_o/U_{mf}=1.5, 2.0, 2.5, and 3.0. Fluidized particles were silica sand (irregular in shape) with d_p=1.1 mm. The bed height was 8". Pressure fluctuation measurements were also conducted to evaluate the maximum force of solid particles. The in-bed tube and the pressure probe locations are shown in Figure 4.3.3.

Firstly, the pressure fluctuation data as a function of U_o/U_{mf} was analyzed to obtain the top five maximum pressure fluctuations and averaged to get $\Delta\Delta P_{max}$. These values were plotted in Figure

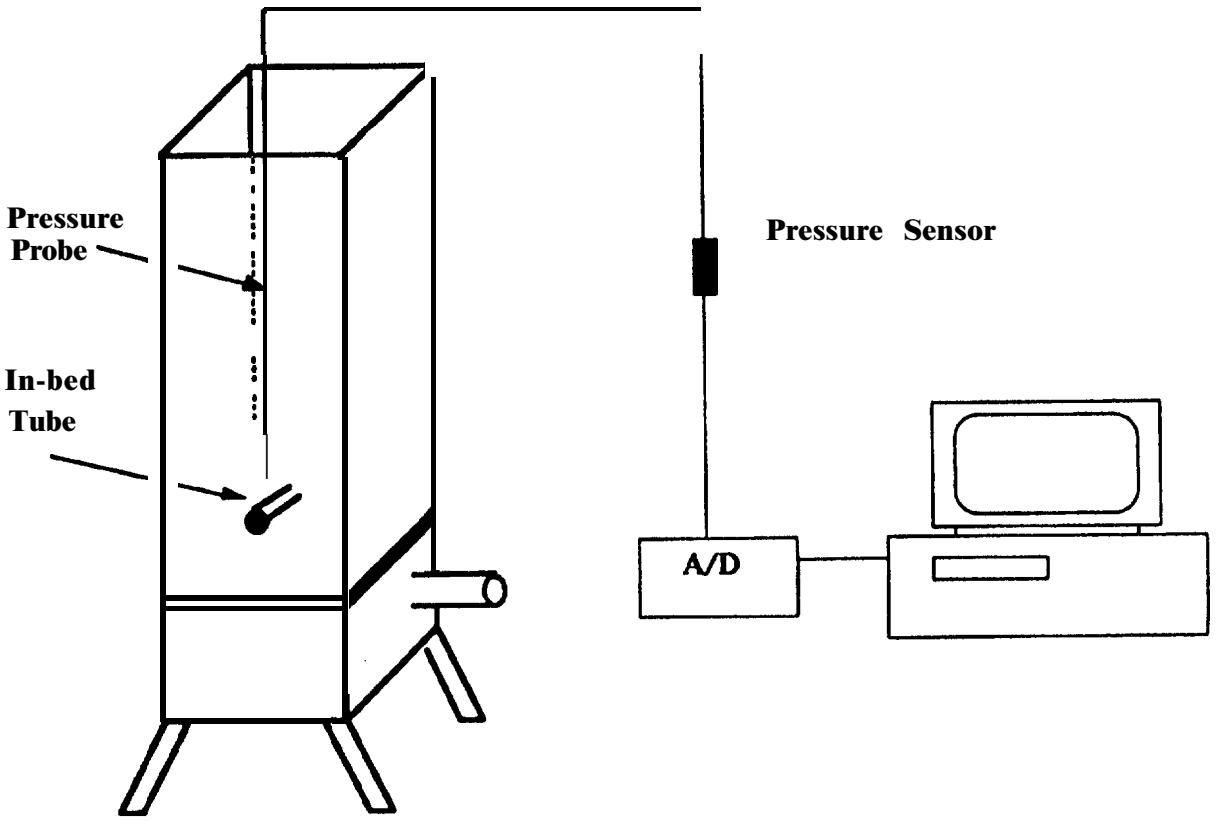

Figure 4.3.2 Experimental set up for erosion tests.

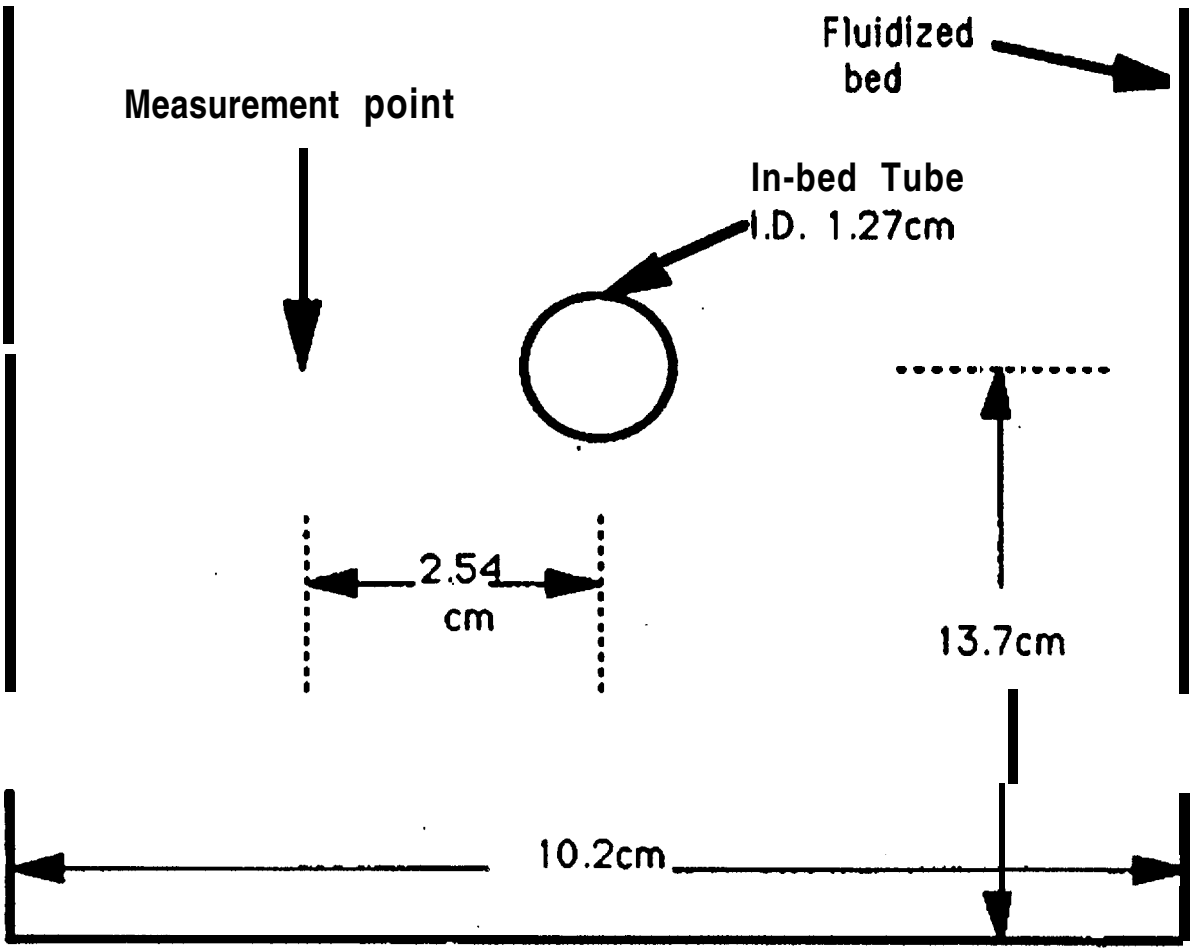

Figure 4.3.3 Schematic diagram of the experimental setting.

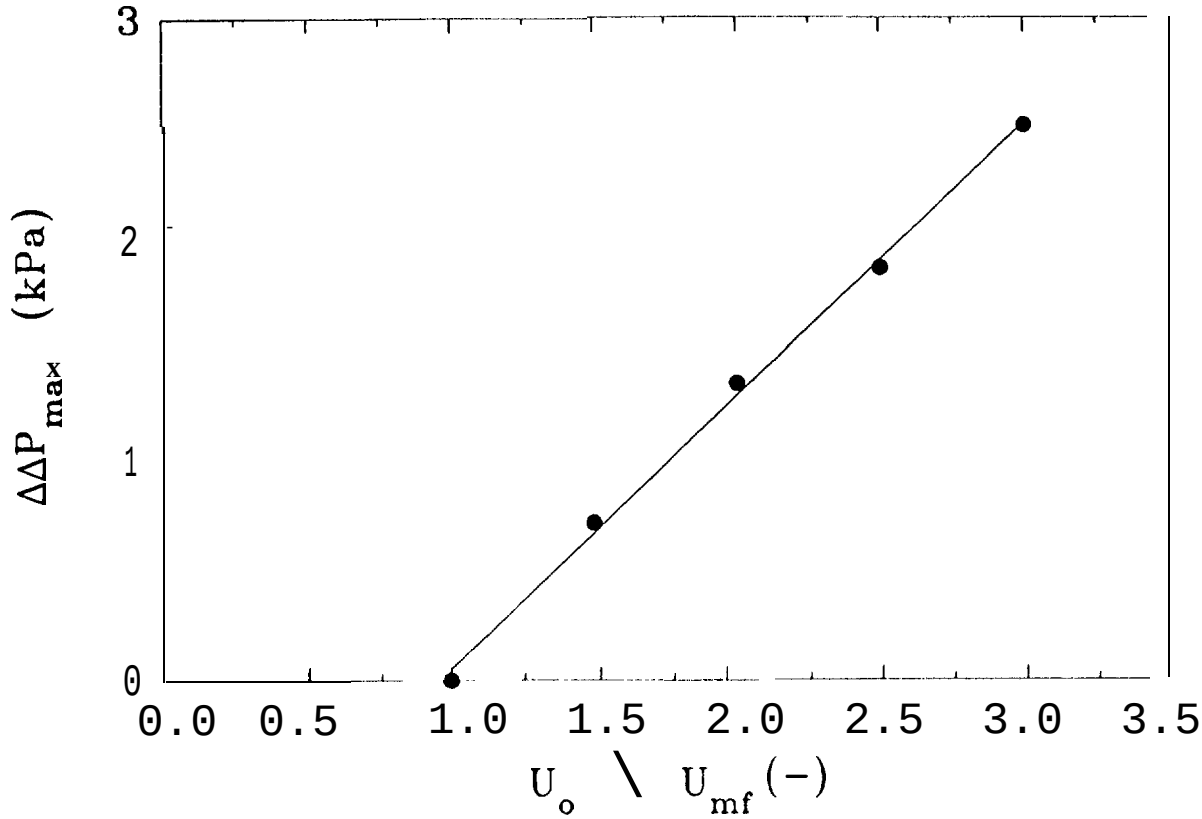

Figure 4.3.4 Relation between the maximum pressure fluctuations and the dimensionless gas velocity.

4.3.4. Therefore, Figure 4.3.4 establishes the relationship between maximum pressure fluctuations and dimensionless gas velocity.

Secondly, the erosion index was evaluated for all the experiments. The detailed data and I values were tabulated in Tables 4.3.1 to 4.3.3 for different tube materials. The erosion index values as a function of $\Delta\Delta P_{max}$ is shown in Figure 4.3.5. As can be seen, there is a good correlation between the erosion index and the maximum pressure fluctuation. It is possible to interpret these results by noting that $\Delta\Delta P_{max}$ is actually the maximum force (i.e., Figure 4.3.1) exerted by the solid particles during their transient motion in the fluidized bed. Thus, as the maximum force increases, the amount of material eroded per unit area per unit time also increases.

On the other hand, the amount of erosion is different for

Table 4.3.1 Erosion Index Data (Aluminum Alloy)
D=15.80 mm L=48.30 mm **A_o=23.97** cm^2 = 2.397x10^3 **m^2**

U_o/U_{mf}		1	2	3	4	5	total
3.0	I	9.850E-5	7.648E-5	9.387E-5	**8.344E-5**	**8.344E-5**	**9.039E-5**
	ΔW	0.017	0.0044	0.0054	0.0048	0.0048	0.0364
	t	72	24	24	24	24	168
2.5	I	**3.477E-5**	**5.389E-5**	**6.605E-5**	6.605E-5	**5.447E-5**	5.041 E-5
	AW	0.006	0.0031	0.0038	0,0038	0.0094	0.0261
	t	72	24	24	24	72	216
2.0	I	**3.592E-5**	**2.781E-5**	3.687E-5	4.581 E-5	2.**177E-5**	**3.443E-5**
	ΔW	0.0062	0.0016	0.0019	0.0028	0,0012	0.0137
	t	72	24	21.5	25.5	23	166
1.5	I	**1.564E-5**	O. **869E-5**	0.869 E-5	1.391 E-5	6.953 E-5	1.101 E-5
	AW	0.0027	0.0005	0.0005	0.0008	0.0012	0.0057
	t	72	24	24	24	72	216

Table 4.3.2 Erosion Index Data (Copper)
D= 15.85 mm L= 101.30 mm **A_o=50.442** cm^2= 5.044x10^3 **m^2**

U_o/U_{mf}		1	2	3	4	5	total
3.0	**I**	22.06 E-5	**20.98E-5**	21. **85E-5**	17.55 E-5	**19.49E-5**	**18.055E-5**
	ΔW	**0.079**	0.0254	0.0270	0.0208	0.0236	0,153
	t	**71**	24	24.5	**23.5**	**24**	168
2.5	**I**	**N/A**	**11.68E-5**	**9.75E-5**	**8.76E-5**	**8.95E-5**	9.806E-5
	AW	**N/A**	0.0277	0.0118	0.0106	0.0325	0.0826
	t	**N/A**	47	24	24	72	167
2.0	**I**	**4.048E-5**	4.520E-5	5.430E-5	**5.121E-5**	**3.910E-5**	**4.410E-5**
	ΔW	0.0049	0.0057	0,0063	**0.0062**	**0.0138**	0.0369
	t	**24**	25	23	24	70	166
1.5	**I**	**2.460E-5**	**1.980E-5**	**2.310E-5**	**1.817E-5**	**1.625E-5**	**1.947E-5**
	ΔW	**0.0032**	0.0022	**0.0028**	**0.0022**	**0.0059**	0.0163
	t	**24**	22	24	24	72	166

Table 4.3.3 Erosion Index Data (Stainless Steel)
D=15.80 mm **L=50.90** mm A=25.26 cm^2 = 2.526x10^3 m^2

U_o/U_{mf}		1	2	3	4	5	total
3.0	I	3.299E-5	3.464E-5	3.629E-5	3.629E-5	2.639E-5	3.323E-5
	ΔW	0.060	0.0021	0.0022	0.0022	0.0016	0,0141
	t	72	24	24	24	24	168
2.s	I	2.584E-5	3.629E-5	2.969E-5	1.979E-5	2.584E-5	2.676E-5
	ΔW	0.0047	0.0022	0,0018	0,0012	0.0047	0.0146
	t	72	24	24	24	72	216
2.0	I	1. 375E-5	O. 825 E-5	2.025 E-5	2.018 E-5	1.549E-5	1.502E-5
	ΔW	0.0025	0.0005	0.0011	0,0013	0.0009	0.0063
	t	72	24	21.5	25.5	23	166
1.5	I	8.248 E-6	4.949E-6	1.650E-6	6.598E-6	2.749E-6	1.502E-6
	ΔW	0.0015	0*0003	0.0001	0.0004	0.0005	0.0028
	t	72	24	24	24	72	216

Table 4.3.4 Mechanical properties of test tubes.

Material	Modulus of Elasticity (kPa)	Tensile Strength (kPa)
Copper	1.17 x 10^8	2.76 x 10^5
Stainless Steel	2.09 x 10^8	5.76 x 10^5
Aluminum Alloy	7.05 x 10^7	2.90 x 10^5

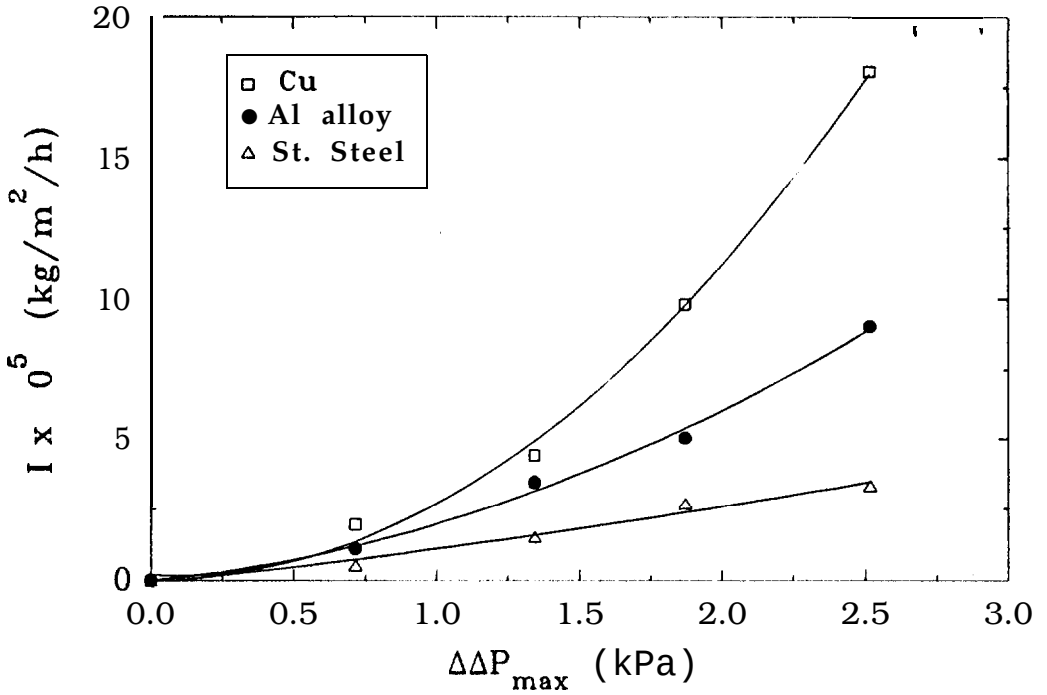

Figure 4 .3.5 Erosion index versus maximum pressure fluctuations for the in-bed tubes.

different materials, as expected. The increase in the erosion rate is more severe in the case of copper than in stainless steel. This material dependency can be explained by referring to the mechanical properties of the tubes. The tensile strength and modulus of elasticity values for the test tubes are listed in Table 4.3.4. From the experimental erosion data, it is possible to develop a prediction equation which includes the mechanical properties of

the test tubes. Figure 4.3.6 shows the plot of the erosion index correlation and the resulting prediction equation is:

$$I = 12{,}939 \left(\frac{\Delta\Delta P_{max}\ E}{\sigma_t^2} \right)^2 \qquad (3)$$

In this equation, I has the units of $kg/m^2/hr$ and correlation coefficient was found to be 0.99. From this equation F_{max} can be calculated by using the reported result of Kono et al. (1987) and correlated as shown in Figure 4.3.7. For this case, the correlation

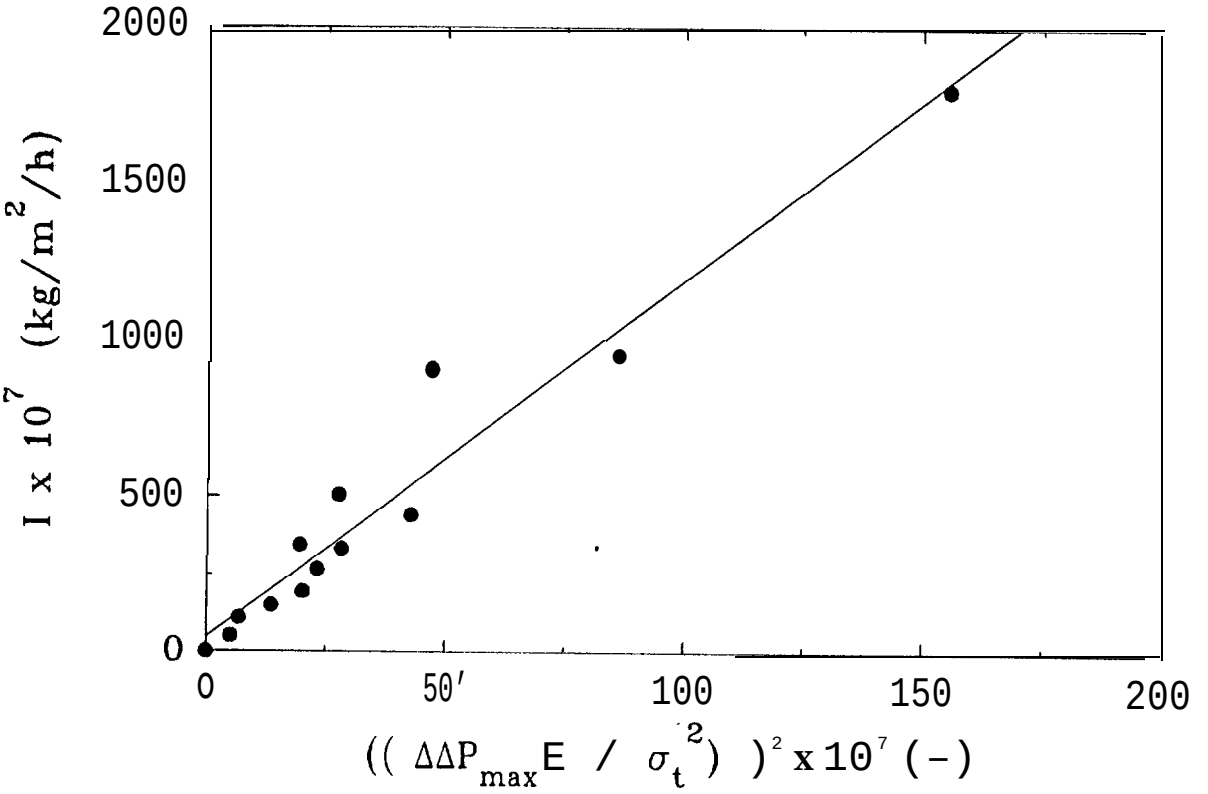

Figure 4. 3.6 Correlation between the erosion index and $\Delta\Delta P_{max}$.

coefficient is 0.97 and the equation becomes:

$$I = 35083.11 \left[\frac{F_{max} E}{\sigma_t^2} \right]^2 \qquad (4)$$

It is important to note that the term $((\Delta\Delta P_{max} E)/\sigma_t^2)$ is a dimensionless number which represents both the properties of the in-bed tube material and the maximum force. This number is called, here, as the dimensionless erosion characteristic number. From Figure 4.3.7, as the erosion characteristic number increases, the erosion rate index also increases. With the help of this correlation, the prediction of erosion rates of in-bed tubes can be achieved when $\Delta\Delta P_{max}$ and E and σ_t of the material are known.

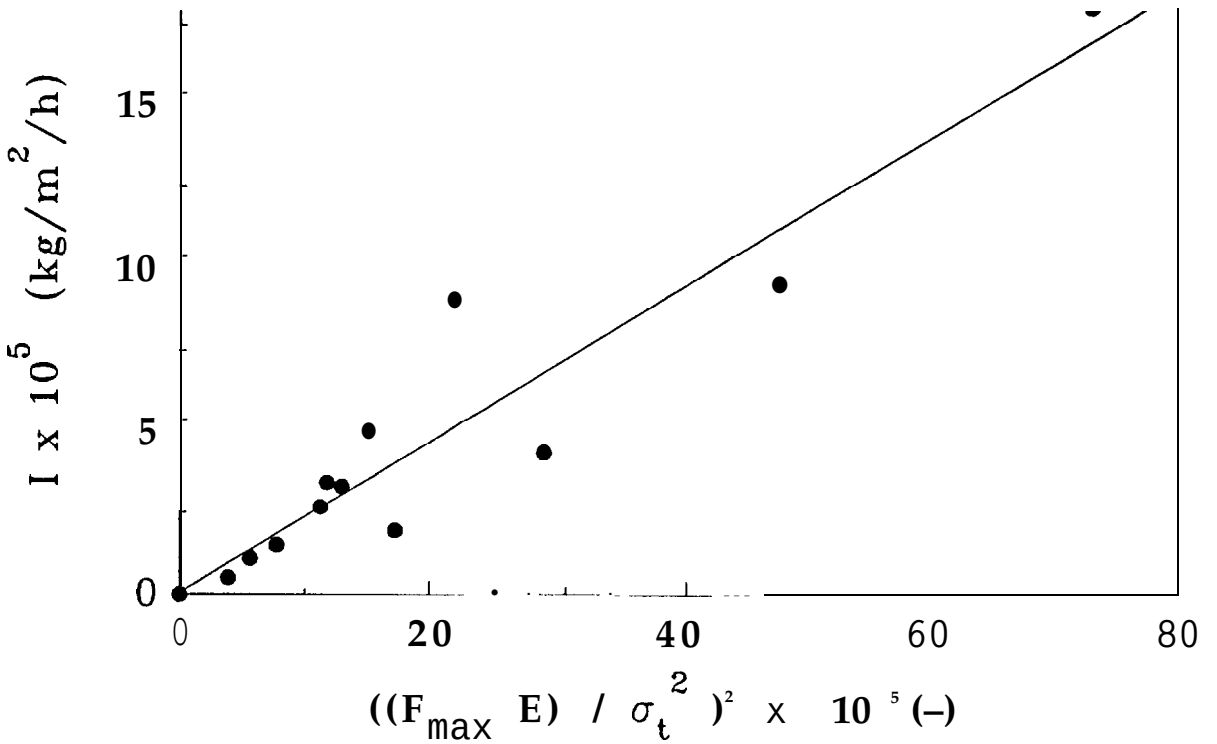

Figure 4.3.7 Correlation between the erosion index and the dimensionless characteristic erosion number.

4.4.2. Effect of fluidization particles

To investigate the particle effect on erosion rates, experiments were carried out by using glass beads (d_p=1 mm). The 4" x 4" square fluidized bed was utilized with a copper test tube. The dimensionless gas velocity values were U_o/U_{mf}=1.50, 2.00, 2.21, 2.94, 3.68, and 4.42. The bed height was again 8".

The erosion data was tabulated in Table 4.3.4. In Figure 4.3.8, the erosion index was plotted as a function of the maximum pressure fluctuation for silica sand and glass beads.

From Figure 4.3.8 it can be seen that silica sand caused considerably higher erosion rates than glass beads. Thus, the

Table 4.3.4 Erosion Index Data (Copper) with glass beads.
D=15.85 mm L=101.3O mm A=50.442cm^2= 5.044x10^{3}m^2

U_o/U_{mf}		1	2	3	4	5	total
4.42	I	9.913 E-5	**1.050E-4**	**9.252E-5**	8.591 E-5	**8.447E-5**	8.963 E-5
	ΔW	0.0120	0.0127	0.0112	0.0195	0.0409	0.0963
	t	24	24	24	45	96	213
3.68	I	4.956 E-5	**5.617E-5**	6.856 E-5	**7.600E-5**	**6.749E-5**	**6.419E-5**
	ΔW	0.0060	0.0068	0.0083	0.0092	0.0016	0.0463
	t	24	24	24	24	**47**	143
2.94	I	**2.643E-5**	**3.056E-5**	3. **800E-5**	2.31OE-5	2.913 E-5	2.932E-5
	ΔW	0.0032	0,0037	0.0046	0.0028	0.0169	0.0312
	t	24	24	24	24	115	211
2.21	I	2.230E-5	3.220E-5	**2.230E-5**	**1.652E-5**	**2.279E-5**	2.316 E-5
	ΔW	0.0027	0,0039	0.0027	0.0020	0.0050	0.0163
	t	24	24	24	24	43.5	139.5
2.00	I	**9.087E-6**	1. **189E-5**	**1.074E-5**	**9.494E-6**	9,637 E-6	9,913 E-6
	ΔW	0.0011	0.0015	0.0013	0.0034	0.0035	0.0108
	t	24	25	24	71	72	216
1.50	I	4. **130E-6**	7.209E-6	**4.506E-6**	**1.950E-6**	**1.652E-6**	3.284E-6
	ΔW	0.0005	0.0008	0.0005	0.0007	0.0002	0,0027
	t	24	22	22	71	24	163

effect of different fluidized particles become **more evident.** However, to characterize this effect it is necessary to further look at the particle properties. A quick literature survey showed that both particles have approximately the same hardness and tensile strength values (Asahara et al. , 1980) . The **only** significant difference, then, is the particle shapes. Since the silica sand is very irregular in shape with sharp edges, it resulted higher erosion rates (note that the glass bead particles are spherical). Therefore, it is possible to state qualitatively that the erosion rate equation will be in the form of:

$$I = \text{constant} \left[\frac{F_{max}\ E}{\sigma_t^2} \right]^2 N_{PC}^m \qquad (5)$$

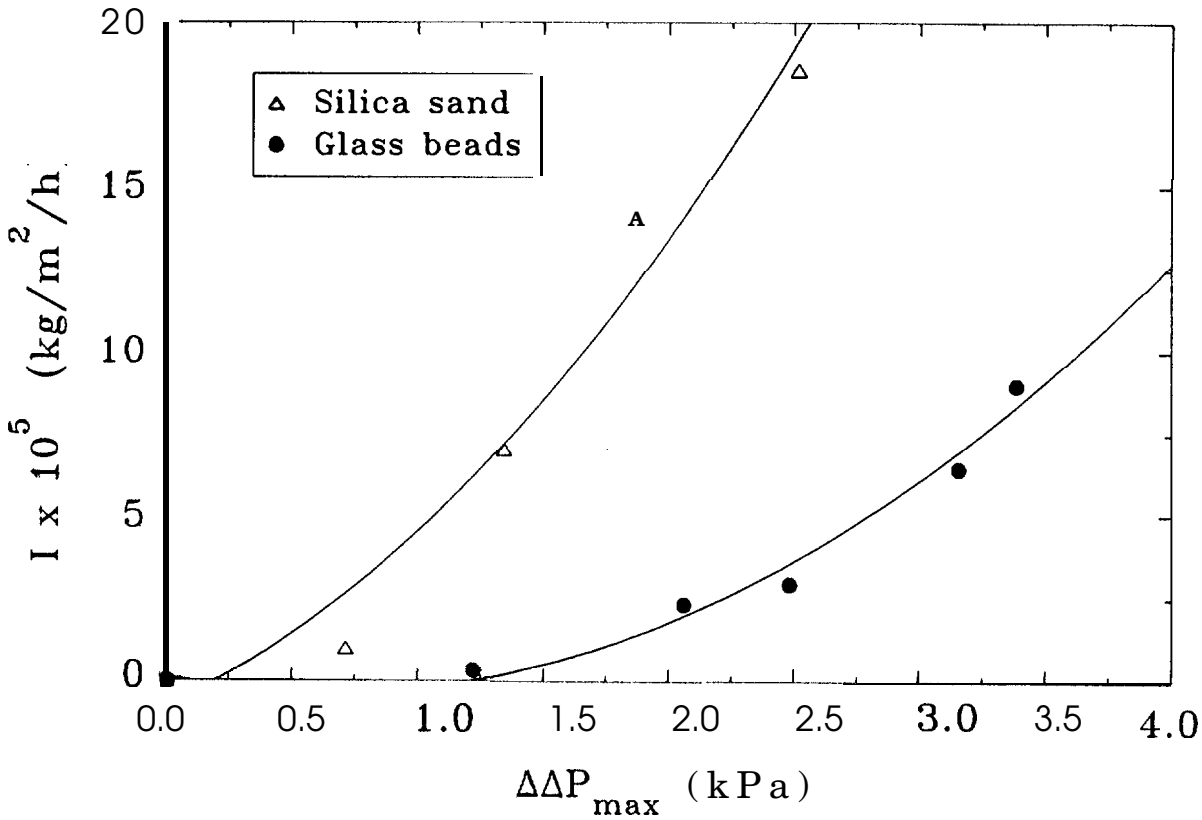

Figure 4. 3.8 Effect of fluidized particles on the erosion index.

where N_{pc} is a dimensionless particle characterization number and it is a function of fluidized particle properties such "as the tensile strength, shape factor, etc.

4.4.3. Measurement of maximum forces in peripheral and longitudinal tube directions

For the measurement of the maximum force in the peripheral direction, a special test tube was constructed. The pressure probe was located on the surface of the test tube from its inside. For each experiment, this tube was rotated inside the bed so that the maximum force can be measured at 0°, 45°, 90°, 135°, and 180°. The

layout of these locations are shown in Figure 4.3.9.

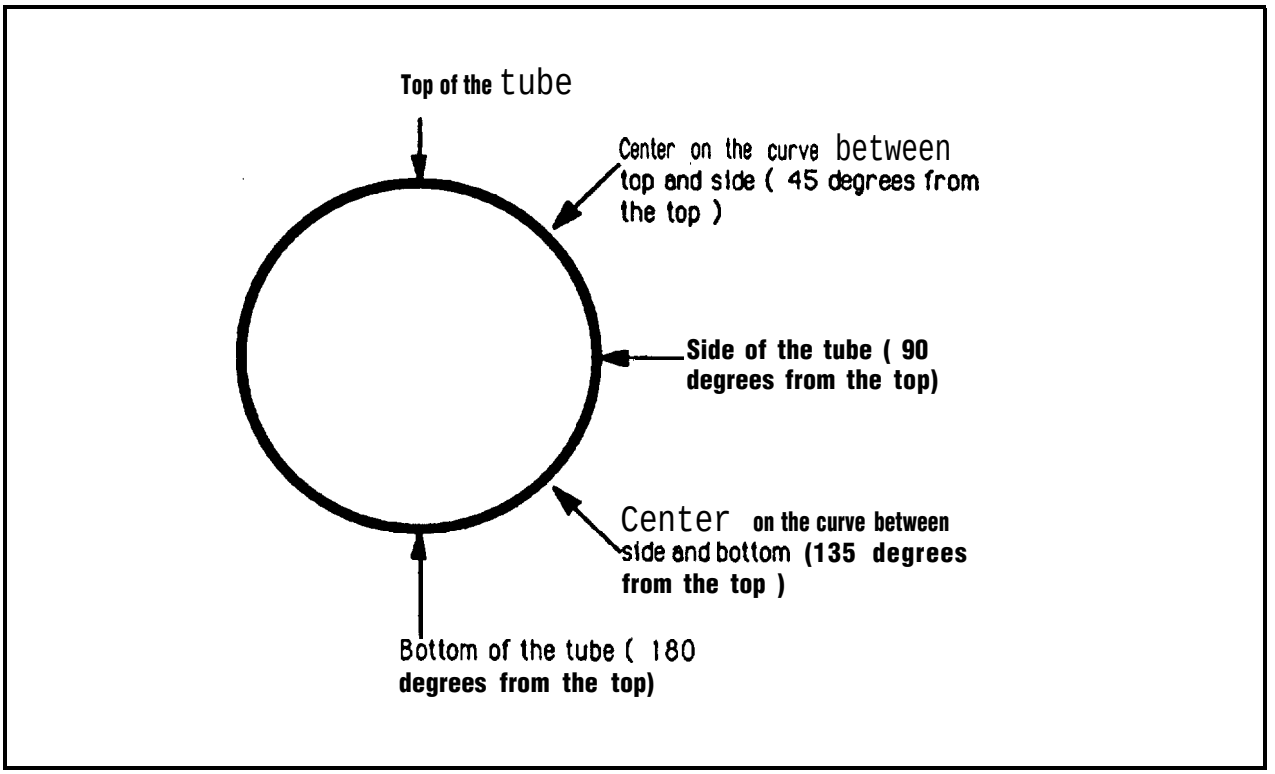

Figure 4.3.9 Peripheral measurement points on the in-bed tube.

In the experiments, silica sand (d_p=1.1 mm) was utilized together with copper sample tube. The bed was 4" x 4" square and the bed height was 8", as dimensionless gas velocities U_o/U_{mf}=1.5, 2.0, 2.5, and 3.0 were used.

Figure 4.3.10 shows the maximum pressure fluctuation versus the degrees from the top of the tube as a function of dimensionless gas velocity. As can be seen, up to U_o/U_{mf}=2.0, there is not so much difference in the maximum pressure fluctuation values. However, starting from U_o/U_{mf}=2.0, the maximum pressure fluctuation values become higher at 90°, 135° and 180°. At U_o/U_{mf}=3.0, $\Delta\Delta P_{max}$ reaches a maximum at 135°. This means that at high gas velocities, at 135° and because of symmetry at 225°, there will be higher material wastage compare to other peripheral points.

Erosion rate distribution was also measured in the longitudinal direction of the test tube. For this purpose, five aluminum rings were installed as shown in Figure 4.3.11. During the experiments, these rings were weighed separately and the erosion index was calculated accordingly.

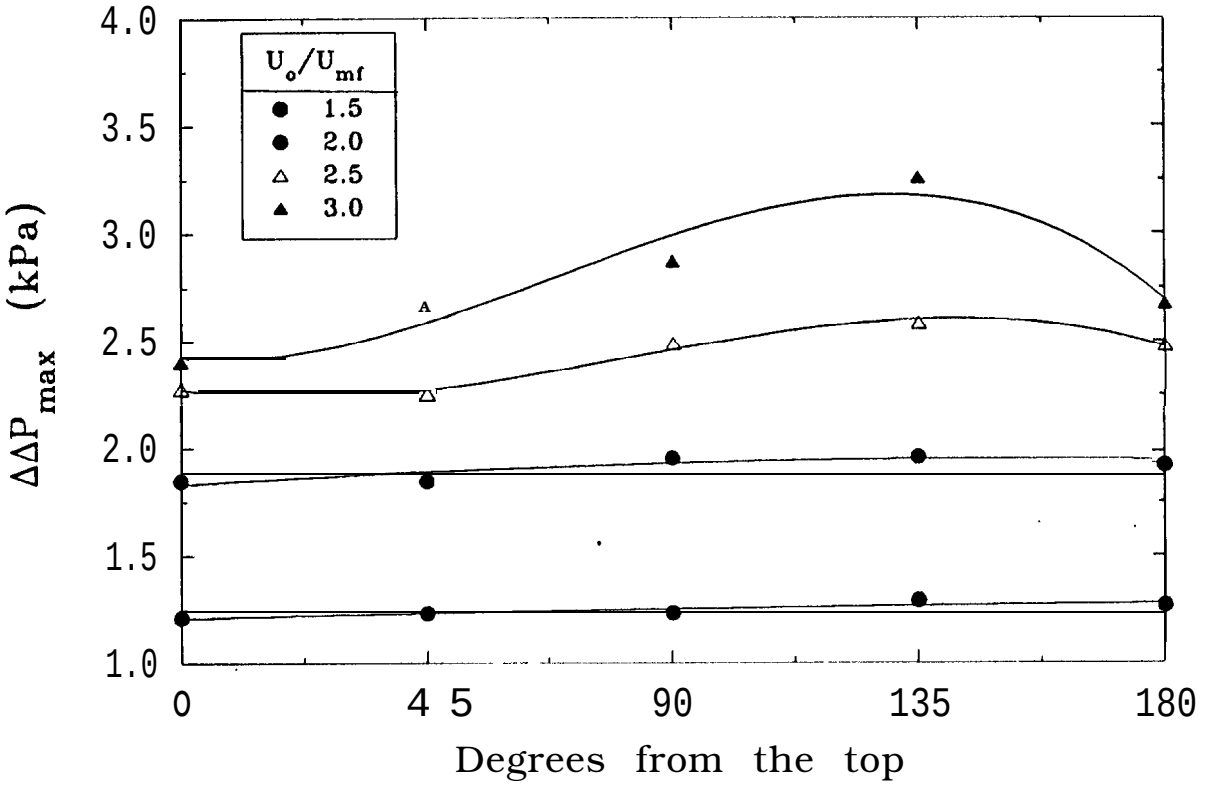

Figure 4.3.10. Distribution of maximum pressure fluctuation along the peripheral direction of the tube.

As fluidized particles, silica sand was used (d_p=1.1 mm). The bed was 4" x 4" square and bed height was 8". Only U_o/U_{mf}=3.0 was employed.

Results were plotted in Figure 4.3.12 as a function of longitudinal tube distance. As can be seen, the general tendency is that the maximum erosion rate is near the tube center, and it decreases towards the walls. This is probably because of the fact that the tube center experiences more-bubble-activities and since each bubble wake has a stronger impact on the tube, the erosion rate obtained was higher. This observation was also reported in the recent literature (Levy et al., 1992).

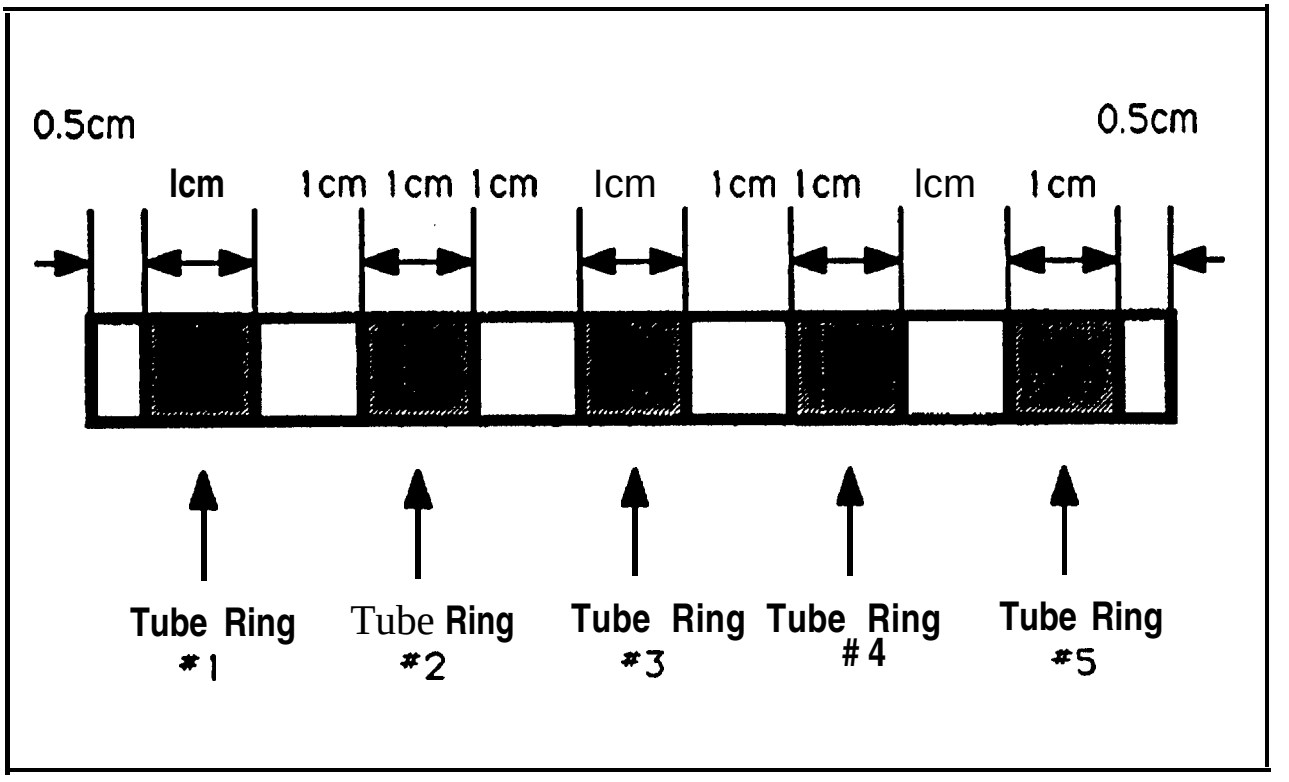

Figure 4.3.11 Tube rings for the measurement of erosion rates in longitudinal direction.

The effect of temperature on the maximum pressure fluctuation $(\Delta\Delta P)_{max}$ is shown in Figure 4.3.12.

The errosion rates of in-bed tubes with the specified properties , e.g., aluminium alloy 6061-T1, copper 122, or 304 stainless steel (refer to Tables 4.3.Oa to 4.3.0c), can be expressed also in the same way for which we developed the predictive equation, i.e.,

$$I = 11.687\,(\Delta\Delta P_{max} E \sigma^{-2})^2 \qquad (6)$$

the experimental results were shown in Figure 4.3.14. The key words used in Figure 4.3.14 were shown in Table 4.3.5. As seen in Figure 4.3.14, when the $(\Delta\Delta P)_{max}$ can be measured at plant site, and the in-bed tube's mechanical properties are provided as the function of temperature, the errosion rate of in-bed tube at a known elvevated temperature can be predicted. This results could be practically a very useful information to design and operate all the types of FBC systems. Using this relation the reverse way, in view of

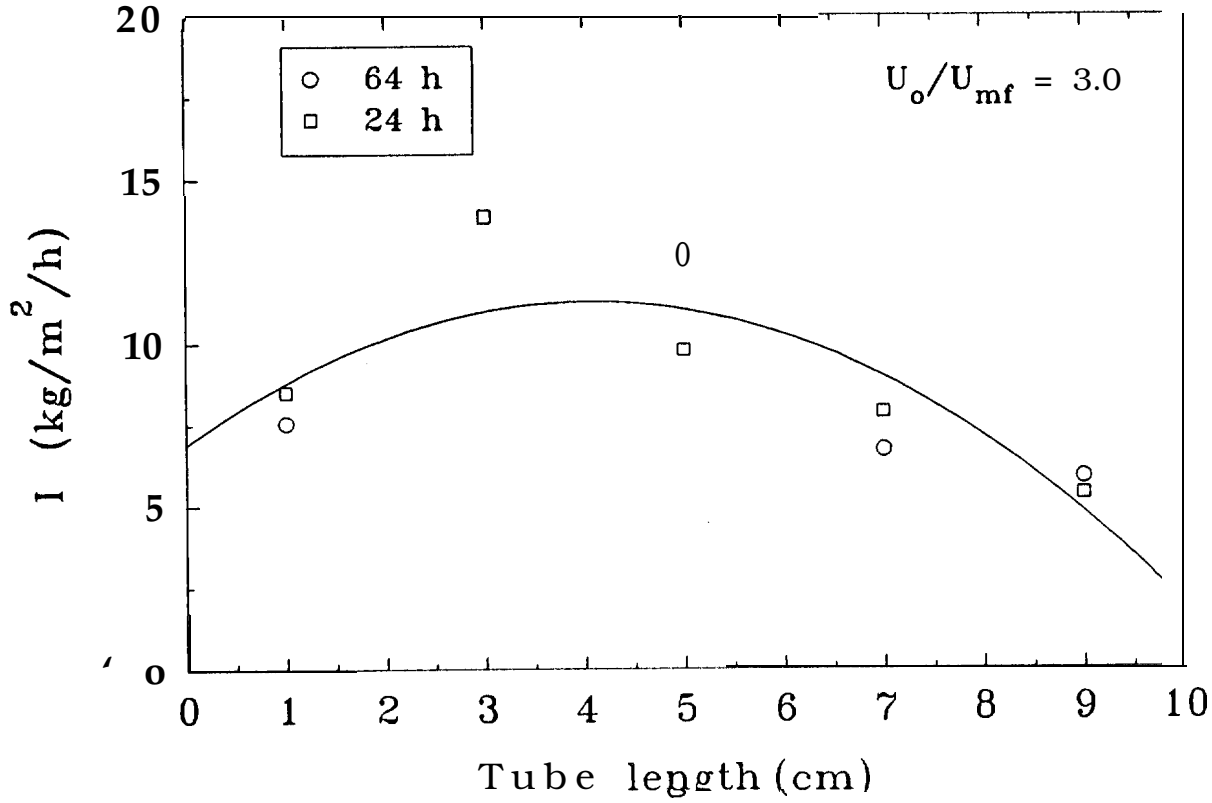

Figure 4.3.12 Erosion index in the longitudinal direction of the in-bed tube.

fundamental scientific view point, the prediction of maximum gas pressure fluctuation can also be accomplished by an errosion test. Further as there is the relation of $\Delta\Delta_{max}$ and $\Delta\Delta P'$ (gas stress gradient), we can determine the intensity of the bubble interaction in the emulsion phase, which could be a useful criterion for fluidization.

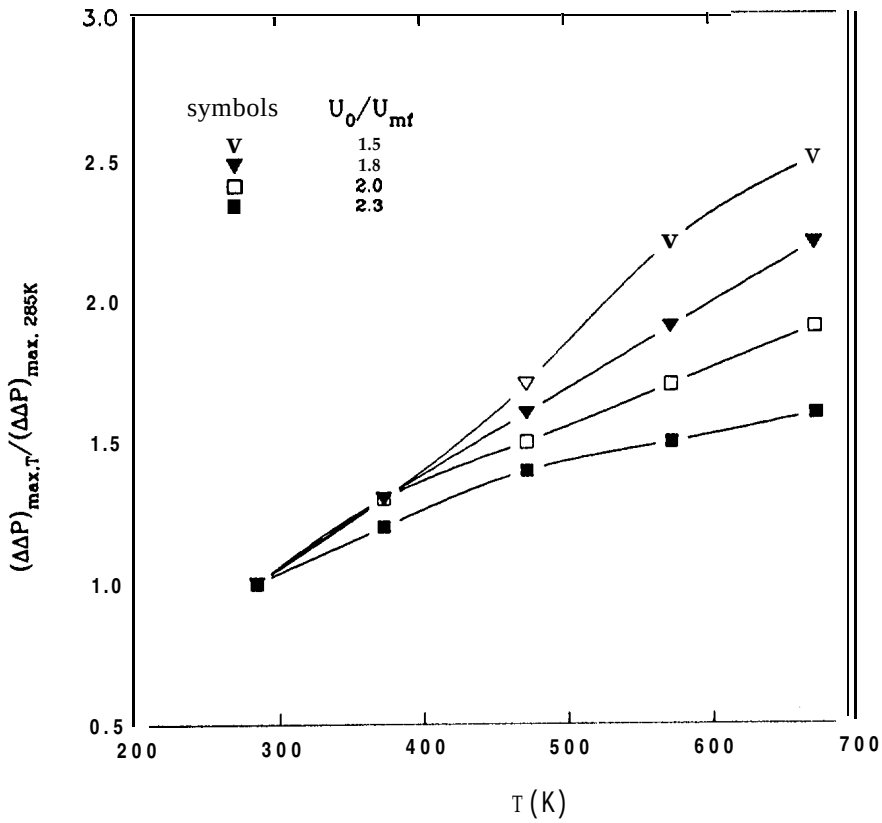

Figure 4.3.13 The effect of temperature on $\Delta\Delta P_{max}$

Table 4.3.5 Keys for Figure 4.3.15

Point	Metal	Temperature (°C)	U_o/U_{mf}
1	Steel	25	1.5
2	Aluminum	25	1.5
3	Steel	100	1.5
4	Steel	25	2
5	Aluminum	25	2
6	Steel	100	2
7	Steel	200	1.5
8	Copper	25	1.5
9	Steel	200	2 "
10	Steel	100	2.7
11	Steel	300	2
12	Aluminum	100	2
13	Steel	200	3
14	Copper	25	2
15	Aluminum	170	2
16	Copper	100	2
17	Copper	200	2
18	Aluminum	200	2
19	Copper	300	2

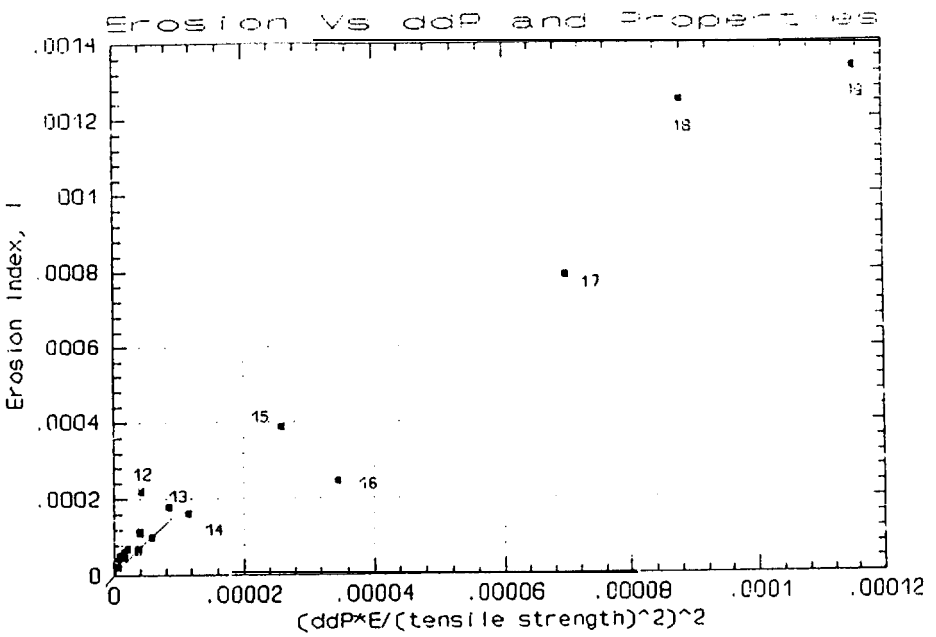

This graph is the enlargement of the lower left corner of the first graph

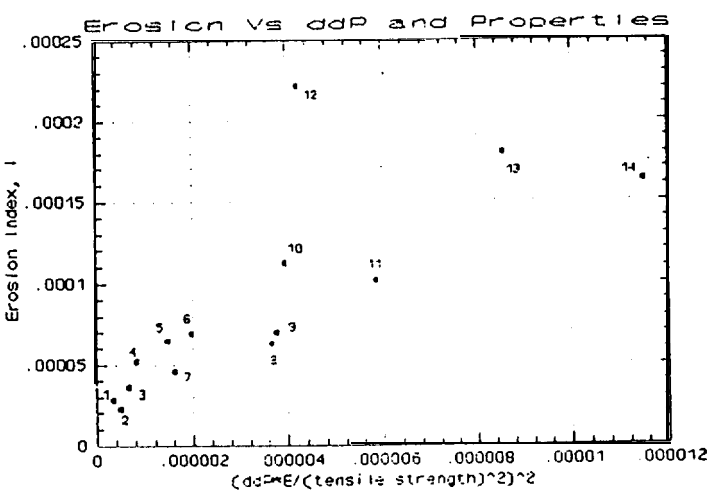

Figure 4.3.14 Erosion vs. ΔΔP and properties of materials

To summarize the results, we can draw:

1) By improving the method developed by Kono et al. (1987), the peaks of the transient forces of solid particles were experimentally measured and characterized by taking the maximum force and the frequency of these forces into account.

2) As a tool for the measurement of the transient forces of solid particles, the gas phase pressure fluctuation method was used.

3) Experimental results indicate that there is a good correlation between the erosion rate index and the characterized maximum force.

4) A prediction model was developed that correlates the erosion rate index to the maximum force through the material properties of in-bed tubes.

5) This correlation was achieved through a dimensionless erosion characterization number which is based on the principles of solid state fracture theory.

6) The effect of fluidized particles on erosion was also investigated. It was seen that the properties of fluidization particles such as shape, significantly affect the erosion rates of in-bed components.

7) Higher erosion rates were observed near the center of the in-bed tube than near the wall.

8) The transient force distribution in the peripheral direction around the in-bed tube surface was also obtained. The transient maximum force has the maximum value at the center of the curve between the side and bottom of the in-bed tube, *i.e.*, at 135° and 225°.

5. CONCLUSIONS

1. The fundamental behavior of transient bubbles was experimentally investigated in two dimensional freely bubbling fluidized bed, taking the video pictures of transient bubbles, and processing the transient bubble images by computers. Very interesting and useful experimental results were obtained, which provided a new insight into the intrinsic physical meaning of freely bubbling fluidization. The results obtained are significantly different from what have been assumed by classical two phase flow model and its related experimental interpretation.

2. New experimental facts of the behavior of transient bubbles in freely bubbling fluidized can be summarized as follows:

- 2.1 Transient bubbles change its size and shaPe very drastically within the very short time interval of 30 milliseconds.
- 2.2 In addition to the known bubbling phenomena of coalescence and splitting, there are considerable bubble disappearance into the adjacent emulsion phase and also bubble reappearance from the adjacent emulsion phase simultaneously.
- 2.3 As the results of experimental evidence of 2.1 and 2.2, there is a significant gas bulk flow between the bubble and the adjacent emulsion phase and also among the transient bubbles.
- 2.4 The bubble rising velocities change transiently and rapidly, e.g., the velocity can change from 0.5 m/s to 3.0 m/s in 30 milliseconds.

All these new experimental facts have been not, at least to our best knowledge, really considered for the design and oPeration of traditional fluidization engineering, but substantially agree with the experimental data of transient bubbling published by J. Halow et al. (1992), which was experimentally observed by using capacitance method in freely bubbling three dimensional fluidized beds.

3. Under a certain definite fluidization operation condition using a specific equipment, there could be two different types of fluidization mode. We named them as normal and abnormal fluidization periods, which can shift from one mode to other or vice versa very stochastically.

4. The erosion rate of in-bed tubes in FBC system is practically a very critical engineering problem, which is strongly affected by the behavior of transient bubbles. At the same time, the erosion rate can be recognized as an important index to understand the transient bubble property. The erosion rates were measured experimentally at ambient and elevated temperature, taking the transiently occurring maximum solid particle's stress and the

properties of the in-bed tube into consideration. The experimental results were analyzed based upon fracture physics and a predictive equation was developed. Measuring the gas phase pressure fluctuation ($\Delta\Delta P$) at plant site and knowing the mechanical properties of in-bed tubes as the function of temperature, the erosion rate of in-bed tubes can be predicted.

6. NOMENCLATURE

A	metal tube surface area
Ar	Archimedes number, $d_p^3 * \rho_{gas} * (\rho_{particle} - \rho_{gas}) / \mu^2$
d_p	diameter of fluidized particle, m
E	Young's Modulus, KPa
F_{max}	maximum transient force, N
G_{mf}	mass minimum fluidization velocity
g	gravitational constant, 9.8 m/s2
H	bed height, m
I	erosion index, (kg/m*/h)
M	mass of the particle in the fluidized bed
RE_{mf}	Renold number at minimum fluidization, $d_p * U_{mf} * \rho_{gas} / \mu$
$\Delta\Delta P^{\#}$	pressure difference between two horizantol points, KPa
$\Delta\Delta P_{max}$	maximum pressure fluctuation, KPa
T	temperature
t	operating time
U_{mf}	minimum fluidization velocity, m/s
U_o	superficial gas velocity, m/s
V	volumetric flow rate, ft^3/min
ΔW	weight change of the metal tube
σ_t	tensile strength, KPa
ρ_{gas}	density of the fluidizing gas, kg/m^3
$\rho_{particle}$	density of the particle, kg/m^3
μ	viscosity of fluidizing agent, Pa*s

7. BIBLIOGRAPHY

Anderson, T. B., and Jackson, R. , I & EC Fundamentals, 6(4), 527, 1967

Asahara, S., et al., Japanese Chemistry Society (eds), Handbook of Chemistry-Applied Chemistry, Maruzen Publ. Co., Tokyo, Japan, 375, 1980

Bordet, J., Borlai, O., Verghes, F. and LeGoff, P., Ind. Chem. Eng. Symp . Ser., 30, 165, 1968

Bouillard, J. X. and Lyczkowski, R. W., Powder Technology, 68, 37, 1991

Clough, David E. and Weimer, Alan W., "Time-Dependent Behavior Of Bubble Volume in Fluidized beds", Ind. Eng. Chem. Fundam. , 24, 235, 1985.

Davidson, J. F. et al , "Fluidized Particles", Cambridge University Press, p.50, 1963.

Ding, J. and Gidaspow, D., "A Bubbling Fluidization Model Using Kinetic Theory of Granular Flow", AIChE Journal, 36, 523, 1990.

Ding, J. and R. W. Lyczkowski, Powder Technology, 73, 127, 1992

Finnie, I, Wear, 19, 81, 1972

Grace, J. R. and Hosny, N., Chem. Eng. Res. Des., 63, 191, 1985

Gyure, Dale C. and Clough, David E., "Dynamic Estimation of Bubble Parameters in a Fluidized Bed Subjected to Load Disturbances", Ind. Eng. Chem. Res., 26, 938, 1987.

Halow, J. S. et al, "Preliminary Capacitance Imaging Experiments of a Fluidized Bed", A. 1. ChE Annual Meeting, San Francisco, 1989.

Halow, J. S. et al, "Advances in Fluidization Engineering", AIChE Symposium Series No. 276, vol. 86, p.41, 1990.

Halow. J. S. and Nicoletti. P., 'lObservations of Fluidized Bed Coalescence Using Capacitance Imaging", Powder Technology, vol. 69, 255, 1992

Kennedy, T. C., Donovan, J. E., and Trigas, A., AIChE J. 27(3), 351, 1981

Kono, H. O. et al, "Kinetic Behavior of Solid Particles in

Fluidized Beds", Annual Report DEAC-21-86MC23249, submitted in 1988.

Kono, H. O. et al, "Kinetic Behavior of Solid Particles in Fluidized Beds", Quarterly Report DEAC-21-86C23249, submitted in Jan 1990.

Kono, H. O., Huang, C. C., and Xi, M., Powder Technology, 62, 13, 1990

Kono, H. O. et al, "Fundamental Study on Transient Bubble (Slug) Behavior by Characterizing transient Forces of Solid Particles in Fluidized Bed", Monthly Report DE-FC21-87MC24207, march 1991.

Kunii, D., and Levenspiel, O. , Fluidization Engineering, R. E. Krieger Publ. Co., Inc., Malabor, Florida, 1984

Levy, E., Wagh, M., Sethu, H. and Pinarbasi, A., Powder Technology, 70, 175, 1992.

Lim, K. S. et al, 'lMeasurement and Modeling of Bubble Parameters in a Two-Dimensional Gas-Fluidized Bed Using Image Analysis", Powder Technology, 60, 159, 1990.

Lyczkowski, R. W. and Bouillard in A. V. Levy (cd.) Proc. Corrosion Erosion of Materials at Elevated Temperatures, Nat. Assoc. Corr. Eng., Houston, 1991

Meijer, J.A.M., Wesselingh, J. A., Clobus, A. and M. L. A. Gossens, Desalination, 58, 1, 1986

Neih, S., Lee, S. W., and Fu, T. T., Powder Technology/ 67, 229, 1991

Nesic, S. and Postlethwaite, J., Corrosion, 8, 582, 1991

Nguyen, T. H., and Grace, J. R., Powder Technology, 19, 255, 1978

Rowe, P. N. et al, "Bubble in Fluidized Beds", Nature, London, 195, 278, 1962.

Sinclair, J. L. and Jackson, R., "Gas-Particle Flow in a Vertical Pipe with Particle Interactions", AIChE Journal, 35, 1437, 1989.

Sung, J. S. and Burgess, J. M., "A Laser-Based Method for Bubble Parameter Measurement in Two Dimensional Fluidized Beds", Powder Technology, 49, 165, 1987'.

Viswanathan, K. and Rae, D. Subba, "Measurement of Bubble Size in Fluidized Beds", Ind. Eng. Chem. process Des. Dev., 23, 573, 1984.